TECHNISCHE UNIVERSITÄT MÜNCHEN

Lehrstuhl für Radiochemie

Evaluation and application of the low energy electron emitter ^{161}Tb

Silvia M. Lehenberger

Vollständiger Abdruck der von der Fakultät für Chemie der Technischen Universität München zur Erlangung des akademischen Grades eines

Doktor der Naturwissenschaften (Dr. rer. nat.)

genehmigten Dissertation.

Vorsitzender: Univ. Prof. Dr. Michael Schuster

Prüfer der Dissertation: 1. Univ. Prof. Dr. Andreas Türler

2. Univ. Prof. Dr. Klaus Köhler

Die Dissertation wurde am 30.09.2010 bei der Technischen Universität München eingereicht und durch die Fakultät für Chemie am 18.11.2010 angenommen.

Die vorliegende Arbeit wurde am Lehrstuhl für Radiochemie der Technischen Universität München in Garching unter Anleitung von Herrn Dr. Konstantin Zhernosekov in der Zeit von September 2007 bis September 2010 durchgeführt.

Abstract

The low energy β^--emitter ^{161}Tb with 6.90 days half-life is very similar to ^{177}Lu. In contrast, ^{161}Tb emits a significant amount of conversion and Auger electrons. Due to the relatively short range in the tissue and consequently high local damage, this particles can provide a very high cytotoxicity and therefore a greater therapeutic effect can be expected in comparison to ^{177}Lu. In addition, ^{161}Tb emits low-energy photons which are useful for imaging purposes by means of a γ-camera.

^{161}Tb was produced via the ^{160}Gd(n,γ)^{161}Gd$\xrightarrow{\beta^-}$^{161}Tb production route by neutron irradiation of massive ^{160}Gd targets (up to 40 mg) in a nuclear reactor. A semi-automated procedure based on cation exchange chromatography was developed and applied for isolation of no carrier added (*n.c.a.*) ^{161}Tb from the bulk of the ^{160}Gd target and from its stable decay product ^{161}Dy. ^{161}Tb was used for radiolabeling of DOTA-Tyr^3-octreotate and the monoclonal antibody chCE7. In addition, experiments with human ovarian carcinoma cells SKOV3ip have been performed and the results have been compared to commercially available *n.c.a.* ^{177}Lu.

The results show that up to 16 GBq of *n.c.a.* ^{161}Tb could be produced by long-term irradiations of Gd targets. Processing on a cation exchange resin allowed obtaining 80 - 90 % of the available ^{161}Tb with highest specific activity, radionuclide- and chemical purity and in quantities sufficient for therapeutic applications. The produced ^{161}Tb could be successfully used for preparations of ^{161}Tb- DOTA-Tyr^3-octreotate and ^{161}Tb-chCE7. Comparison of experiments with SKOV3ip cells showed similar results for the components ^{161}Tb-chCE7 and ^{177}Lu-chCE7.

Zusammenfassung

Der niederenergetische Elektronenstrahler ^{161}Tb mit einer Halbwertszeit von 6.90 Tagen ähnelt sehr dem Lanthanoid ^{177}Lu. Im Gegensatz dazu emittiert ^{161}Tb zusätzlich eine hohe Anzahl an Konversions- und Augerelektronen. Aufgrund ihrer relativ geringen Reichweite im menschlichen Gewebe, und der demzufolge hohen lokalen Schädigung, ermöglichen diese Teilchen eine sehr hohe Zytotoxizität, wodurch verglichen mit ^{177}Lu ein erhöhter therapeutischer Effekt erwartet werden darf.

^{161}Tb wurde über die Kernreaktion ^{160}Gd(n,γ)^{161}Gd$\xrightarrow{\beta^-}$^{161}Tb durch Bestrahlung von massiven ^{160}Gd-Proben mit thermischen Neutronen hergestellt. Ein halbautomatisierter Prozess auf der Grundlage der Kationenaustauschchromatografie wurde entwickelt, und für die Isolierung von trägerfreiem (no carrier added, *n.c.a.*) ^{161}Tb von den ^{160}Gd-Proben, sowie seinem stabilen Zerfallsprodukt ^{161}Dy, angewendet. ^{161}Tb wurde für die Markierung des Peptids DOTA-Tyr^3-octreotat und des monoklonalen Antikörpers chCE7 verwendet. Zusätzlich wurden Experimente mit menschlichen Ovarialkarzinomzellen, SKOV3ip, durchgeführt, und die Ergebnisse mit kommerziell erhältlichem trägerfreiem ^{177}Lu verglichen.

Die erhaltenen Ergebnisse zeigen, dass bis zu 16 GBq trägerfreies ^{161}Tb durch Langzeitbestrahlung von Gd-Proben hergestellt werden konnte. Mittels Kationenaustauschchromatografie war es möglich, 80 - 90% des zur Verfügung stehenden ^{161}Tb mit höchster spezifischer Aktivität sowie radionuklidischer- und chemischer Reinheit in für therapeutische Anwendungen ausreichenden Mengen zu produzieren. Dieses ^{161}Tb konnte erfolgreich für die Herstellung von ^{161}Tb- DOTA-Tyr^3-octreotat und ^{161}Tb-chCE7 eingesetzt werden. Vergleichende Studien mit SKOV3ip-Zellen lieferten für ^{161}Tb-chCE7 ähnliche Ergebnisse wie für ^{177}Lu-chCE7.

Acknowledgements

The research described in this thesis was performed partly at the Lehrstuhl für Radiochemie at the Technische Universität München and partly at the Center of Radiopharmaceutical Science at the Paul Scherrer Institute, Switzerland.

First of all special thanks go to my „Doktorvater“ Prof. Dr. Andreas Türler, for giving me the opportunity to work on such an interesting topic and for giving me the chance to participate at a cooperation with the Paul Scherrer Institute, and my supervisor Dr. Konstantin Zhernosekov. I thank both for supporting me in every possible way, for their confidence and for spending their time for reading and correction of this thesis.

Also I would like to thank the group of Prof. Dr. Roger Schibli at the Paul Scherrer Institute, where I was able to perform the antibody experiments, especially Susan Cohrs, Eliane Fischer, Dr. Jürgen Grünberg, Anja Saage, Prof. Dr. Roger Schibli and Kurt Zimmermann. Thank you for having so much patience with me and helping me with the chCE7 study. I know you had a lot of work to do preparing all the stuff and introducing me into the radiopharmaceutical field.

Many thanks to ITM/ITG, especially Sabrina Büdel, Dr. Mark Harfensteller, Dr. Richard Henkelmann, Paula Juntunen, Oliver Leib, Sebastian Marx, Dr. Josue Moreno and Leena and Dr. Tuomo Nikula for helping me with the irradiations, Tb/Lu shipments, several experiments, and for the countless GBq of free ^{177}Lu.

Further I would like to thank all the people at the research reactors for irradiating my samples, Dr. Heiko Gerstenberg, Dr. Xiaosong Li, Volker Loder and Alfred Richter from FRM II (Munich), Gregor Bukalis from BER II (Berlin), Dr. Ulli Köster from HFR (Grenoble, France) and the irradiation group from SCK-CEN (Mol, Belgium).

A big thank you goes to all the people from the Lehrstuhl für Radiochemie at the Technische Universtität München. All of you did a great job and made it possible for me to do all my work. Especially Guy Birebent and Dr. Xiasong Li for helping me with the γ-spectrometers, Rolf Bühnemann, Herbert Größlhuber and Gerhard Mattheis for the technical support, Siegfried Firley for preparing my columns and sealing my ampoules, Dr. Hansjörg Zott for doing all the IT-stuff, Dr. Denis Jurkin for his advices and reading my thesis, Dr. Dirk Dautzenberg for the ICP-OES measurements, Irene Höpfl, Manuela Hoffmann and Susanne Runde for the nice „brainstorming“ coffee breaks, Christoph Barkhausen, Dr. Reimar Graeger and Annett Klaschwitz for being such good friends and my boss Dr. Christoph Lierse von Gostomski for giving me all the time I needed to finish my thesis.

Special thanks go to Dr. Thorsten August for his patience and uncompromising help, and my parents who always supported me over the years so much. Without them standing by my side, this work could hardly be finished. Thank you very much!!!

Table of Content

1 Introduction

Radiopharmaceuticals are molecules labeled with a radionuclide to deliver therapeutic doses of ionizing radiation to specific disease sites. Most of the therapeutic radiopharmaceuticals are small organic or inorganic compounds with definite composition (Volkert, et al., 1999; Heeg, et al., 1999). Also, they can be macromolecules like monoclonal antibodies or antibody fragments labeled with a radionuclide. The radiopharmaceutical should be able to localize the tumor sites in adequate concentration to deliver a cytotoxic radiation dose to the tumor cells and additionally offer a rapid blood clearance to minimize radiation damage to normal tissues.

The beginning of radiotherapy was in the 1960's starting with radioiodine for treatment of thyroid cancers. Later ^{111}In-DTPA-octreotide was used for diagnosis of somatostatin receptor positive tumors (Liu, et al., 2001).

Today radiopharmaceuticals are used in nuclear medicine as tracers in diagnosis and treatment of many diseases (Nijsen, et al., 2007). In this context, the interest in radiometals (non-Tc, non-Re) has increased over the last years because of their successful clinical application in nuclear oncology. Over the chart of the nuclides there is a multitude of relevant radioactive isotopes. But not only their use in nuclear medicine, also the production of radiometals is an important field of nuclear research.

1.1 Metalloradiopharmaceuticals

Endoradiotherapy (targeted radionuclide therapy) of malign diseases, especially the radioimmuno- and peptidreceptor radionuclide therapy, is used with promising results. Thereby radioactivity is transported directly into the tumor via specific labeled antibodies. Due to the cross-fire-effect it is possible to destroy tumor cells that cannot be directly addressed by antibodies. This may happen, for example, if single tumor cells are antibody-negative or if the antibody is not able to reach the epitope because of a poor vascularization of the tumor (Wilder, et al., 1996; Postema, et al., 2001; Witzig, et

al., 2002; Wisemann, et al., 1999). A broader application of these methods in clinical routine can be expected in the coming years (Schmaljohann, et al., 2005; Kwekkeboom, et al., 2005; Buchmann, et al., 2005).

For endoradiotherapeutic treatment, radiolabeled molecules are used that selectively transmit a high therapeutic dose to the target tissue. Antibodies and antibody fragments as well as peptides are used as tracer molecules. The radionuclides are particle emitters that are able to deposit a high amount of energy in small volumes *via* a high "linear energy transfer" (LET) of the projectile. Especially β^-, α, and also Auger electron emitters are used or considered as useful for therapeutic applications (Kwekkeboom, et al., 2005; Zalutsky, 2003; Buchegger, et al., 2006; Rösch, et al., 2004; Kwekkeboom, et al., 2003; Stahl, et al., 2006).

Because of the development of effective radiochemical labeling procedures an increasing number of radioisotopes of heavy metals are adjuvant for therapy (Rösch, 2007; Liu, et al., 2001). β emitting radiolanthanides including ^{90}Y are of special interest (Mäcke, et al., 2003; Rösch, 2007; Rösch, et al., 2004). These elements are very similar in their chemical properties and can be used for labeling with the same method. Therefore, the influence of different nuclear properties (e.g. mode of decay, decay energy, half-life) can be compared and thereby the therapeutic effect can be optimized.

Currently the radionuclides ^{90}Y and ^{177}Lu are commercially available for medical applications. ^{90}Y is a high energy β^- emitter suitable for treatment of large tumors. It provides no γ component for visualization by means of a γ-camera. In contrast, ^{177}Lu is a low energy β^- emitter with a measureable γ component (11% of decays) with an energy of 208 keV (Table 1-3). Because of the lower mean energy of the β^- particles and therefore shorter range it is preferred for therapy of small tumors. Certainly, in spite of promising clinical studies a further optimization of the treatment is necessary (Kwekkeboom, et al., 2005). Here, primarily evaluation of alternative radionuclides that can intensify the therapeutic effect of radiopharmaceuticals is required.

A typical metalloradiopharmaceutical consists of the following components: the radionuclide, which provides the therapeutic effect and is useful for visualization, a bifunctional chelator (BFC), a linker/spacer and a targeting biomolecule e.g. a peptide

or an antibody (ab) (vector molecule), which delivers the attached radionuclide to the target cells (Liu, et al., 2001; Rösch, 2003) (Figure 1-1). The linker/spacer is often used as a pharmacokinetic modifier (PKM) depending on the requirements for the radiopharmaceutical.

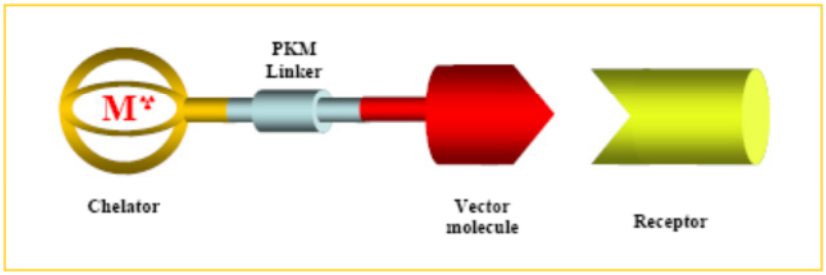

Figure 1-1: Construction of a receptor mediated metalloradiopharmaceutical.
The radiometal is bound to the vector molecule via a bifunctional chelator.

Like mAbs, peptides consist of a number of amino acids, though they are much smaller (up to 50 amino acids). Due to this smaller size, peptides can be cleared faster from the blood pool and most normal tissues. Additionally, they are able to penetrate faster into tumors and thus are distributed more rapidly in the tumor. Because of the smaller immunogenicity of peptides compared to mAbs, a multiple dose administration is possible. Also the synthesis of peptides is much more convenient by using automated solid phase procedures (Zalutsky, 2003).

But there are also a few disadvantages. For instance, by using regular peptides for targeted radiotherapy their corresponding receptors in certain tumor cells are also existent in some normal tissue, like the receptors in the gastrointestinal tract (Warner, et al., 2002). Moreover, these regular peptides cause physiological effects at small concentrations, thus a high specific activity of radiolabeled peptides must be reached. Furthermore, these peptides degrade rapidly *in vivo*, therefore it is essential to use analogues with a higher grade of stability (Reubi, 1997). Hence, an insertion of D-amino acids at critical points or a cyclization of a part of the molecule is accomplished (Lamberts, et al., 1987).

Table 1-1: Peptides and corresponding receptors that are over expressed on human tumors (Zalutsky, 2003).

peptide/receptor	amino acids	tumor overexpressing receptor
Somatostatin	14, 28	neuroendocrine, small cell lung cancer medullary thyroid carcinoma, astrocytoma
vasoactive intestinal peptide	28	small cell lung cancer, colon carcinoma, pancreatic cancer, stomach cancer
α-melanocyte stimulating hormone	13	melanoma
Bombesin, gastric releasing peptide	14, 27	small cell lung cancer, colon carcinoma, glioblastoma
Substance P	11	glioblastoma, astrocytoma, medullary thyroid carcinoma, breast tumors, small cell lung cancer
Neurotensin	13	pancreatic cancer, colon carcinoma, small cell lung cancer, prostate cancer
Cholecystokinin B	17, 12	medullary thyroid carcinoma, small cell lung cancer, ovarian cancer astrocytoma
epidermal growth factor	53	glioblastoma, squamous cell carcinoma, breast carcinoma

Table 1-1, some of the regulatory peptides and corresponding receptors evaluated for targeted radiotherapy are listed. So far, the most widely investigated peptide is somatostatin and its analogues (Kwekkeboom, et al., 2001; Heppeler, et al., 2000). Somatostatin is a neuropeptide produced by neuroendocrine, inflammatory and immune cells in response to different stimuli and inhibits different cellular functions including secretions, motility and proliferation. Its effectiveness is caused by five specific somatostatin receptors (sstr1-sstr5) which belong to the G protein-coupled receptor family. These receptors are able to bind the peptide with high affinity but only sstr2, sstr3 and sstr5 bind the short synthetic analogues used to treat patients with neuroendocrine tumors (Benali, et al., 2000).

There are several ways a radiopharmaceutical behaves *in vivo*. Besides the desired receptor binding, also excretion, metabolisation, decomposition, metal-exchange, dissociation, chelat exchange or the binding to a different protein. In the worst cases dissociation and metal exchange the radiometal exists as a free radionuclide.

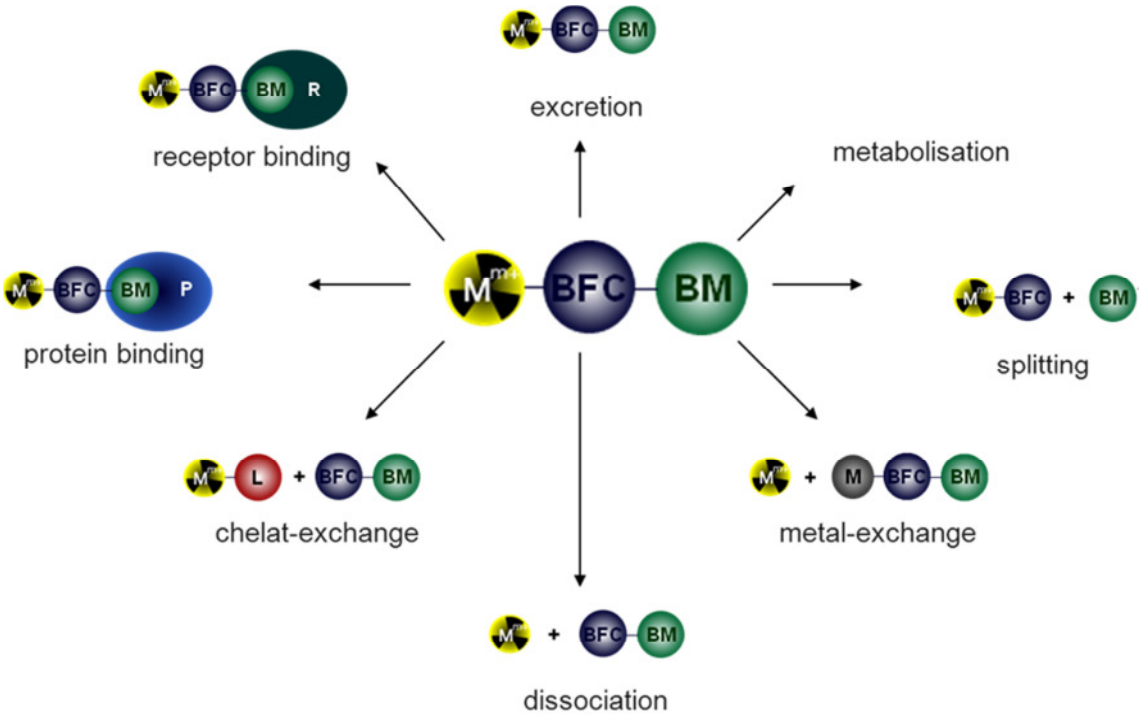

Figure 1-2: Possible behavior of targeted specific radiopharmaceuticals *in vivo*.

1.1.1 Bifunctional chelators (BFC) and their conjugation

The bifunctional chelator is supposed to complex the radiometal while it is covalently attached to the biomolecule. It has to form strong complexes with high thermodynamic and kinetic inertness at $5 < pH < 7.5$. This is an important property because the release of the radionuclide would cause a number of side effects by accumulation in non-target organs. Free radionuclides show a high toxicity, for example metals like ^{177}Lu(III) and ^{90}Y(III) are known as "bone seekers" and cause bone marrow damages (Volkert, et al., 1999; Mäcke, 2002; Liu, et al., 2001; Heppeler, et al., 2000). Besides, the conjugation of the BFC with the biomolecule is supposed to create as few isomers as possible since those are reflected in the properties of the entire radiopharmaceutical construct.

In a chelate complex, bonds or other attractive interactions between at least two separate binding sites within the same organic ligand and a single central atom (metal) are present. The larger the number of ring closures to a metal atom, the more stable the compound. This phenomenon is called the chelate effect and causes an increase in the stability of the complexes. Monodentate ligands, which have one coordinating atom like H_2O or NH_3 are easily broken by other chemical processes, whereas polydentate chelators, donating multiple bounds to a metal ion, provide more stable complexes.

The kinetic inertness is characterized by the rate of dissociation of the radiometal from the BFC. Complexes with acyclic chelators or chelators with suboptimal denticity (e.g. EDTA, DTPA, Figure 1-3) provide a low *in vivo* stability. Complexes based on macrocyclic framework (e. g. DOTA, Figure 1-3) often show much higher kinetic inertness (Jurkin, 2009). These chelating agents are capable of a strong interaction with the metallic ion as all four aza- and carboxyl-binding sites can participate.

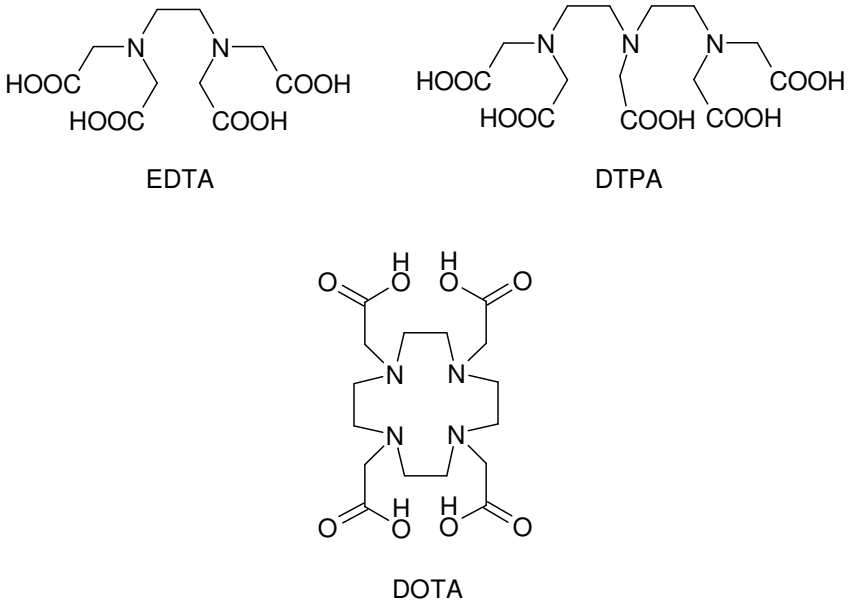

Figure 1-3: Selected chelators with carboxylate functionalization.

Macrocyclic BFC's often require extreme labeling conditions like high temperature to achieve an appropriate labeling yield. However, for the labeling of antibodies high temperatures may cause problems because of the unfolding of the protein and loss of binding affinity to the desired target receptor. The BFC also has to be stable against ionizing radiation.

The linker is chosen depending on the pharmacokinetic requirements of the pharmaceutical. It may influence the hydrophilicity and therefore improve the pharmacokinetics. The linker also interacts as a separator between the BFC and the vector molecule to prevent steric influence of the chelator on the binding affinity of the receptor targeting part of the radiopharmaceutical (Volkert, et al., 1999; Mäcke, 2002; Heppeler, et al., 2000).

Monoclonal antibodies used for endoradiotherapy are obtained from mice via the hybridoma technique. However, these murine antibodies are often considered as foreign intruders and destroyed by the human immune system. Therefore, these biomolecules have to be "humanized". In this regard, the constant parts of the murine antibody are substituted by groups from human antibodies. The variable section, which induces the recognition of the antigen, is not modified. The resulting chimeric antibody consists of

65% to 90% human material and is not recognized by the human immune system as foreign. Accordingly, the efficiency of the endoradiotherapy is drastically enhanced (Levene, et al., 2005).

A typical feature of many different types of cancer is the overexpression of the epidermal growth factor receptor (EGFR). EGFR is a transmembrane proteine promoting cell proliferation consisting of the specific binding of the epidermal growth factor and the transforming growth factor α (TGFα). It is assumed that the activity of this factor contributes to the progression of cancers (Gullick, 1991; Ramos-Suzarte, et al., 1999). Therefore, many antibodies for cancer treatment are anti-EGFR-antibodies.

1.1.2 Methods for the conjugation of mAbs to BFCs

An overview of different methods for conjugating mAbs to BFCs is given by Liu and Edwards (Liu, et al., 2001). For these reactions, the parameters of the BFC are important, for example the binding linker and its functional group, which is necessary for the connection to the biomolecule.

There are several groups possible to conjugate the linker to the antibody, e.g. activated disulfides, acidic chlorides, acidic anhydrides, bromoacetamides, iodoacetamides, N-hydroxysuccinimide esters, aldehydes, ketones or maleimides. These groups are all electrophilic, so the biomolecule has to provide a nucleophilic group. In case of antibodies this is a primary amine.

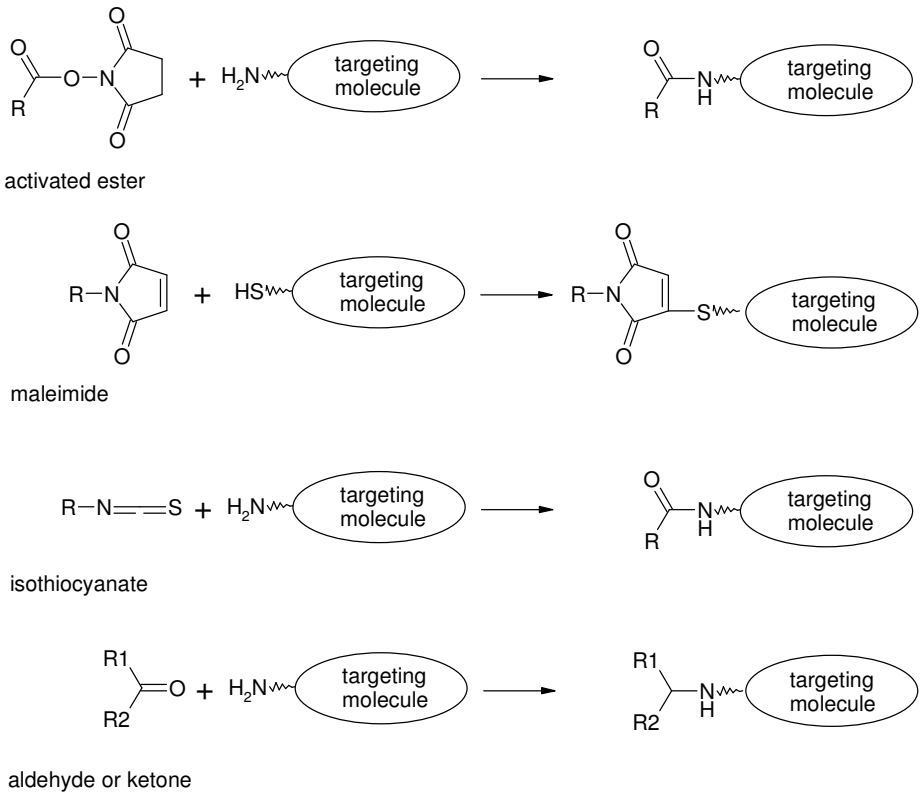

Figure 1-4: Methods of conjugation.

1.2 Production of therapeutic radionuclides at nuclear reactors

Most of the therapeutical radionuclides decay by emitting β^- particles. Therefore, they are neutron-rich and thus predominantly produced at nuclear reactors. Radionuclides are used for the production of pharmaceuticals for diagnosis and therapy, for example ^{99m}Tc ($T_{1/2}$ = 6.0 h), ^{131}I ($T_{1/2}$ = 8.0 d), ^{133}Xe ($T_{1/2}$ = 5.2 d) and the lanthanides ^{166}Ho (26.82 h) and ^{177}Lu ($T_{1/2}$ = 6.7 d). 70% of all nuclides used in nuclear medicine are produced in research reactors, because their thermal neutron flux allows a controlled production of these specific nuclides.

Table 1-2: Therapeutically relevant radionuclides (Firestone, et al., 1996).

isotope	**half-life**	**mode of decay**	$\overline{E}_{\beta-/\alpha}$ **[MeV] (%)**	$\overline{E}_{\gamma}$ **[keV] (%)**
^{90}Y	2.67 d	β^-	0.93 (100)	no γ
^{188}Re	16.98 h	β^-	0.766 (100)	155 (15)
^{67}Cu	2.58 d	β^-	0.19 (20), 0.12 (57)	93 (16), 185 (49)
^{213}Bi	46.0 min	α	0.49 (65), 0.32 (32)	440 (27)
^{225}Ac	10.0 d	α	5.83 (51)	100 (3.5)
lanthanides	**half-life**	**mode of decay**	$\overline{E}_{\beta-/\alpha}$ **[MeV] (%)**	$\overline{E}_{\gamma}$ **[keV] (%)**
^{177}Lu	6.71 d	β^-	0.15 (79)	208 (10.36)
^{161}Tb	6.9 d	β^-	0.155 (100)	75 (9.8)
^{166}Ho	26.8 d	β^-	0.69 (51), 0.65 (48)	80.6 (6.2)
^{153}Sm	1.95 d	β^-	0.23 (43), 0.2 (35)	103 (28)
^{149}Pm	53.1 h	β^-	0.37 (97)	286 (2.9)
^{175}Yb	4.2 d	β^-	0.48 (100)	396 (13.2), 283 (3.1)

A widely used radiolanthanide is ^{177}Lu, which can be produced in nuclear reactors via the direct

$$^{176}\text{Lu}(n,\gamma)^{177}\text{Lu} \qquad 1$$

or the indirect (n,γ) production route

$$^{176}\text{Yb}(n,\gamma)^{177}\text{Yb} \xrightarrow{\beta^-} {}^{177}\text{Lu}. \qquad 2$$

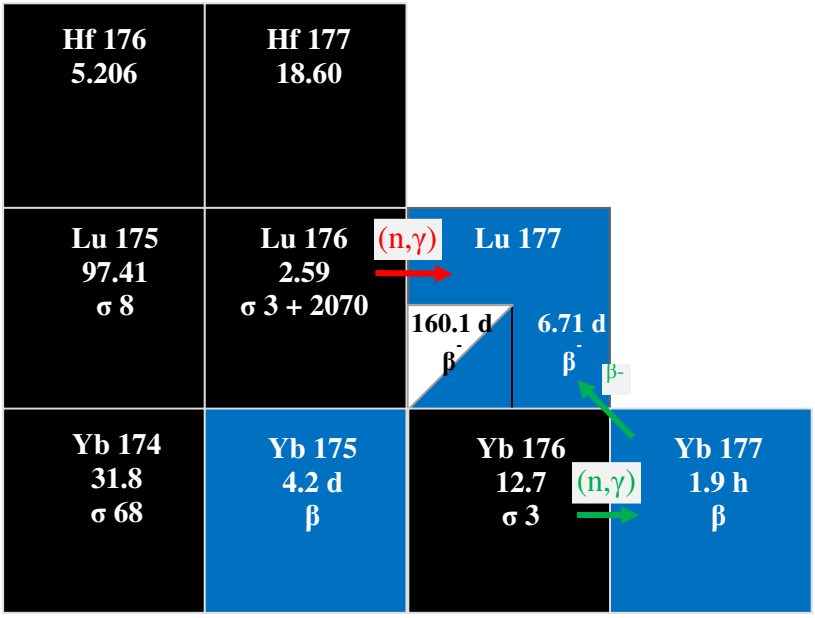

Figure 1-5: Cut out of the chart of the nuclides: direct (red arrows) and indirect (green arrow) production route of ^{177}Lu (Magill, et al., 2006).

Because of the rather large cross section of ^{176}Lu, ^{177}Lu can be produced directly with high specific activity at nuclear reactors with a high neutron flux (10^{13} - 10^{15} cm^{2}s^{-1}) via the (n,γ) production route. However, during irradiation of the ^{176}Lu target, the long-lived isomer ^{177m}Lu ($T_{1/2}$ = 160.1 d) is also produced via the ^{176}Lu(n,γ)^{177m}Lu reaction (Figure 1-5). ^{177m}Lu lowers the radionuclidic purity of ^{177}Lu. Due to the presence of stable ^{176}Lu the specific activity of ^{177}Lu in this case only reaches a value of about 0.9 - 1.2 TBq/mg (25 - 33 Ci/mg) compared to the maximal theoretical value of 4.1 TBq/mg (110 Ci/mg). In addition, formation of a long-lived radionuclide leads to complications with radioactive waste disposal in hospitals (Bakker, et al., 2006).

Alternatively, ^{177}Lu can be produced *n.c.a* via the indirect production route ^{176}Yb(n,γ)^{177}Yb $\xrightarrow{\beta^-}$ ^{177}Lu with the absence of long-lived by products. The expression *n.c.a.* (no carrier added) defines a preparation of a given radionuclide, where special attention has been paid to procedures, equipment and materials in order to minimize the introduction of stable and radioactive isotopes of the element in question in the same chemical form or as a species enabling isotopic exchange reactions (de Goeij, et al., 2005) (Figure 1-5). The natural abundance of ^{176}Yb is only 12.7%. Therefore, highly enriched target material is required. An enrichment of natural ytterbium up to 97% of ^{176}Yb is already commercially available.

In case of the indirect production route, the desired nuclide is an isotone of the target nuclei and can be isolated chemically. If the desired and the target nuclide are adjacent lanthanides, the separation is challenging because of their high chemical similarity. The chemical separation becomes even more complicated by the use of massive targets.

1.2.1 Irradiation yield of the (n,γ) reaction followed by β$^-$ decay

The irradiation yield of radionuclides Z that are produced by β$^-$ decay following a (n,γ) reaction is expressed by

$$\frac{dN_Z}{dt} = N_X\left(1 - e^{-\lambda_Y t}\right)\phi\sigma_X - N_Z\lambda_Z \qquad 3$$

Under the assumption that no target burn-up occurs the number of target atoms can be considered as constant due to the relatively small capture cross section. At the start of irradiation (t=0), $N_Y = N_Z = 0$, equation 4 is obtained by integration of equation 3 (Lieser, 1980):

$$N_Z = N_X \phi \sigma_X \left[\left(\frac{1 - e^{-\lambda_Z t}}{\lambda_Z} + \frac{e^{-\lambda_Y t} - e^{-\lambda_Z t}}{\lambda_Y - \lambda_Z} \right) e^{-\lambda_Z t_d} + \frac{\left(1 - e^{-\lambda_Y t}\right)\left(e^{-\lambda_Y t_d} - e^{-\lambda_Z t_d}\right)}{\lambda_Z - \lambda_Y} \right] \quad (4)$$

N_X: number of target atoms X

N_Z: number of radioactive atoms Z formed

Φ: neutron flux ($cm^2 s^{-1}$)

σ_X: neutron capture cross section of X (cm^2)

λ_Y: decay constant of Y (s^{-1})

λ_Z: decay constant of Z (s^{-1})

t: irradiation time (s)

t_d decay time after the end of irradiation

For example, the irradiation yield of ^{177}Lu can be expressed by equation 5:

$$N_{Lu-177} = N_{Yb-176} \phi \sigma_{Yb-176} \left[\left(\frac{1 - e^{-\lambda_{Lu-177} t}}{\lambda_{Lu-177}} + \frac{e^{-\lambda_{Yb-177} t} - e^{-\lambda_{Lu-177} t}}{\lambda_{Yb-177} - \lambda_{Lu-177}} \right) e^{-\lambda_{Lu-177} t_d} + \frac{\left(1 - e^{-\lambda_{Yb-177} t}\right)\left(e^{-\lambda_{Yb-177} t_d} - e^{-\lambda_{Lu-177} t_d}\right)}{\lambda_{Lu-177} - \lambda_{Yb-177}} \right] \quad (5)$$

1.2.2 Separation of lanthanides

The most intensively studied system for isolation a microconstituent from a macroconstituent of two adjacent trivalent lanthanides is the system Yb/^{177}Lu (Lebedev, et al., 2000; Horwitz, et al., 2005; Hashimoto, et al., 2003). With the cementation process it was possible to obtain *n.c.a.* ^{177}Lu in radiochemically pure form with about 75% overall separation yield (Lebedev, et al., 2000). As an alternative, the following

chromatographic systems have been used: extraction chromatography (Horwitz, et al., 2005) or reversed-phase ion-pair chromatography (Hashimoto, et al., 2003). A detailed process for separating adjacent lanthanides was described recently for the systems Pr/^{140}Nd and Ce/^{140}Nd (Zhernosekov, et al., 2007). It was possible to isolate *n.c.a.* ^{140}Nd from a massive Pr- respectively Ce-target using ion-exchange chromatography. This method showed a strong dependence on the mass of the used macroconstituent and has to be developed and optimized for every single pair of lanthanides.

Separation of lanthanides by extraction or solvent chromatography is another possibility due to different extractabilities with organophosphorus extractants. The extractants used for lanthanide separations are for example HDEHP (di(2-ethylhexyl) orthophosphoric acid) and HEH[EHP] (2-(ethylhexyl) phosphonic acid mono-2-ethylhexyl ester). Separation of lanthanides by means of extraction chromatography was intensively studied by Horwitz (Horwitz, et al., 1975; Horwitz, et al., 1976). ^{177}Lu with high specific activity (at least 3.7 TBq/mg; 100 Ci/mg), separated from a 10 mg Yb-target by elution with increasing concentrations of HCl with the Eichrom LN resin (HDEHP) was produced by the group of Knapp (Knapp, et al., 2005).

Among the lanthanides the system Tb/Gd has the greatest separation factor α (ratio of α-HIB complex stability constants). For example the factors for Lu/Yb are 1.92 (HDEHP) and 1.99 (HEH[EHP]), but 5.66 (HDEHP) and 6.96 ((HEH[EHP]) for Tb/Gd (Sivaraman, et al., 2002; Horwitz, et al., 2005; Breeman, et al., 2003; Horwitz, et al., 1972)

However, the use of extraction chromatography for lanthanide separations is time consuming and produces large volumes of radioactive waste. In addition, the target nuclide is eluted after the target material, which is present in large amounts, and, therefore this is not a convenient method. There are also reports that it was not possible to reach the chemical purity requirements for radiopharmaceuticals (Mikolajczak, et al., 2005).

For separation or purification of radionuclides in nuclear medicine, ion exchangers are widely used. It is possible to separate micro amounts of *n.c.a.* radionuclides from macro amounts of the target material after irradiation at nuclear reactors or cyclotrons. For

example, ^{166}Ho could be separated from Dy using the sulfonic type cation exchanger resin AMINEX A6 and α-HIB as mobile phase (Lahiri, et al., 2004). Cyclotron produced ^{114m}In was separated from its Cd-target material via the strong anion exchange resin AG 1 (Tolmachev, et al., 2000).

In nuclear medicine, ion exchangers are also used as column material for radionuclide generators. Usually, a radionuclide generator is a column filled with an inorganic ion exchanger and loaded with a longer-lived parent nuclide from which the shorter-lived daughter nuclide can be obtained by periodical elution in *n.c.a.* form. Mostly inorganic ion exchangers like hydrated aluminum, iron oxides, titanium, zirconium and antimony oxides are used due to their stability against radiation damage. Other properties like exchange capacity or kinetics are less important (Rösch, 2003). The most widely used generator is the ^{99}Mo/^{99m}Tc (^{99}Mo: $t_{1/2}$ = 66.0 h, ^{99m}Tc: $t_{1/2}$ = 6.0 h (Magill, et al., 2006)) generator system, where Mo is adsorbed on aluminum oxide and sodium pertechnetate is eluted with saline solution.

Separation of actinides and lanthanides was already successfully performed by cation resin columns using ammonium lactate solutions as eluting agent (Dunlavey, et al., 1953; Mayer, et al., 1953; Wish, et al., 1954; Thompson, et al., 1954; Glass, 1955). Although much better results have been achieved with the eluent α-hydroxy-isobutyrate (Ghiorso, et al., 1955). While using a cation exchanger for separating Tb and Gd, Tb is eluted first and can therefore be collected much easier producing less radioactive waste compared to the extraction chromatography. Because of the peak tailing, the Tb fraction would contain too much gadolinium if the elution order would be reversed like e. g. in extraction chromatography. On the other hand, a large volume of eluent is needed for the cation exchange method which can lead to higher chemical impurities in the Tb-fraction.

It appears that strong cation exchange resins like AMINEX A6 from BioRad laboratories are the most efficient ones (Lahiri, et al., 2004; Schädel, et al., 1977). For instance the separation of *n.c.a.* ^{166}Ho from irradiated Dy_2O_3 target was performed with HPLC using BioRad AG 50W-X8 (200 - 400 μ) (Figure 1-6) or AMINEX A6 (17.5 ± 2.0 μm) (Figure 1-7) cation exchanger and 0.1 M α-HIB (pH 4.2) as eluent (Lahiri, et al., 2004). ^{166}Ho is produced via double neutron capture from ^{164}Dy. The separation

from the Dy target (1.0 mg) can be done quantitatively by using the AMINEX resin. In contrast, no separation occurred by the use of the DOWEX 50 resin. Unfortunately, the AMINEX resin is no longer commercially available. In addition, one has to try to scale up the separation to ≥ 50 mg target material to produce an adequate amount of ^{166}Ho for use in nuclear medicine.

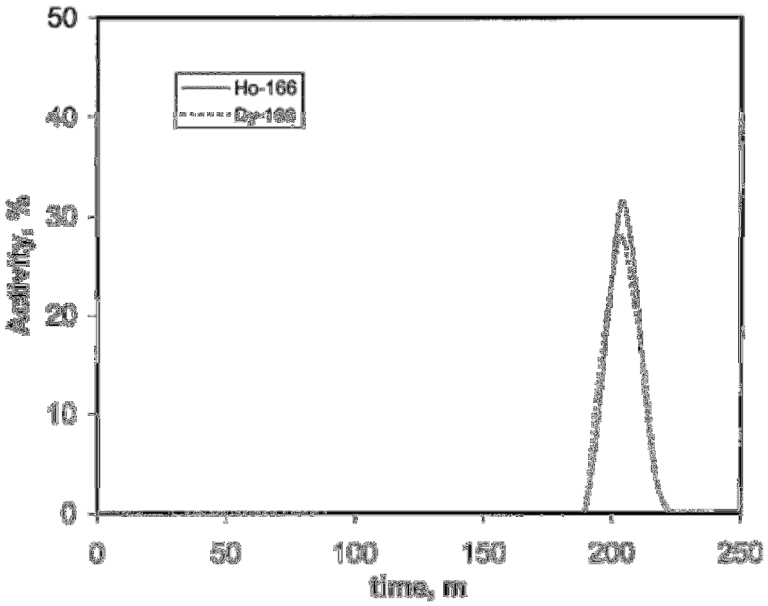

Figure 1-6: Separation of *n.c.a.* ^{166}Ho from irradiated Dy-targets (1mg) using DOWEX 50 cation resin (Lahiri, et al., 2004).
Solid line: Ho; dotted line: Dy.
No separation of Ho and Dy occurs.

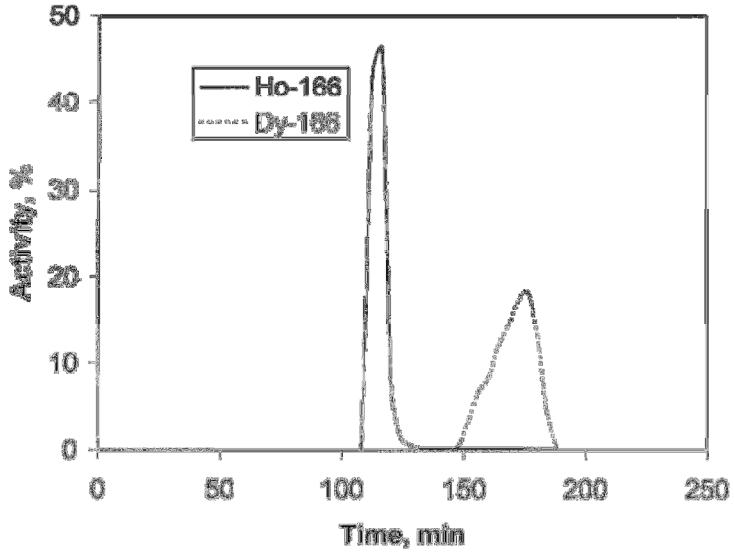

Figure 1-7: Separation of *n.c.a.* ^{166}Ho from irradiated Dy-targets (1mg) using AMINEX A7 cation resin (Lahiri, et al., 2004).
Solid line: Ho; dotted line: Dy.
Ho can be separated from the Dy target material.

In nuclear medicine and radiochemistry, ion exchangers are exposed to ionizing radiation. As a result of radiolysis, deteriorative effects can be observed on the ion exchange material. In addition, the ion exchanger is affected by radiolysis reactions of the solvents and solutes present in the system on the ion exchange matrix. One of the results is the decrease of ion exchange capacity and increased swelling, which changes the volume. Being exposed to radiation, the ion exchanger becomes more susceptible to physical and chemical damages. Cation exchangers are more stable with regard to deterioration than anion exchangers. For example, radiation damage in cation exchange resins of the sulfonic acid type (e.g. Dowex 50) is mainly caused by the breakage of cross-linkages. The loss of capacity by cation exchangers is observed at total adsorbed doses of $\geq 10^6$ Gy (Pillay, 1986; Dorfner, 1991).

Inorganic ion exchangers are more stable in the presence of ionizing radiation. There are only a few reports showing the radiation stability limits of inorganic ion exchangers because it is difficult to conduct an experiment with high dose rates of more than 10^8 Gy. However, Zeolites show a decrease in exchange capacity after receiving integral doses of $5 \cdot 10^7$ - 10^8 Gy (Marhol, 1982; Pillay, 1986).

Inorganic exchangers exhibit much higher thermal stability than organic resins. Strong acidic cation exchangers in H^+ form, for example, should not be used above 80 °C, while inorganic material can be heated up to several hundred degrees.

Strongly acidic cation exchangers are stable in the whole pH range, but the stability decreases in oxidizing agents like nitric acid ($c > 2.0$ M). Inorganic exchangers often are not stable in strongly acidic or basic solutions, yet they are resistant to oxidation and organic solvents.

Also, the specific column load is of great importance. By increasing the amount of stable lanthanides, a gradual increase in the peak width occurs. This leads to a deterioration of the separation. This effect becomes especially significant when the amount of the stable elements exceeds 5 - 10 mg related to 1 cm^2 of the column cross section. 30 – 40 mg of the element related to 1 cm^2 of the column cross section is recommended, provided that the ratio of the exchanger column height to its diameter is ≥ 50, to achieve a satisfactory separation of two neighboring lanthanides (Marhol, 1982).

1.3 Current applications and trends in clinical nuclear oncology

There is already a great experience in clinical endoradiotherapy with ^{90}Y and ^{177}Lu. For example, a large number of studies is known for treatment of neuroendocrine tumors. The somatostatin receptor is over-expressed on this kind of tumors. Therefore, they can be treated successfully with ^{90}Y and ^{177}Lu labeled somatostatin analogs (DOTATOC, DOTATATE) (Kwekkeboom, et al., 2005; Waldherr, et al., 2002; Kwekkeboom, et al., 2003; Stahl, et al., 2006; Essen, et al., 2007). Furthermore, a relatively high tumor response rate up to 30 – 35% can be achieved with ^{177}Lu-labeled somatostatin analogs such as ^{177}Lu-DOTATOC or ^{177}Lu-DOTATATE (Kwekkeboom, et al., 2005). ^{177}Lu is also considered for preparation of alternative therapeutic agents, particularly ^{177}Lu-labeled antibodies. In spite of the promising clinical studies, a further optimization of the treatment is necessary (Kwekkeboom, et al., 2005; Kwekkeboom, et al., 2003; Stahl, et al., 2006). Here, primarily the evaluation of alternative radionuclides is required that can intensify the therapeutic effect of the radiopharmaceuticals.

Because of the relatively short range in tissue and consequently high local damage, low energy electrons (e.g. Auger and conversion electrons) can provide a very high cytotoxicity (Buchegger, et al., 2006; Michel, et al., 2003; Behr, et al., 2000). Currently there are no therapeutically relevant metallic conversion or Auger electron emitters commercially available and the only experience is based on the practice with the diagnostic radionuclides ^{111}In ($t_{1/2}$=2.8 d) and ^{67}Ga ($t_{1/2}$=3.26 d). After internal conversion ^{111}In and ^{67}Ga emit a large quantity of conversion and Auger electrons, but have also a large γ component (Table 1-3). The dosimetric evaluation of these radionuclides shows that ^{111}In and ^{67}Ga are not appropriate to endoradiotherapy because of their high unspecific dose rate (Bernhardt, et al., 2001). Therapeutic application of pure Auger electron emitters (e.g. ^{67}Ga, ^{111}In) is limited by the targeting strategy required to reach close proximity to radiosensitive targets. In further clinical studies for treatment of neuroendocrine tumors with conversion and Auger electron emitters, therapeutic doses of ^{111}In labeled somatostatin analog DTPA-octreotide (Octreoscan®) led to numerous side effects (Valkema, et al., 2002; Anthony, et al., 2002). Thus, the application could not be considered positive (Kwekkeboom, et al., 2005).

Table 1-3: Modes of radioactive decay of selected radionuclides (Firestone, et al., 1996).

isotope	max/mean β energy [keV]	conversion and Auger electrons [keV] (%)	photons [keV] (%)
^{90}Y	2.3/0.94	-	-
^{177}Lu	0.5/0.14	48 (17)	56 (5), 113 (6.6), 208 (11)
^{161}Tb	0.55/ 0.15	1.5 - 8.0 (254), 17 - 26 (51), 40 - 49 (54)	26 - 55 (63), 75 (9)
^{111}In	EC	0 - 4 (293), 19 - 22 (16), 145 - 167 (10) 219 - 242 (6)	25 (95), 171.3 (90.3), 245.4 (94)
^{67}Ga	EC	0 - 1 (169), 7 - 10 (61), 84 - 92 (31)	9 (56), 93 (40), 184.6 (20.4) 208.9 (2.3), 300.2 (16.6), 393.5 (4.6)

Monoclonal antibodies (mAb) show a higher antitumor efficiency when they are labeled with low energy Auger electron emitters compared to β^- emitters (Meredith, et al., 1995; Welt, et al., 1996; Behr, et al., 2000). The high linear energy transfer of Auger electrons gives a high relative biological efficiency similar to that of α particles. But, in contrast, Auger electrons offer a lower toxicity if they are emitted outside the tumor cells. Because of the short range (Figure 1-8), Auger electrons can only reach the DNA if the antibody is internalized in the tumor tissue (Kassis, et al., 1987).

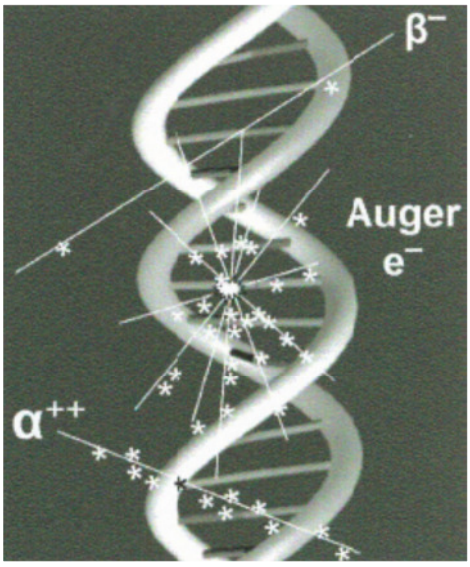

Figure 1-8: Range of α, β and Auger electrons compared to DNA strang.

2 Motivation

2.1 Evaluation of ^{161}Tb for endoradiotherapy

Table 2-2 lists the energies and frequencies of electrons and photons emitted after decay of ^{90}Y, ^{177}Lu and ^{161}Tb. For comparison, the decay characteristics of the Auger electron emitters ^{67}Ga and ^{111}In are also given. The therapeutic efficiency of these radionuclides was quantitatively evaluated by a group of the university of Göteburg (Bernhardt, et al., 2001; Uusijärvi, et al., 2006). They presented the dosimetric simulation of the ratio between the absorbed dose rate in tumor and normal tissue (TND) in relation to the emitted particle energy, photon-to-electron energy ratio and tumor size for several β^- emitters (Figure 2-1). A high dose rate in tumor tissue (high TND factor), for example, can only be achieved with ^{90}Y if the tumor size is several millimeters. In contrast, the adsorbed dose rate in smaller tumors tends towards zero because of the high range of the β particles. Low and medium energy β emitting lanthanides such as ^{177}Lu and ^{161}Tb can be used effectively for relatively small tumor cell clusters (about 0.2 mm).

^{111}In and ^{67}Ga are inefficient for therapeutic treatments although they emit a large quantity of conversion and Auger electrons (Table 1-3). An enormous amount of γ-rays leads to a very high, unspecific dose rate. Even at big tumor cell clusters only a TND-factor of about 10 with ^{67}Ga and 5 - 6 with ^{111}In can be reached (Figure 2-1). In contrast, ^{161}Tb and ^{177}Lu provide a TND of about 23.

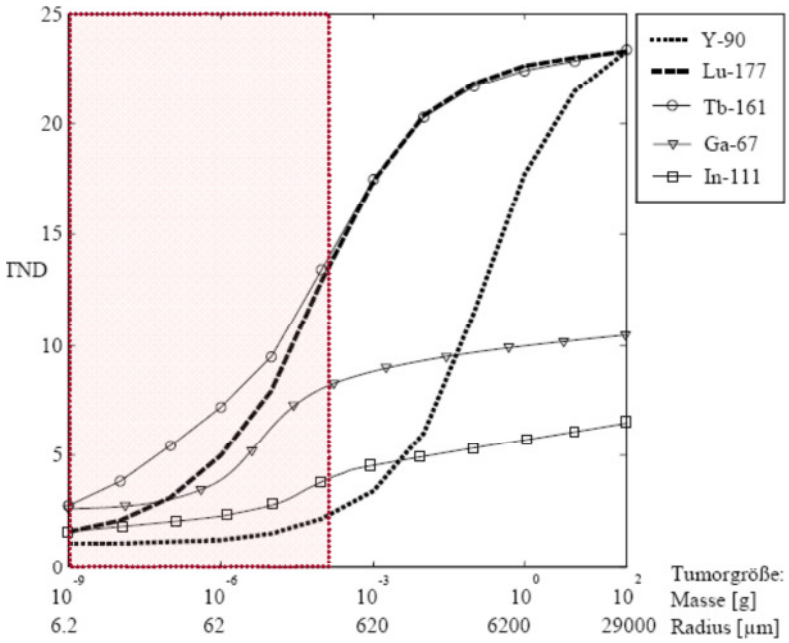

Figure 2-1: Tumor to normal tissue mean adsorbed dose rate (TND).
TND for some β emitting radionuclides versus tumor radius/mass.
The results are from dosimetric simulation in humans assuming uniform distribution within tumor and normal tissue with 25 times higher activity concentration in the tumor compared to normal tissue (Uusijärvi, et al., 2006).

With a half-life of 6.90 d and a relatively low mean energy of the emitted β^- particles the radiolanthanide ^{161}Tb is very similar to ^{177}Lu. Due to its chemical similarity to ^{177}Lu it can also be applied with already established radiolabeling chemistry. ^{161}Tb emits only a few photons with an energy of 75 keV (10% yield), which can be used for imaging purposes by means of a gamma camera. In contrast to ^{177}Lu, after β decay of ^{161}Tb, a significant quantity of conversion and Auger electrons is emitted (Figure 2-2 and Table 1-3). In addition to the energy provided by the beta particle, about 27% of the mean beta energy is released by secondary electrons emitted with energies between 3 and 50 keV (National Nuclear Data Center) (Figure 2-3). With this yield of conversion and Auger electrons, ^{161}Tb is comparable to radionuclides such as ^{67}Ga and ^{111}In.

Due to the relatively short range in the tissue and consequently high local damage, low energy electrons can provide a very high cytotoxicity (Buchegger, et al., 2006; Michel, et al., 2003; Behr, et al., 2000). Therapeutic application of pure Auger electron emitters (e.g. ^{67}Ga, ^{111}In) is limited by the targeting strategy required to reach close proximity to radiosensitive targets. Here, ^{161}Tb presents a unique situation provided by the decay of

both components, β^- and conversion/Auger electrons. Additionally emitted low energy electrons can enhance the crossfire effect of β particles, if the radiopharmaceutical is directly bound on the malignant cell surface or internalized into the cell. The dosimetric evaluation of the therapeutic efficiency of electron emitting radiolanthanides shows that ^{161}Tb provides better energy transfer in small volumes than ^{177}Lu because of the high component of conversion and Auger electrons (Uusijärvi, et al., 2006) (Figure 2-1). Therefore, it can be expected that ^{161}Tb-labeled compounds might have a better anti-tumor efficiency, especially regarding the treatment of small tumor cell clusters or even in the targeting of single cells. Furthermore, a higher cytotoxicity can be expected if the radionuclide internalizes and is transported to the cell nucleus because of the Auger effect (Pomplun, et al., 2004; Pomplun, 2000).

^{161}Tb emits one β^- and 2.23 Auger and conversion electrons per decay, ^{177}Lu only one β^- and 0.22 Auger and conversion electrons. Hence, it is assumed that ^{161}Tb might have a better antitumor efficiency regarding small tumor-cell clusters or single tumor cells.

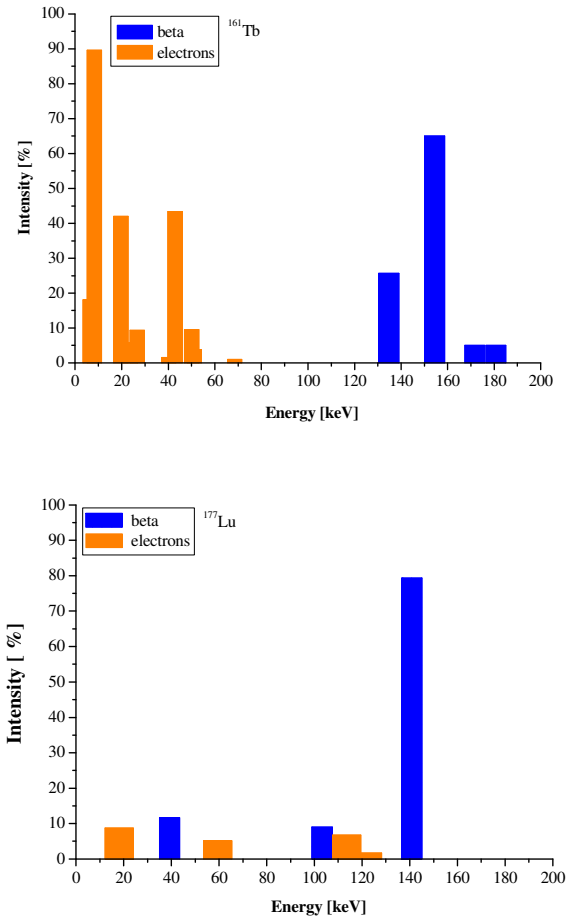

Figure 2-2: Profiles of ^{161}Tb- and ^{177}Lu decay.
^{161}Tb decay: Per decay 1 β and 2.23 Auger and conversions electrons occur.
^{177}Lu decay: Per decay 1 β and 0.22 Auger and conversions electrons occur (National Nuclear Data Center).

In addition, the released energy per decay (dose, [MeV/Bq·s]) is higher for ^{161}Tb than for ^{177}Lu (Table 2-1, Figure 2-3). Per decay the total dose for ^{177}Lu is 0.146 MeV/ Bq·s and 0.193 MeV/ Bq·s for ^{161}Tb.

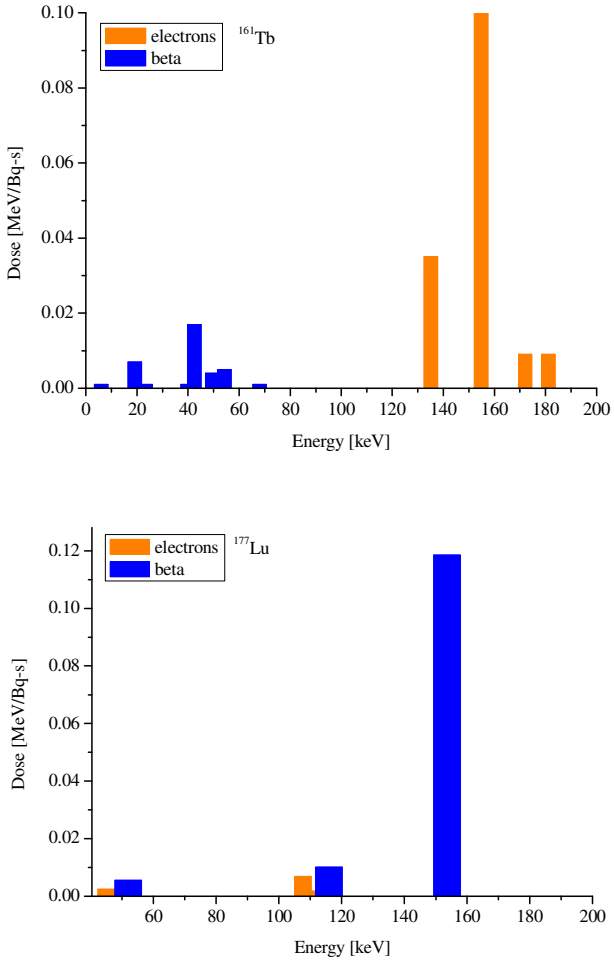

Figure 2-3: Profiles of ^{161}Tb- and ^{177}Lu decay: dose (released energy) [MeV/ Bq·s].
^{161}Tb-decay: Per decay 0.134 MeV/ Bq·s are released by β^- radiation and 0.012 MeV/ Bq·s by conversion and Auger electrons .
^{177}Lu-decay: Per decay 0.155 MeV/ Bq·s are released by β^- radiation and 0.038 MeV/ Bq·s by conversion and Auger electrons (National Nuclear Data Center).

Compared to ^{177}Lu, ^{161}Tb generates a higher dose (about 16% more by β^- radiation and about 216% more by conversion and Auger electrons). Referred to the sum of β^- radiation and conversion and Auger electrons, the ^{161}Tb dose is about 33% higher than the ^{177}Lu dose. The Auger and conversion electrons increase the dose of ^{161}Tb by 25% (Table 2-1, Figure 2-3). For endoradiotherapeutic treatment this is an important factor since the dose that is deposited in the tissue is relevant for therapy.

Table 2-1: Dose of ^{161}Tb and ^{177}Lu β^- decay and Auger electrons (National Nuclear Data Center).

element	dose β^- [MeV/ Bq·s]	dose Auger electrons [MeV/ Bq·s]
^{161}Tb	0.155	0.042
^{177}Lu	0.134	0.014

2.2 Availability of ^{161}Tb

2.2.1 Production of ^{161}Tb at nuclear reactors

^{161}Tb is a neutron rich radionuclide that can be produced at nuclear reactors. For the production from stable ^{159}Tb (natural abundance: 100%) a double neutron capture is required (Figure 2-7). Owing to the relatively low cross section the ^{159}Tb(2n,2γ)^{161}Tb reaction can only achieve limited specific activity and contamination with long-lived ^{160}Tb ($t_{1/2}$ = 72.3 days) can not be avoided. In an alternative production route *n.c.a.* ^{161}Tb can be obtained from β^-decay of short-lived^{161}Gd ($t_{1/2}$ = 3.66 min) produced by neutron capture of ^{160}Gd at a nuclear reactor: ^{160}Gd(n,γ)^{161}Gd ^{161}Tb.

The research reactor FRM II in Garching is located next to RCM and, therefore, the irradiated targets can easily be transported to the RCM laboratories. This neutron source is based on a single U_3Si_2 fuel element with an uranium enrichment up to 93% and cooled with light water and surrounded by heavy water in a large moderator tank. There, a high flux of thermal neutrons builds up.

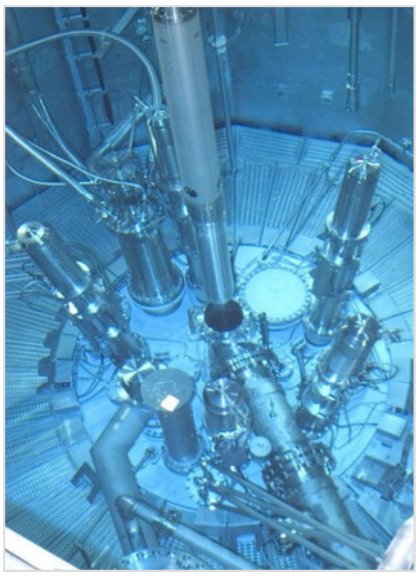

Figure 2-4: View on the moderator tank of FRM II Technische Universität München (FRM-II).

For the production of neutron rich radioisotopes, there is a pneumatic rabbit system with six independent channels for irradiation of samples up to a volume of 12 cm^3 in a maximum thermal flux of $7.3 \cdot 10^{13}$ n $cm^{-2}s^{-1}$ for up to 15 h. Larger volumes up to 30 cm^3 without any time limit can be performed in a two-channel hydraulic rabbit system for encapsulated samples with a thermal flux of $1.3 \cdot 10^{14}$ n $cm^{-2}s^{-1}$ (Lin, et al., 2006).

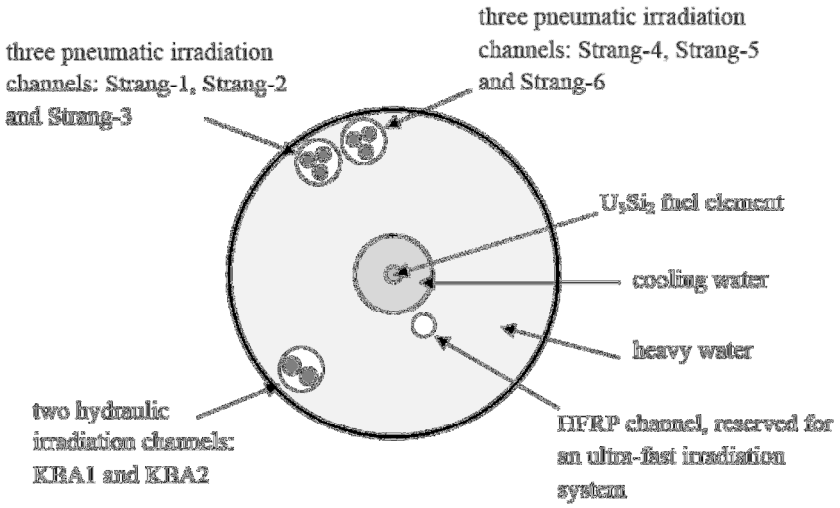

Figure 2-5: Schematic diagram of the irradiation devices in the research reactor FRM II (Lin, et al., 2006).

For irradiations at an even higher neutron flux the high flux reactor (HFR) at the Institute Laue-Langevin (ILL) in Grenoble was used. It produces an intense continuous neutron flux in the moderator region with $1.5 \cdot 10^{15}$ n $cm^{-2}s^{-1}$ and delivers neutron beams to 34 high technology scientific instruments. The reactor uses a fuel element enriched to 93% in ^{235}U moderated by D_2O. In order to optimize the neutron fluxes for off-thermal neutron energies the reactor has been equipped by a cold source and a hot source.

Figure 2-6: View on the moderator tank of High Flux Reactor (HFR) Institute Laue-Langevin Grenoble (Laue-Langevin).

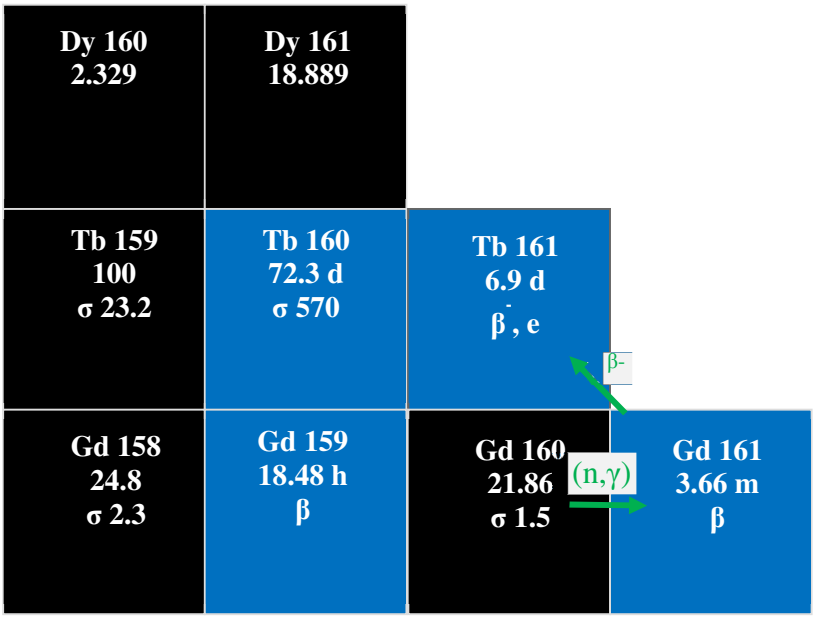

Figure 2-7: Cut-out from the chart of nuclides showing the isotopes of Gd, Tb and Dy (Magill, et al., 2006).

2.2.2 Specific activity of ^{161}Tb

A successful application of metallic radionuclides is limited by the specific activity that can be achieved during production. The specific activity is defined as the activity of the nuclide divided by the total mass of all of its radioactive and stable isotopes [Bq/mg, Ci/mg]. This definition is already in use for several decades and it is widely accepted. A high specific activity is necessary to reach a site-specific uptake without saturating these

binding sites with stable isotopes, which leads to a suboptimal tumor uptake (Breeman, et al., 2003). Therefore, the application of a *n.c.a.* radiometal for labeling is preferred.

Natural gadolinium consists of only 21.66% of the target isotope ^{160}Gd and, consequently, highly enriched material has to be employed. Presence of the stable isotope ^{158}Gd (24.84% natural abundance; σ = 2.3 b) in the target results in accumulation of stable ^{159}Tb during irradiation *via* the $^{158}Gd(n,\gamma)^{159}Gd \xrightarrow{\beta^-} {}^{159}Tb(st)$ nuclear reaction and thus decreases the technically achievable specific activity of ^{161}Tb. Furthermore, natural Gd contains 15.65% ^{157}Gd with a cross section of 254000 barn (Magill, et al., 2006). Estimations of the specific activity, which can be achieved utilizing currently available ^{160}Gd of 98.2% isotopic enrichment with a content of 0.85% of ^{158}Gd at 10^{14} $cm^{-2}s^{-1}$ as a function of time is given in Figure 2-8.

A high specific activity of 4.03 TBq/mg (109 Ci/mg) (as related to total terbium mass in the system) can be theoretically achieved after 14 days of irradiation and isolation of ^{161}Tb from the highly enriched target material. This value is about 93% of the theoretical specific activity of 4.34 TBq/mg (117.3 Ci/mg). After the end of irradiation, due to the low content of stable terbium the specific activity decreases slowly and evens out at ~ 3.89 Tbq/mg (105 Ci/mg) even after a cooling period of 5 days. In contrast, irradiation of natural gadolinium, under the same conditions, would provide only ~ 2.48 Tbq/mg (67 Ci/mg) as a result of a significant accumulation of stable terbium during irradiation as consequence of neutron activation of ^{158}Gd.
However, decay of ^{161}Tb leads to the formation of stable ^{161}Dy. This chemically similar neighboring lanthanide can interfere with radiolabeling reactions with ^{161}Tb. The specific activity of ^{161}Tb related to total terbium and dysprosium mass in the system during irradiation is given in Figure 2-8. It is significantly lower because of accumulation of ^{161}Dy(st) during irradiation and averages ~ 2.22 TBq/mg (60 Ci/mg) after 14 days. Furthermore, it decreases proportional to the ^{161}Tb activity after the end of irradiation and is ~ 1.37 TBq/mg (37 Ci/mg) after only 5 days of cooling period. Thus, an isolation of ^{161}Tb from ^{161}Dy should be taken into consideration, although the basic radiochemical strategy aims at the isolation of ^{161}Tb from macro-amounts of the gadolinium target.

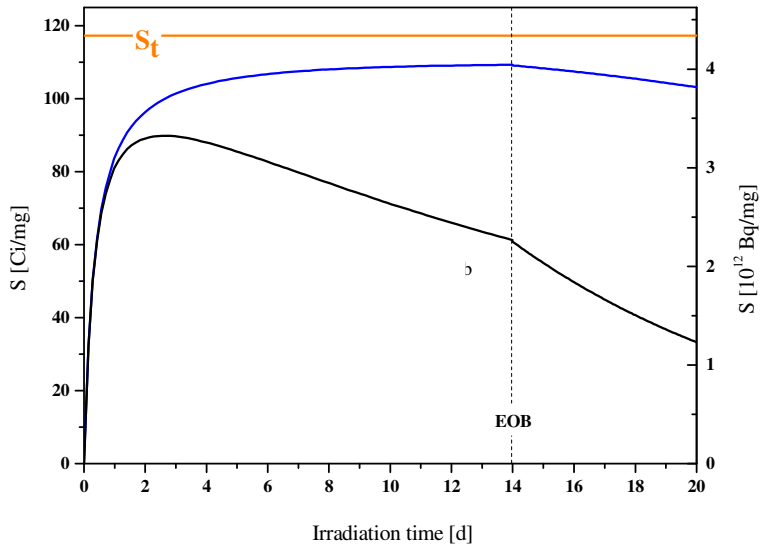

Figure 2-8: Specific activity of ^{161}Tb as a function of time
neutron flux: 10^{14} cm^{-2} s^{-1}.
Orange line: theoretical specific activity of ^{161}Tb (118.2 Ci/mg).
Blue line: theoretical specific activity of ^{161}Tb calculated for the ^{160}Gd-target (98.2% enrichment) used in this work.
Black line: theoretical specific activity of ^{161}Tb calculated for the ^{160}Gd-target used in this work if also the content of Dy (46 ppm) is taken into account.

Gadolinium oxides enriched in ^{160}Gd up to ≈ 98% are commercially available. To obtain *n.c.a.* ^{161}Tb of maximum specific activity, radiochemical separation of the Gd(macro)/Tb(micro) system is necessary because of the competition of Gd with Tb in complexation reaction during production of radiopharmaceuticals. Furthermore, the low cross section for the reaction ^{160}Gd(n,γ)^{161}Gd of only 1.5 b (versus 3.0 b for ^{176}Yb(n,γ)^{177}Yb) requires a massive Gd-target even for irradiations at high neutron flux nuclear reactors.

In general, all lanthanides are chemically quite similar and the separation of two neighbors is challenging. Nevertheless, separating adjacent trivalent lanthanides has been well documented (Forsberg, et al., 1983; Cotton, 2006). Among the lanthanides, the Tb(III)/Gd(III) system shows the highest possible separation factor α even for the established system cation exchanger/α-HIBA (2.40 versus e.g. 1.54 for Lu(III)/Yb(III) (Marhol, 1982)) as well as for the extraction system HDEHP and HEH[EHP] (factors 5.66 and 6.96 versus 1.92 and 1.99 for Lu(III)/Yb(III), respectively (Marhol, 1982) see 1.2.2). In addition to a targeted separation of this system, the production of the stable

isotope ^{161}Dy has to be taken into account. Due to the radioactive decay of ^{161}Tb (Figure 2-7) and dependent on the time of irradiation a significant mass of ^{161}Dy is accumulated. With irradiation times of more than two times $t_{1/2}$ more ^{161}Dy than ^{161}Tb atoms are generated. Accordingly also the separation ^{161}Dy/^{161}Tb has to be optimized to reach the highest possible specific activity of *n.c.a.* ^{161}Tb.

2.2.2.1 Radionuclide purity

By neutron activation of a Gd target, no long-lived impurities are co-produced. A content of 5 ppm of ^{159}Tb(st), however, would lead to accumulation of the relatively long-lived β^- and photon emitter ^{160}Tb ($T_{1/2}$ = 72.3 d) *via* the ^{159}Tb(n,γ)^{160}Tb reaction. After 14 days of irradiation, ^{161}Tb contains ~ 10^{-3}% of ^{160}Tb activity. Cooling time increases the ratio of ^{160}Tb to ^{161}Tb due to its significantly longer half-life. Thus, after 7 days the content equals ~ $2 \cdot 10^{-3}$% of the activity.

2.2.2.2 Irradiation yield

Up to 0.45 GBq of ^{161}Tb can be theoretically produced after 14 days irradiation time of 1 mg ^{160}Gd target in nuclear reactor at 10^{14} $cm^{-2}s^{-1}$. The intermediate nuclide ^{161}Gd shows a high neutron capture cross section σ of 20 000 b. Due to by its short half-life ($T_{½}$ = 3.66 min), however, there are no significant losses through its activation to ^{162}Gd. ^{161}Gd quantitatively decays to ^{161}Tb even at higher neutron flux. There is no data available for the neutron capture cross section of ^{161}Tb. Presence of ^{155}Gd (14.80% natural abundance) and ^{157}Gd (15.65% natural abundance) in the target might cause self-shielding effects and consequently a decrease of the activation rate due to the high cross sections of 61 000 b and 254000 b, respectively.

2.2.2.3 Chemical strategy

Production of adequate ^{161}Tb activities requires irradiation and processing of massive gadolinium targets (tens of milligrams). 14 days irradiation of a highly enriched ^{160}Gd target at 10^{14} $cm^{-2}s^{-1}$ results in a Gd to ^{161}Tb ratio of about 10^4. Thus, gadolinium must be reduced by a factor > 10^5 and ^{161}Dy by a factor > 10 to obtain high quality ^{161}Tb preparations. Here, column chromatography can be successfully applied for the target processing. Along with the relatively high separation factor, the Tb(III) fraction is

eluted first, resulting in its better isolation from macro amounts of Gd(III). Additionally, the system provides a relatively high separation factor of 2.30 for the Dy(III)/Tb(III) pair. Increasing the target mass can complicate isolation of micro amounts of ^{161}Tb and specific optimization of the column process must be performed.

Depending on the conditions of the irradiation and the properties of the target material, the mass ratio of gadolinium to terbium can be in the range of several hundred to several thousand. To obtain ^{161}Tb for applications with a high specific activity the following points are essential:

- high chemical and radionuclidic purity
- high overall yield of ^{161}Tb (> 85%)
- ^{161}Tb has to be present in a suitable chemical form for radiolabeling reactions
- Gd has to be recovered for the next irradiation to save target material
- the separation process should be fast, reliable, reproducible and able to be scaled up and handled remotely

2.3 Preparation and evaluation of ^{161}Tb labeled compounds

2.3.1 ^{161}Tb labeled Peptides

A large number of primary and metastatic human tumors show a high affinity to somatostatin receptors. Radiometal labeled somatostatin analogs are successful used in diagnostics and therapy (Forssell-Aronsson, et al., 1995; Krenning, et al., 1993). Animal studies using ^{90}Y-DOTA-octreotide showed complete regression of rat pancreatic tumors. A maximal labeling efficiency is essential, because with decreasing efficiency the uptake in octreotide receptor-positive organs also decreases (de Jong, et al., 1995). The labeling efficiency is a function of pH and molar ratio of the radionuclide and the peptide (Breeman, et al., 2003) (Figure 2-9).

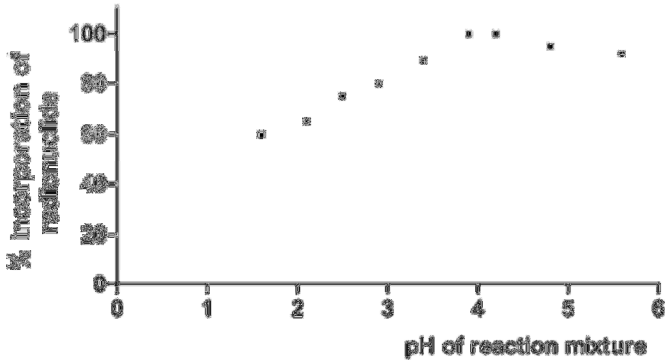

Figure 2-9: Formation of ^{177}Lu-DOTATOC as a function of pH.
After 20 min at 80 °C, as measured by the% incorporation of the radionuclide. Similar results were found with ^{90}Y and DOTATATE as ligand (Breeman, et al., 2003).

Peptides are short polymers formed via linking of amino acids. Peptides are smaller than proteins like monoclonal antibodies, so their clearance from the blood pool and normal tissue is faster. Moreover, they have a lower molecular weight and thus they penetrate faster into tumors and rapidly achieve homogeneous distribution of the radionuclide in the tumor. In addition, the synthesis of peptides is more convenient than the synthesis of antibodies (Ladner, 1999). Because of their configuration, it is possible to change or add amino acids without any consequences for receptor binding. However,

there are also a few disadvantages in application of labeled peptides. Most of them are regulatory peptides and are also present in some normal tissues especially in the gastrointestinal tract (Warner, et al., 2002). Even in small concentrations these regulatory peptides cause physiological effects and therefore a maximized specific activity is required (Zalutsky, 2003).

In addition a successful peptide labeling is an indicator that the radionuclide has a high purity and, for instance, can be used for labeling experiments with antibodies.

There is already a large experience in labeling of peptides with lanthanides, so it is possible to use this established models for labeling with ^{161}Tb.

2.3.2 Monoclonal antibodies (mAbs)

The cell surface protein L1-CAM is a target antigen involved in cell proliferation and gets more and more important as marker for cancers like neuroblastoma, renal cell carcinomas, melanomas and ovarian and endometrial carcinomas (Primiano, et al., 2003; Meli, et al., 1999; Fogel, et al., 2003; Fogel, et al., 2004). The highly affine chimeric monoclonal antibody chCE7 ($K_d \approx 10^{-10}$ M) binds to L1-CAM and is internalized into tumor cells. It has been especially useful in radioimmunodiagnosis of neuroblastoma cells (Hoefnagel, et al., 2001). It shows a great internalization into neuroblastoma cells. For example, treatment with ^{67}Cu and ^{125}I-labeled chCE7 showed antitumor activity (Novak-Hofer, et al., 1992; Amstutz, et al., 1993; Novak-Hofer, et al., 1994).

Neuroblastoma is a type of cancer that occurs during formation of the nervous system and appears mostly at young children. Survival rates are minimal at an advanced stage of disease. This is a result of the fact that this type of cancer infiltrates quite early into bone marrow and metastasizes into bones and further organs. These metastases are rather inert against chemotherapy. In this case, radioimmunotherapy might be successful.

First clinical studies of chCE7 antibodies in diagnosis showed a rapid and high accumulation in bone metastases (Dörr, et al., 1993). *In vitro* and *in vivo* studies with human neuroblastoma cells SK-N-AS showed that the chCE7 antibody internalizes into

tumor cells with high selectivity and is stable in radiolabeling without loss of immunoreactivity (Novak-Hofer, et al., 1992). ^{125}I and ^{67}Cu labeled antibodies have been studied. ^{67}Cu-chCE7 showed a higher accumulation in tumor tissue, a longer retention time and a higher tumor/blood ratio than ^{125}I-chCE7 (Figure 2-10) (Novak-Hofer, et al., 1992; Novak-Hofer, et al., 1997).

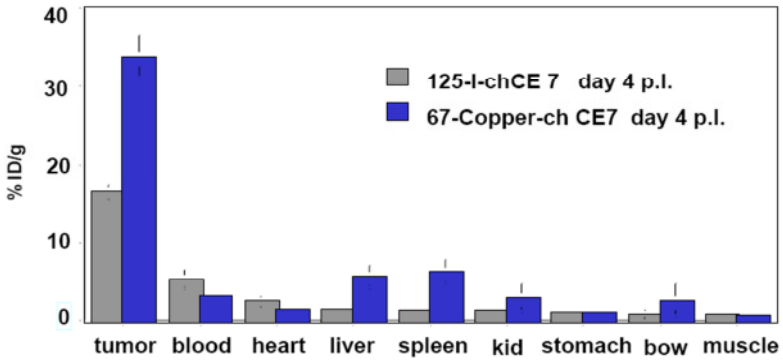

Figure 2-10: Biodistribution of ^{67}Cu-CPTA-labeled vs. ^{125}I-labeled antineuroblastoma mAb chCE7 in tumor mice.
Most of the labeled antibody is bound to tumor cells. Only low uptake in other organs like liver and heart is observed (PSI).

There are a few studies with internalizing mAb labeled with Auger electron emitters. This antibodies show a higher tumor efficiency compared to mAbs conjugated to β emitters (Meredith, et al., 1995; Welt, et al., 1996). As a result of their short path lengths, Auger electrons only reach the DNA if the antibody is internalized. Therefore, ^{161}Tb has to be conjugated to an internalizing mAb to examine the tumor efficiency caused by emitted Auger electrons.

3 Experimental

3.1 Production of ^{161}Tb in nuclear reactors

Highly enriched ^{160}Gd (98.2% enrichment) in its oxide form was purchased from Isoflex (Russia). The target material comprised 0.85% of stable ^{158}Gd, 0.27% ^{157}Gd, 0.39% ^{156}Gd, 0.24% ^{155}Gd and 0.04% ^{154}Gd. Terbium content in gadolinium was 46 ppm. $^{160}Gd_2O_3$ was dissolved in HNO_3 and evaporated. The residue was dissolved in pure water resulting in a solution with a ^{160}Gd(III) concentration of ~ 0.2 mg/µl. Aliquots from the stock solution were taken to prepare 5.0 – 40.0 mg ^{160}Gd samples in its nitrate form by evaporating to dryness in quartz ampoules. For investigation of the Dy(III) behavior a sample containing a mixture of 10.0 mg ^{160}Gd and 0.2 mg ^{nat}Dy in nitrate form was used. Neutron irradiations were performed at the research reactor FRM II (Munich, Germany). For model experiments the ^{160}Gd targets were irradiated for one hour at a neutron flux of $3.57 \cdot 10^{13}$ $cm^{-2}s^{-1}$, with a cooling period of one hour. Fourteen day irradiations were performed at a neutron flux of $1.3 \cdot 10^{14}$ $cm^{-2}s^{-1}$ and with a 24 h cooling period. Absolute radionuclide activities or relative distributions were measured using a pre-calibrated HPGe detector.
After irradiation and about two days decay time the sample was transported to our lab in a lead shielded container.

For production of higher activities (~ 20 GBq), the sample was irradiated for up to 14 days in the nuclear reactors FRM II Munich ($1.3 \cdot 10^{14}$ cm^2s^{-1}), ILL Grenoble ($1.35 \cdot 10^{15}$ cm^2s^{-1}), BER II Berlin ($1.6 \cdot 10^{14}$ cm^2s^{-1}) and BR2 Belgian ($3 \cdot 10^{14}$ cm^2s^{-1}).

For the model experiments, ^{160}Gd has been irradiated at the position “Strang 1” at FRM II. The neutron flux of this position has been determined by irradiating two flux monitors: Al-Co wire with 0.1043±0.0013% Co and Al-Au wire with 0.1049±0.0013% Au. The flux monitors have been irradiated for one hour. Afterwards, the activity of the Al-Au monitor was determined by γ-spectrometry.

^{161}Tb has been produced by irradiation of 1 to 40 mg ^{160}Gd mass in the chemical form $^{160}Gd(NO_3)_3$. The composition of the $^{160}Gd_2O_3$ target material from Isoflex, Russia is given in Table 3-1. This values have been verified ICP-OES.

Table 3-1: Isotopic distribution of the target material from Isoflex, Russia.

isotope	**^{152}Gd**	**^{154}Gd**	**^{155}Gd**	**^{156}Gd**	**^{157}Gd**	**^{158}Gd**	**^{160}Gd**
content [%]	-	0.04	0.24	0.39	0.28	0.85	98.2

Table 3-2: Chemical admixtures of the target material from Isoflex, Russia.

element	**Na**	**Mg**	**Al**	**Si**	**K**	**Ca**	**Cr**
content [%]	0.016	< 0.0005	< 0.001	< 0.005	0.006	< 0.004	< 0.003

element	**Fe**	**Ni**	**Cu**	**Sn**	**Nd**	**Sm**	**Eu**
content [%]	< 0.004	0.008	< 0.005	< 0.003	< 0.02	0.037	< 0.01

element	**Tb**	**Dy**	**Er**	**Pb**
content [%]	0.044	< 0.02	< 0.01	0.009

The activity of ^{161}Tb after irradiation (A_0) for the reaction $^{160}Gd(n,\gamma)^{161}Gd \xrightarrow{\beta^-} {}^{161}Tb$ is calculated according to equation 6:

$$A_0 = \sigma \Phi N_0 (1 - e^{-\lambda * t_b}) \qquad 6$$

Where σ is the cross section of ^{160}Gd (1.5 barn (Magill, et al., 2006)), Φ the neutron flux at the used irradiation position, N_0 the number of ^{160}Gd atoms in the target, λ the decay constant of ^{161}Tb (for $T_{1/2}$ = 6.9 days (Magill, et al., 2006)) and t_b is the time of irradiation. Due to the relative short half-life of ^{161}Gd of 3.66 min (Magill, et al., 2006),

one can assume that ^{161}Gd is already completely decayed before the material is loaded on the column.

The actual activity of ^{161}Tb after a certain decay time ($A_{Tb\text{-}161}$) is given in term 7:

$$A_{Tb-161} = A_0 \cdot e^{-\lambda t_a} \qquad 7$$

Where t_a is the decay time.

3.2 Experimental procedures

3.2.1 Chemicals and instruments

Chemicals and solvents are used from Sigma Aldrich (Schnelldorf, Germany), ^{160}Gd (98.2% enrichment) from Isoflex (Moscow, Russia), *n.c.a.* ^{177}Lu from ITG GmbH (Garching, Germany) the cation exchange resins AG 50W-X8 (200 - 400 μ) and AMINEX from BioRad (Munich, Germany), and the macroporous cation exchange resin from Sykam (Fuerstenfeldbruck, Germany). In all experiments and for all preparations deionized water from a Milli-Q Plus water purification system (Millipore, U.S.A.) was obtained. The required acid solutions were prepared by dilution of commercial concentrated HCl and HNO_3 acids. All experiments were performed at temperatures of 20 ± 2 °C. The glass columns and the dispenser needed for the separations was ordered from Sykam (Fuerstenfeldbruck, Germany). For the elution a gradient pump ISC 3000SP from Dionex (Idstein, Germany) was used. For preparing the ampoules for irradiation Heraeus Quarzglas HSQ300 (Vogelsberger Quarzglastechnik, Munich, Germany) was used.

Determination of the radioactivity of the samples during the ion-exchange column experiments and in case of irradiated Gd/Tb targets was carried out by γ-spectrometry. γ-spectra were acquired using a high purity germanium detector coupled to a multichannel analyzer (Canberra, Germany). The energy calibration of the detector was performed regularly by a multi-element γ-ray standard covering the energy range from 59.5 keV (^{241}Am) to 1332.5 keV (^{60}Co). Samples were measured at a distance of 0, 5 and 25 cm from the detector.

The resin (V = 3.24 ml) was washed with 4.0 M HCl solution until the pH of the eluted solution was about two and with 0.5 M NH_4Cl (pH ≈ 4.5) to obtain the NH_4^+ form of the resin. Then it was washed with 2.5 ml pure H_2O, 5.0 ml 0.5 M α-HIBA solution and again with 10.0 ml pure H_2O.

3.2.2 Radiochemical isolation of ^{161}Tb from the target material

The ampoule was brought into a glove box and broken with a "crusher" by compression of two aluminum blocks. After that, the target was dissolved in 2.0 ml loading solution (0.05 M NH_4Cl solution, pH = 3) and transferred to the column.

Figure 3-1: Crusher - interior view.
Via the tubing at the bottom of the Teflon tube water and loading solution can be brought into the tube and the solved activity can be transported to the column.

In this work, three different columns were used. The first one was filled with 16.4 cm BioRad AG 50W-X8 200-400 µ resin (1.7 meq), the second one with 17.3 cm respectively 14.3 cm macroporous cation exchange resin (1.7 meq) and the last one with 14.3 cm AMINEX A6 (1.7 meq) (Table 3-3). The resin bed height was measured in NH_4^+-form.

The cation exchange resin BioRad AG 50W-X8 200 – 400 µ, macroporous cation exchange resin and AMINEX A6 in NH_4^+-form were used to prepare chromatographic columns of 180 × 5 mm and 150 × 5 mm dimension and ~ 1.4 ml free column volume (FCV). The columns were connected to a standard 3-way valve using PTFE capillary 1/16″ OD. Switching the valve allowed to change the direction to the column from a 2.5 ml syringe pump (Variodisp[8], ScintOmics) to a HPLC pump (Dionex Ultimate 3000

PEEK construction). The irradiated material was dissolved in 2.0 – 3.0 ml of 0.05 M NH_4Cl solution (pH 3) and loaded on the column with a syringe pump at a flow rate of 0.125 ml/min. After loading, the column was washed with 2.0 – 3.0 ml H_2O. Separations were performed by isocratic elution of the column with 0.2 ml/min flow rate using a HPLC pump with α-HIBA (α-hydroxyisobutyric acid) solutions titrated with ammonia to pH 4.5 as eluent. Absolute or relative activities in the fractions were determined for the radionuclides ^{161}Tb, ^{159}Gd and ^{165}Dy.

During the separation of the short time irradiated samples (production up to 33 MBq), fractions with a volume of 0.5 ml have been taken. The content of the different fractions was examined by γ-spectroscopy. As soon as there is only a little amount of ^{161}Tb detectable, the concentration of the α-HIB/NH_3-solution was increased to 0.5 M to elute ^{159}Gd.

Because of the relatively high dose rate of several mSv/h of the 14 days irradiated samples (production up to 21 GBq), the process was observed only by the dose rate. When the dose rate increased, the eluted solution was collected in a clean 20 ml glass vial (washed with 4 M HCl and pure water) until the dose rate decreased again. After that, the column was eluted with 0.5 M α-HIB/NH_4^+-solution.

Table 3-3: Ion exchanger resins used in this work

resin	**BioRad AG 50W-X8**	**AMINEX A6**	**macroporous cation exchange resin**
particle size [µ]	20 - 40	17.5 ± 2.0	16.0
cross linkage [%]	8	8	16
functional group	$R\text{-}SO_3^-$	$R\text{-}SO_3^-$	$R\text{-}SO_3^-$

3.2.2.5 γ-spectrometry

The activity of the eluted fractions were measured at distances of 0, 5 or 25 cm to the detector, depending on the rate of the activity. For calculating the activities of the isotopes, the most intense γ-peak was used. ^{161}Tb was calculated via the 74.5 keV γ-line (intensity 10.2%), ^{159}Gd via 363.5 keV γ-line (intensity 11.78%) and ^{165}Dy via 94.7 keV γ-line (intensity 3.8%). The activity is calculated according to equation 8:

$$A = \frac{counting\ rate}{intensity \cdot detector\ efficiency} \qquad 8$$

The counting rate is measured with a γ-detector and given in the unit counts per second (cps) or minute (cpm), the detector efficiency was determined by calibration of the detector in the specific positions.

3.2.2.6 Target recovery

It is feasible to recycle the irradiated target because the cross section of ^{160}Gd is low and practically no target burn-up occurs. Therefore, the cation exchange resin BioRad AG 50W-X8 (200 - 400 μ) was used to prepare a column of 35 × 10 mm dimension. The target dissolved in α-HIBA was loaded on the column. After loading the column was washed with 5.0 ml H_2O. Finally, $^{160}Gd(NO_3)_3$ could be eluted with 15.0 – 20.0 ml 4.0 M NH_3-solution and was evaporated under nitrogen flow.

3.2.3 Labeling of DOTATATE (DOTA-Tyr^3-octreotate)

About 3.0 – 3.5 ml ^{161}Tb fraction obtained after column processing was mixed with 1.0 ml 1.0 M HCl solution in order to adjust the pH to ~ 1. The mixture was loaded on a small secondary column of 26 × 5 mm dimension filled with BioRad AG 50W-X8 cation exchanger in H^+-form. The column was washed with 5.0 ml 1.0 M HCl solution and finally stripped with 5.0 – 10.0 ml 4.0 M HCl. ^{161}Tb in hydrochloric acid solution was evaporated under nitrogen flow and redissolved in 200 to 300 μl 0.05 M HCl.

DOTA-Tyr^3-octreotate was provided by ABX chemicals (Radeberg, Germany). The peptide was dissolved in pure water to obtain 1.0 mg/ml solution. 400 MBq aliquots of

^{161}Tb solution were mixed with 0.04 M HCl and 0.5 M sodium acetate solution to obtain samples of 25 µl total volume with pH in the range 3- 5. 5 to 15 µg f DOTATATE were added and mixtures were incubated at ~ 100 °C within 30 min in 2 ml Eppendorf tubes. The radiolabeling yield was controlled by TLC on aluminum sheets, silica gel 60 and 0.1 M Na_3Citrate pH 4.5 as mobile phase (Malja, et al., 2000).

3.2.4 Stability of labeled peptides in human serum

Stability of ^{161}Tb- and ^{177}Lu-DOTA-compounds was investigated by incubation of 50 MBq (up to 4 µl aliquots from the labeling mixture from 3.2.3) in 1.0 ml human plasma 20% HAS (Novartis-Behring) for 10 days at 37 °C. Aliquots were taken at different time points and the unbound fraction of the radionuclides was determined by TLC.

3.2.5 Labeling of the monoclonal antibody chCE7

The monoclonal antibody chCE7 was produced in HEK-293 cells (Knogler, et al., 2005; Grünberg, et al., 2003) and purified from tissue culture supernatants with protein G-Sepharose (Amersham, Biosciences, Otelfinger, Switzerland). For all experiments, the aglycosylated form of chCE7 was used.

For labeling with radiometals proteins were substituted with p-SCN-benzyl-DOTA.

80 (11 · excess) and 160 µg (22 · excess) p-SCN-benzyl-DOTA were added to 200 to 400 µl of 0.1 M sodium phosphate buffer (pH 8). The pH was adjusted using Na_3PO_4 (saturated solution) to pH 9 - 10 and the reaction mixture was incubated for 8 h at 4 °C. Excess ligand was then removed by centrifugation dialysis (Vivascience, Winkel, Switzerland) and the buffer changed to 0.1 M ammonium acetate buffer (pH 5.5). The number of chelators coupled per antibody was determined by mass spectroscopy.

After substitution, chCE7 (1.5 µg) was labeled with 200 MBq ^{161}Tb or ^{177}Lu in 25 µl 0.25 M NH_4-solution (pH 5.5) at 37 °C for 30 min. Afterwards, 25 µl 50 mM EDTA-solution was added and again incubated for five minutes to complex free radiometal ions. The labeling yield was analyzed by fast protein liquid chromatography (FPLC) on a Superose 12 HR 10/30 column (Amersham, Biosciences, Otelfinger, Switzerland)

with PBS as eluent (0.5 ml/min). The activity of the different fractions was measured by Berthold FPLC Radioactivity Monitor (Berthold Technologies, Regensdorf, Switzerland)

3.2.6 Cell experiments with ^{161}Tb-chCE7 and ^{177}Lu-chCE7

Radioligand binding assays can be used in quality control to examine important characteristics of the labeled antibody by characterization of the binding of the labeled ligand to the membrane-receptor. The first assay was performed in 1970 by Lefkowitz (Lefkowitz, et al., 1970). He determined the binding affinity for the receptor of a radiolabeled hormone by using the same principle as described originally for radioimmunoassay (Yalow, et al., 1959). The assay is based on the competitive interaction between a labeled ligand and an analyst for the same receptor binding site (Lefkowitz, et al., 1970; de Jong, et al., 2005).

For all experiments, SKOV3ip human ovarian carcinoma cells were used, provided by PSI, Switzerland. They have been maintained in Dulbecco's modified Eagle's medium (4.5 g/k glucose). All media were supplemented with 10% fetal calf serum, 2 mmol/l glutamine, 100 units/ml oeniccillin, 100.0 Ag/ml streptomycin and 0.25 Ag/ml Fungizone. All media and additives were obtained from BioConcept (Allschwil, Switzerland).

3.2.6.1 Preparation of the solutions

PBS-buffer (PBS = Phosphate buffered saline) pH 7.2:

- NaCl: 8.0 g
- KCl: 0.2 g
- Na_2HPO_4: 1.44 g
- K_2HPO_4: 0.24 g
- ddH_2O: to 1000 ml
- adjust pH with 1M HCl

Acid wash buffer pH 2.8:

- NaCl: 0.6 g
- Glycine: 0.4 g
- ddH_2O: to 100 ml
- adjust pH with 1M HCl

Separating gel:

- Acrylamide solution: 2.5 ml
- 4 · Resolving gel buffer: 2.5 ml
- 10% SDS: 0.1 ml
- ddH_2O: 4.9 ml
- Ammoniumpersulphate: 40 µl
- TEMED: 15 µl

4 · Resolving gel buffer pH 8.8:

- Tris-Cl (FW 121.1): 36.3 g
- ddH_2O: to 200 ml
- Adjust pH with HCl

Stacking gel:

- Acrylamide solution: 0.44 ml
- 4 · Stacking gel buffer: 0.83 ml
- 10% SDS: 33 µl
- ddH_2O: 2.03 ml
- Ammoniumpersulphate: 15 µl
- TEMED: 15 µl

4 · Stacking gel buffer pH 6.8:

- Tris-Cl (FW 121.1): 3.0 g
- ddH_2O: to 50 ml
- adjust pH with HCl

3.2.6.2 Scatchard analysis

The Scatchard-assay allows the graphical representation of an equation that describes protein-ligand binding and analyzes equilibrium binding data. The raw data is obtained from the radioreceptor-assay ligand binding experiment. Therewith the amount of bound antibodies referred to the concentration of antibodies is specified. The graphical analysis of Scatchard delivers the dissociation constant K_D and the maximum of the binding capacity B_{max}. B_{max} is multiplied by the reaction volume and divided by the number of cells. The resulting amount of antibodies is equal to the amount of antibodies per cell. This value is divided by the molecular mass of immunoglobulines G (150 kDa) and multiplied by N_A. The resulting amount of bound antibodies is equal to the binding sites B per cell (Scatchard, 1949; Rosenthal, 1967).

To obtain the Scatchard-plot, the ratio bound/free ligand is plotted against the number of bound radioligands (Rosenthal plot). The equation for the line is:

$$\frac{L_{bound}}{L_{free}} = \frac{1}{K_D}\ bound + \frac{B_{max}}{K_D} \qquad 8$$

The affinity of chCE7 for its binding site on SKOV3ip cells and the number of binding sites/cell was determined by incubating 10^5 – 10^6 cpm ^{161}Tb-chCE7 or ^{177}Lu-chCE7 and increasing the concentration of unlabeled chCE7 (1 – 800 ng). Cells were suspended in duplicate samples in 0.4 ml PBS/BSA and 0.1 ml of the labeled chCE7-solution. Incubation was made on a shaking platform at 37 °C for two hours. Cells were then washed twice with 2.0 ml ice cold PBS/BSA by centrifugation. The radioactivity associated with the cell pellets was measured by γ-spectroscopy.

3.2.6.3 Immunoreactivity assay

Another opportunity for quality control is the Lindmo-assay. There, the immunoreactive fraction of the radiolabeled antibody can be determined. The fraction of immunoreactive antibody is defined by linear extrapolation to conditions representing infinite antigen excess. This assay is based on a double-inverse plot of the binding data, which is a kind of modification of the Lineweaver-Burk plot. The data is plotted in a double inverse plot of total applied radioactivity/specific binding as a function of the inverse of cell concentration. The immunoreactive fraction can be determined from the intercept value obtained by linear extrapolation to the y-axis (Lindmo, et al., 1984).

The line follows equation 9, if only a fraction r of the total amount of the antibody is immunologically reactive:

$$\frac{total\ applied\ radioactivity}{specific\ binding} = \frac{1}{r} + \frac{1}{r \cdot K_a \cdot cell\ concentration} \qquad 9$$

where K_a is the association constant.

The immunoreactivity of radiolabeled chCE7 antibodies was measured by cell binding assays in duplicate wells using increasing the number of cells ($0.2 \cdot 10^6$ to $6 \cdot 10^6$) in 1.5 ml PBS/BSA (1:1). Nonspecific binding was determined by adding 5 µg of unlabeled chCE7. The probes were incubated for two hours at 37 °C on a shaking platform. After incubation 2.0 ml of ice cold PBS/BSA was added and the probes have been centrifuged for 5 min at 1500 rpm at 4 °C. After drawing off the supernatant, again 2.0 ml PBS/BSA were added and the procedure repeated. The cells were measured in a γ-counter.

3.2.6.4 SDS-PAGE electrophoresis (western-blot)

The western-blot is an analytical technique to detect specific proteins in a given sample. For separation of the proteins, gel electrophoresis is used. This is a method to separate the molecules based on their size and charge. For the separation of proteins, polyacrylamide gels are used, which consist of a network of polymers that contain spaces between them that can act like a sieve. The size of this spaces decreases with increasing gel monomer concentration. Small molecules tend to migrate more quickly trough the gel than big ones. Performing SDS-PAGE (SDS polyacrylamide gel electrophoresis) the process results in the separation of proteins into discrete bands along the gel according to their electrophoretic mobility. By using a reducing agent like DTT (dithiothreitol), the disulfide linkages get reduced and the quaternary protein structure is broken up. SDS-PAGE is the most common method used to separate proteins (Laemmli, 1970; Shapiro, et al., 1967; Weber, et al., 1969; Raymond, et al., 1959).

About 2 - 4 µg labeled chCE7 was mixed with sample buffer. For reducing SDS-PAGE additionally 2 µl DTT (Dithiothreitol) was added. After heating to 95 °C for five minutes, the samples were briefly pelleted by centrifugation. Non reduced samples (25 µl) were run on 10%, the reduced onces on 7.5% SDS gel (1 h, 150 V). The Coomassie-Blue stained and dried gels were autoradiographed using Amersham Hyperfilm MP (Amersham, Biosciences, Otelfinger, Switzerland) and Kodak intensifying screens.

3.2.6.5 Internalization of labeled chCE7

Because of their short path length, low energy Auger electrons can reach the nuclear DNA only if the antibody is internalized. In this case, higher anti-tumor efficacy at lower toxicity can be expected (Kassis, et al., 1987). The most common used Auger electron emitter is ^{125}I ($T_{1/2}$ = 60.1 d). It releases 21 low energy Auger and conversion electrons (Martin, et al., 1981; Daghighian, et al., 1996). With a path length of 0.06 – 17.00 µm the electrons are only able reach the DNA if the decay occurs within the cell.

The monoclonal antibody chCE7 was found to be taken up into neuroblastoma cells (Novak-Hofer, et al., 1994; Novak-Hofer, et al., 1992). Internalized ^{161}Tb-labeled chCE7 antibodies enhance the cytotoxic effect of additionally emitted low energy electrons. The electrons are able to get more closely to the nucleus and thereby the probability to cause DNA-damage increases. Hence, it is an important task to examine the grade of internalization of ^{161}Tb-labeled antibodies.

The internalizing fraction of labeled chCE7 antibodies was determined by adding 2.0 ml of PBS (binding medium) to SKVO3ip cells and 10^5 – 10^6 cpm ^{161}Tb-chCE7 or ^{177}Lu-chCE7 to duplicate wells and put them for four hours on ice. The internalization starts by taking off the binding medium, washing the cells with 5.0 ml ice cold PBS, adding 5.0 ml of complete medium (37 °C) and placing the dishes in the incubator at 37 °C. After desired points in time, the dishes have been washed two times with 5.0 ml ice cold PBS. After that, the non internalized fraction can be obtained by adding 2.0 ml ice cold acid wash, pooling the solution and counting. The remaining cells were washed again with ice cold PBS and covered with 0.5 ml 1 M NaOH to solve the cells for counting purposes.

3.2.7 Stability of labeled chCE7 in human serum

0.5 ml of human serum obtained from volunteers was incubated at 37 °C for 48 h with 200 MBq ^{161}Tb- and ^{177}Lu-chCE7 of labeled immunoconjugates with p-SCN-benzyl-DOTA as linker (250 µg antibody). Labeling was performed at 37 °C for 2.5 hours. Samples were analyzed immediately after addition, 24 h and 48 h later. EDTA was added to a final concentration of 5 mM to complex free radiometal ions.

Stability of the labeled antibodies after desired points in time was analyzed by fast protein liquid chromatography on a Superose 12 HR 10/30 column (Amersham, Biosciences, Otelfinger, Switzerland) with PBS as eluent (0.5 ml/min).

3.2.8 SPECT imaging performance of ^{161}Tb

Tomography uses computer technology to convert numerous planar images into a three-dimensional slice through the object. This data processing is also used with CT and MRI. With radioactive tracers it is called emission computed tomography, which includes single photon emission computed tomography (SPECT) and positron emission tomography (PET).

SPECT images are usually obtained with Auger cameras, which rotate around the patient. Numerous images are obtained at different angles. Faster and bigger computers give better image quality, while improved graphics capabilities allow three-dimensional imaging.

In this study, a Derenzo phantom was used, a common device in nuclear medicine imaging (Budinger, et al., 1977; Park, et al., 2008). The Derenzo phantom consists of six pieshaped wedges, each with different diameters from 0.8 to 1.3 mm.

The Derenzo phantom was filled with 48.1 MBq ^{161}Tb. The diameters of the holes ranged from 0.8 to 1.3 mm with 0.1 mm steps. The visualization was performed with X-SPECT/CT; Gamma Medica – Ideas GE. The detector was equipped with a 1 mm tungsten-based single pinhole collimator. The 75 keV gamma line was used for the reconstruction.

4 Results and Discussion

4.1 Production of ^{161}Tb in nuclear reactors

The thermal neutron flux at the irradiation position "Strang 1" of the munich research reactor FRM II with a theoretical value of $3.57 \cdot 10^{13}$ cm^{-2} s^{-1} has been monitored two times with Au and Co wires.

Table 4-1: Monitoring of the thermal neutron flux at irradiation position "Strang 1" from irradiation of the monitors Au and Co.

irradiation date	monitor	γ-peak [keV]	calculated neutron flux [cm^{-2} s^{-1}]
25.02.2008	Au	70.38	$3.81 \cdot 10^{13}$
25.02.2008	Au	411.68	$3.69 \cdot 10^{13}$
25.02.2008	Au	675.54	$3.64 \cdot 10^{13}$
25.02.2008	Co	1173.23	$4.04 \cdot 10^{13}$
25.02.2008	Co	1332.49	$3.89 \cdot 10^{13}$
17.12.2008	Co	1173.23	$3.89 \cdot 10^{13}$
17.12.2008	Co	1332.49	$3.90 \cdot 10^{13}$

Average value Au: $3.71 \cdot 10^{13}$ cm^{-2} s^{-1}

Average value Co: $3.93 \cdot 10^{13}$ cm^{-2} s^{-1}

The published value of the thermal neutron flux at irradiation position "Strang 1" with $3.57 \cdot 10^{13}$ cm^{-2} s^{-1} could be confirmed with the Au and Co monitors measured values of about $3.71 \cdot 10^{13}$ cm^{-2} s^{-1} (Au) and $3.93 \cdot 10^{13}$ cm^{-2} s^{-1} (Co). The slight aberrances ($< 0.4 \cdot 10^{13}$) might originate in measurement inaccuracies for example of the weight of the wires or in γ-spectroscopy. Also it might be of importance at which place in the irradiation position the sample is located. It cannot be guaranteed that in every

irradiation the sample was placed at the same position. Therefore, for all calculations of the produced activity at the irradiation position "Strang 1" for model experiments the published value of $3.57 \cdot 10^{13}$ cm^{-2} s^{-1} was used (Lin, et al., 2006).

^{161}Tb activities obtained after irradiation at different neutron intensities were in good agreement with the theoretically expected values.

At long-term irradiations, the estimated specific activity of ^{161}Tb, as related to total terbium amount in the system produced at FRM II and BER II was about 2.8 TBq/mg (75 Ci/mg) after 1 – 3 days cooling period. The specific activity of ^{161}Tb achieved at ILL was about 4.0 TBq/mg (~ 108 Ci/mg) at the end of the irradiation. After 24 days cooling and transport time the specific activity, as related to total terbium mass was ca. 2.1 TBq/mg (58 Ci/mg). Traces of stable terbium (46 ppm) in the target material reduced the specific activity from the maximum achievable one by about 35% and 7% for irradiations at FRM II or BER II and ILL, respectively.

4.2 Radiochemical isolation of ^{161}Tb from target material

For the elution profile of the separations, the percentage of the total measured activity is plotted against the used volume of α-HIBA-solution [ml]. Every fraction contains 0.5 ml solution.

Due to micro amounts of ^{161}Tb it is not reasonable to give the column efficiency as percentage of total number of millimoles of exchangeable ions of the resin (millimoles of exchangeable ions of the resin divided by 3 mmol Ln^{3+}). Nevertheless, the unit mg/cm^2 resin is used. Consequently the column efficiency just depends on the target mass and the radius of the used column.

4.2.1 Resin: BioRad AG 50W-X8

An elution profile of the processing of 3.0 mg ^{160}Gd (15.3 mg/cm^2 lanthanide mass to column cross section) on a chromatographic column is presented in Figure 4-1. The peak of the ^{161}Tb fraction could be eluted with 0.12 M α-HIBA solution after about 45.0 ml (~ 32 FCV [free column volume]). Gadolinium was eluted by increasing the

α-HIBA concentration up to 0.5 M. The gadolinium content in ^{161}Tb was estimated by ^{159}Gd measurements with a detection limit of 10^{-5}% of its total amount.

In the following Figures the blue line represents ^{161}Tb, the orange line ^{159}Gd and the violet line ^{165}Dy.

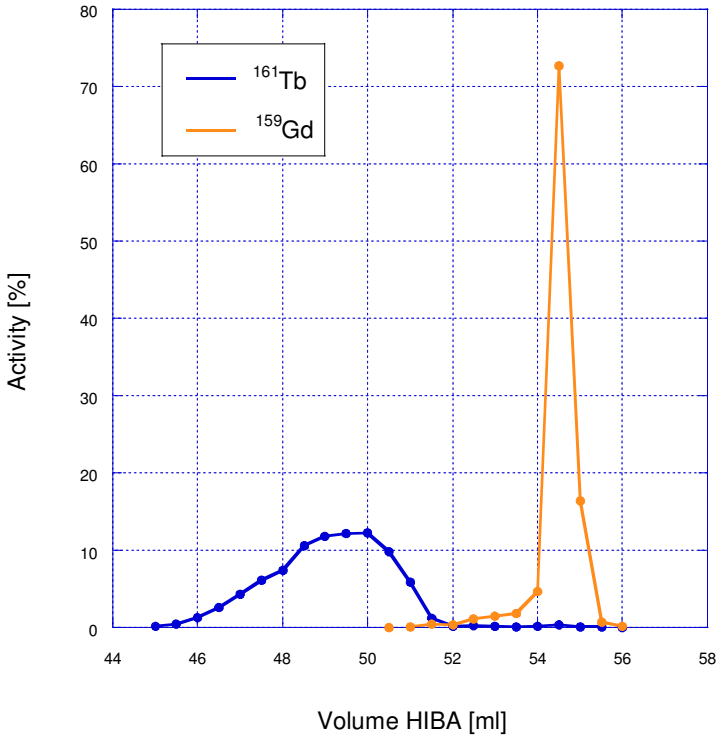

Figure 4-1: Elution profile of the Gd/Tb separation (BioRad, 3.0 mg, 0.12 M).
79.23% of the ^{161}Tb activity could be separated from Gd.
Target mass: 3.0 mg ^{160}Gd, c(α-HIBA): 0.12 M; after 52.0 ml: 0.5 M.
Resin bed length: 16.3 cm, inner diameter: 0.5 cm, resin: BioRad AG W50-X8.
Column efficiency: 15.3 mg/cm^2.

After 45.0 ml, the elution of ^{161}Tb begins. The range from 48.0 – 50.0 ml (volume = 2.0 ml) contains most of the activity. The ^{159}Gd-activity starts to elute after 50.0 ml. The main activity is contained in the fractions eluted after 54.0 ml (volume = 0.5 ml). 79.23% of the overall measured ^{161}Tb activity could be separated without any detectable content of ^{159}Gd.

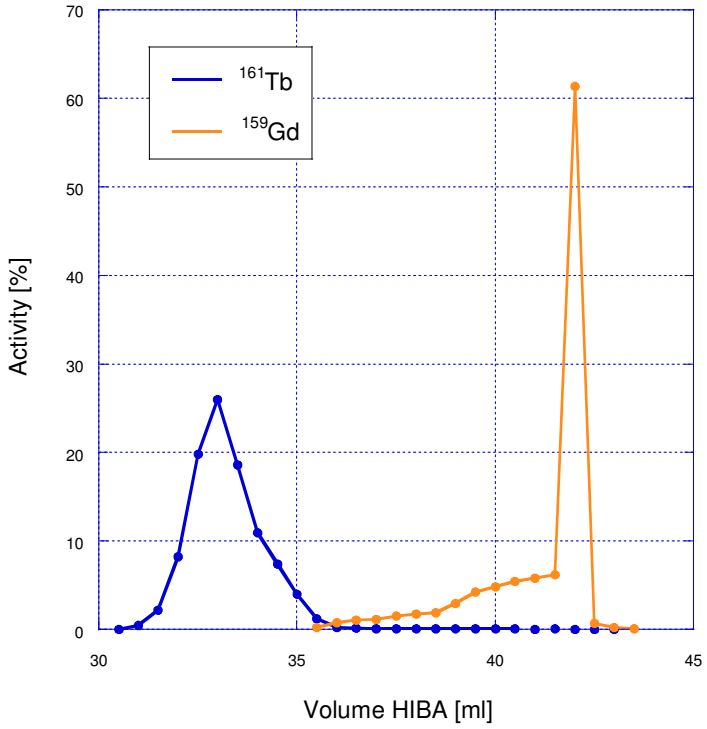

Figure 4-2: Elution profile of the Gd/Tb separation (BioRad, 3.0 mg, 0.13 M).
97.57% of the ^{161}Tb activity could be separated from Gd.
Target mass: 3.0 mg ^{160}Gd, c(α-HIBA): 0.13 M; after 39.0 ml: 0.5 M.
Resin bed length: 16.3 cm, inner diameter: 0.5 cm, resin: BioRad AG W50-X8.
Column efficiency: 15.3 mg/cm^2.

With 0.13 M HIBA-solution, it was possible to obtain 97.57% of the total measured ^{161}Tb activity without any measurable ^{159}Gd. ^{161}Tb starts to be eluted after 29.5 ml and has its main peak at 31.5 – 34.0 ml (volume = 2.5 ml). After 34.5 ml, ^{159}Gd is eluted. Most of the ^{159}Gd activity is contained in the fraction at 44.0 ml (volume = 0.5 ml).

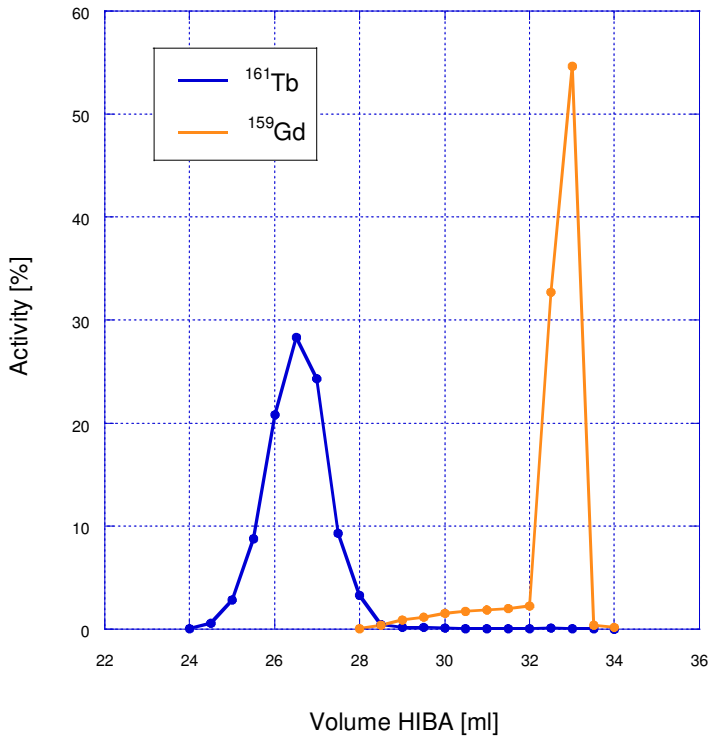

Figure 4-3: Elution profile of the Gd/Tb separation (BioRad, 3.0 mg, 0.14 M).
95.03% of the ^{161}Tb activity could be separated from Gd.
Target mass: 3.0 mg ^{160}Gd, c(α-HIBA): 0.14 M; after 31.0 ml: 0.5 M.
Resin bed length: 16.3 cm, inner diameter: 0.5 cm, resin: BioRad AG W50-X8.
Column efficiency: 15.3 mg/cm^2.

After 24.5 ml, the elution of ^{161}Tb sets in. The range from 26.5 – 28.5 ml (volume = 2.0 ml) contains most of the activity. The ^{159}Gd-activity starts to elute after 28.5 ml. The main activity is contained in the fractions eluted at 33.5 and 34.0 ml (volume = 1.0 ml). 95.03% of the total measured ^{161}Tb activity could be separated without any detectable content of ^{159}Gd.

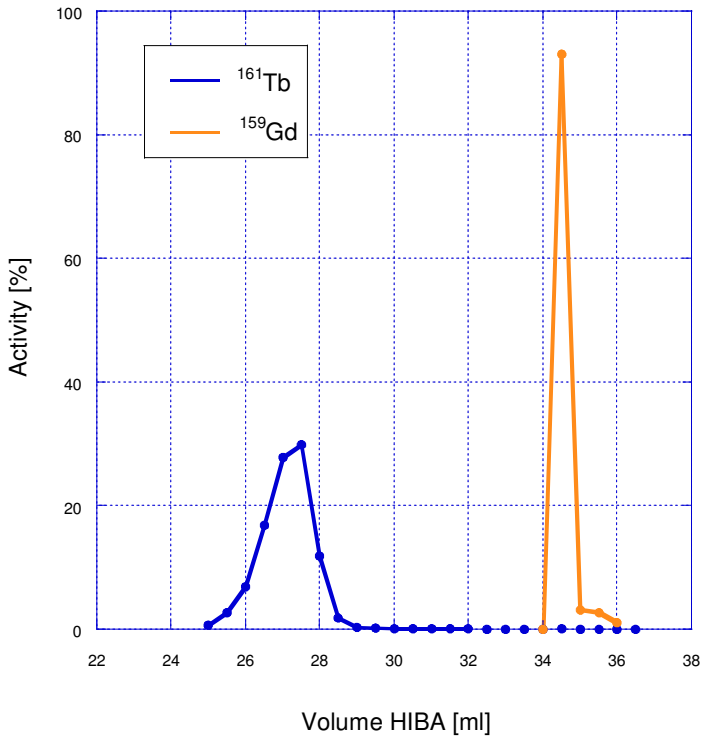

Figure 4-4: Elution profile of the Gd/Tb separation (BioRad, 5.0 mg, 0.14 M).
96.66% of the ^{161}Tb activity could be separated from Gd.
Target mass: 5.0 mg ^{160}Gd, c(α-HIBA): 0.14 M; after 31.5 ml: 0.5 M.
Resin bed length: 16.3 cm, inner diameter: 0.5 cm, resin: BioRad AG W50-X8.
Column efficiency: 25.5 mg/cm^2.

96.66% of the total measured ^{161}Tb activity was separated without any measurable ^{159}Gd content. After 25.0 ml ^{161}Tb starts to elute. The main activity is contained in the fractions at 26.0 – 27.5 ml (volume = 1.5 ml). ^{159}Gd is eluted after 34.0 ml and has its main peak at 34.5 and 35.0 ml (volume = 1.0 ml).

With a higher concentration of α-HIBA less volume is required to start the elution of the lanthanides. It can be seen clearly that the activity peak of ^{161}Tb also decreases; consequently the radiometal is solved in a reduced amount of solution, which makes it easier to evaporate the solvent afterwards.

Additionally, the Tb-fraction is contaminated with less Gd if a higher concentration is used. It seems like Tb is eluted even faster with a higher concentration of α-HIBA in the solution than Gd. This can especially be seen in Figure 4-1 and Figure 4-3. If the target mass is increased as well, the micro amounts of Tb can be separated from the macro amounts of Gd even better (Figure 4-4). Thus, it can be concluded that a smaller mass

of lanthanide is eluted faster and it takes more and more time to elute the element if the mass increases.

4.2.2 Resin: macroporous cation exchange resin

The first column filled with macroporous cation exchange resin has a resin bed length of 17.3 cm. The theoretical column efficiency for Ln^{3+} of this column was 1.92 mmol.

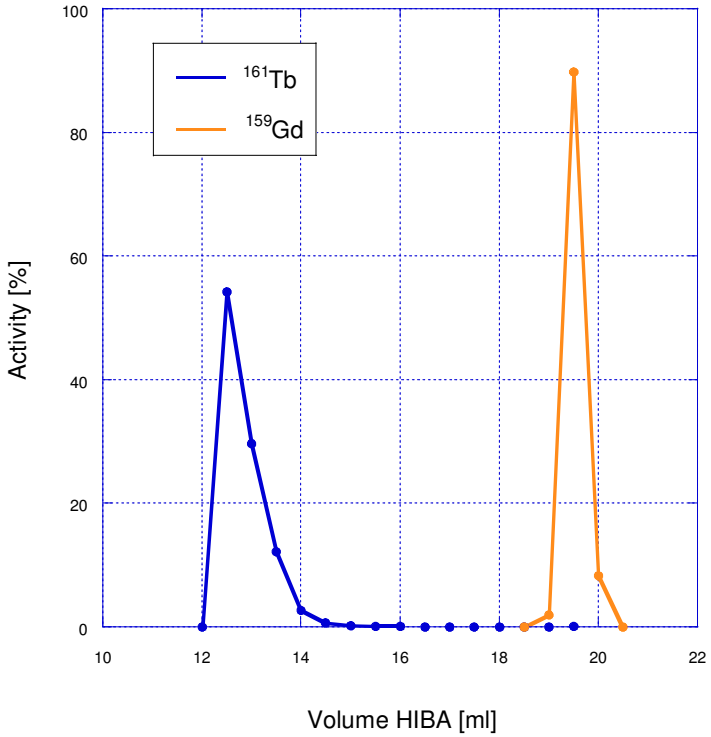

Figure 4-5: Elution profile of the Gd/Tb separation (macroporous resin, 5.0 mg, 0.14 M).
99.90% of the ^{161}Tb activity could be separated from Gd.
Target mass: 5.0 mg ^{160}Gd, c(α-HIBA): 0.14 M; after 17.0 ml: 0.5 M.
Resin bed length: 17.3 cm, inner diameter: 0.5 cm, resin: macroporous cation exchange resin.
Column efficiency: 25.5 mg/cm^2.

With the macroporous cation exchange resin, ^{161}Tb elution sets in at less than 12.0 ml elution volume. The main activity is approximately in the fractions 12.5 and 13.0 ml (volume = 1.0 ml). After 18.0 ml ^{159}Gd is eluted with most of the activity at 19.5 ml (volume = 0.5 ml). With this separation it was possible to separate 99.90% of the total measured ^{161}Tb activity without any detectable ^{159}Gd.

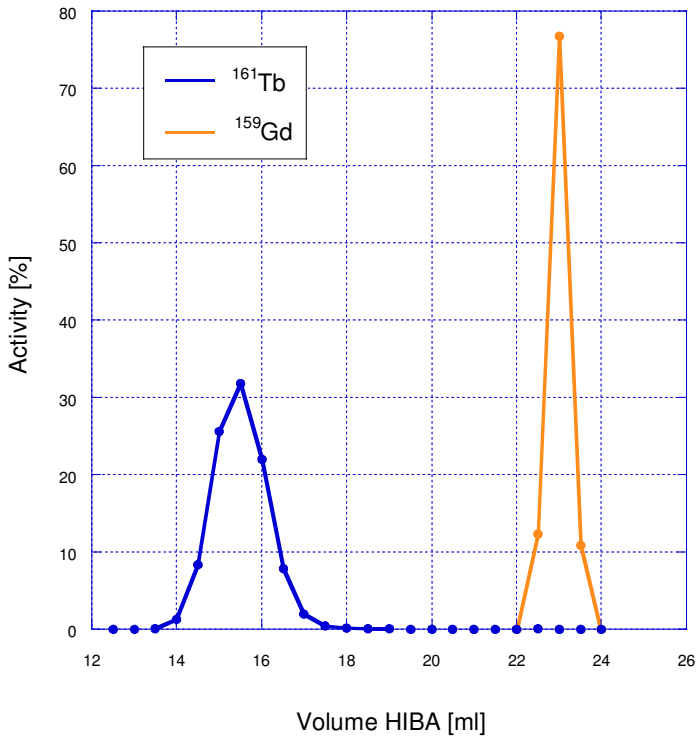

Figure 4-6: Elution profile of the Gd/Tb separation (macroporous resin, 5.0 mg, 0.13 M).
99.99% of the ^{161}Tb activity could be separated from Gd.
Target mass: 5.0 mg ^{160}Gd, c(α-HIBA): 0.13 M; after 20.0 ml: 0.5M.
Resin bed length: 17.3 cm, inner diameter: 0.5 cm, resin: macroporous cation exchange resin.
Column efficiency: 25.5 mg/cm^2.

This separation yielded 99.99% of the total measured ^{161}Tb activity without any measurable ^{159}Gd. ^{161}Tb elution starts after 12.0 ml and has its main peak at 15.0 – 16.0 ml (volume = 1.0 ml). After 21.5 ml ^{159}Gd is eluted. Most of the ^{159}Gd activity is contained in the fraction at 23.0 ml (volume = 0.5 ml).

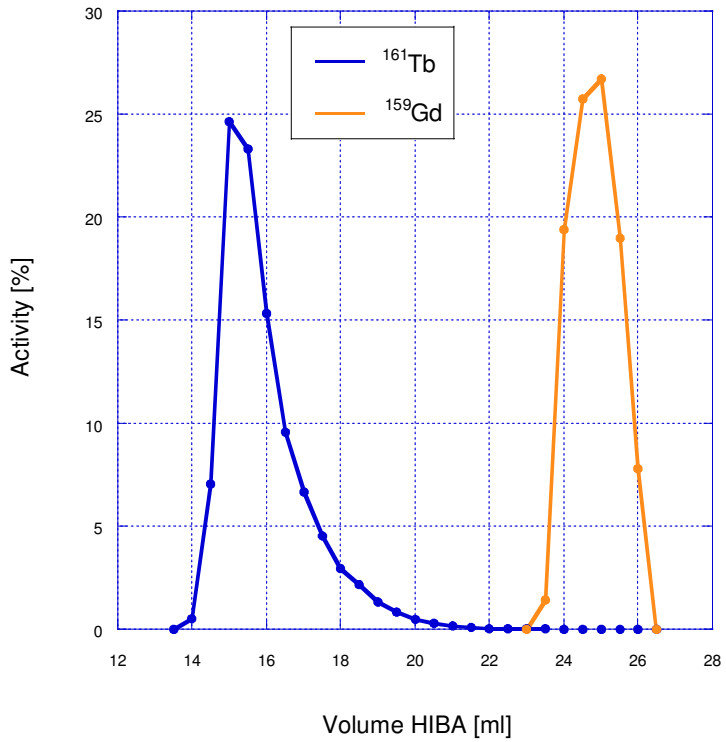

Figure 4-7: Elution profile of the Gd/Tb separation (macroporous resin, 20.0 mg, 0.13 M).
99.78% of the ^{161}Tb activity could be separated from Gd.
Target mass: 20.0 mg ^{160}Gd, c(α-HIBA): 0.13 M; after 21.0 ml: 0.5 M.
Resin bed length: 17.3 cm, inner diameter: 0.5 cm, resin: macroporous cation exchange resin.
Column efficiency: 102.0 mg/cm^2.

After 13.0 ml the elution of ^{161}Tb begins. The range from 14.5 – 17.0 ml (volume = 2.5 ml) contains most of the activity. The ^{159}Gd-activity starts to elute after 22.5 ml. The main activity is contained in the fractions 24.0 – 26.0 ml (volume = 2.0 ml). 99.78% of the total measured ^{161}Tb activity could be separated without any detectable content of ^{159}Gd.

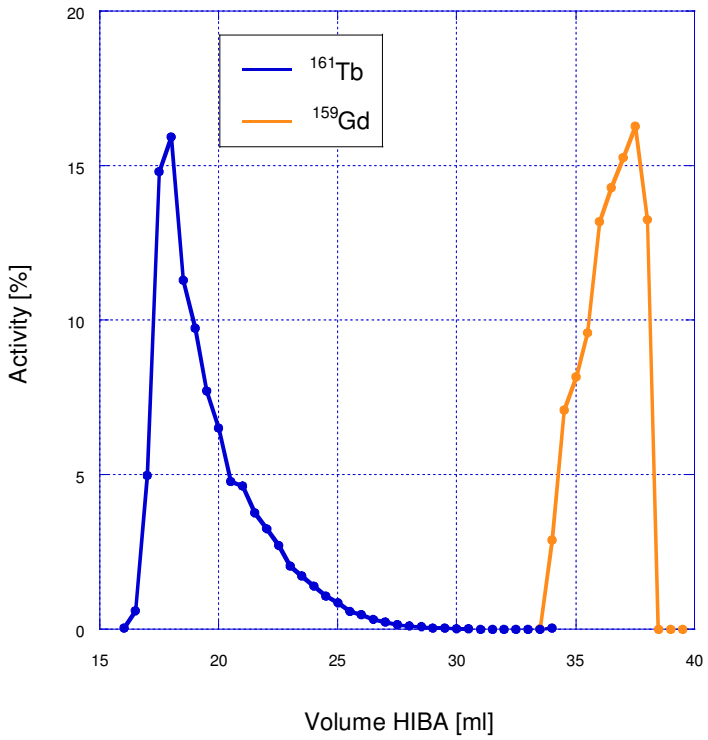

Figure 4-8: Elution profile of the Gd/Tb separation (macroporous resin, 40.0 mg, 0.13 M).
99.96% of the ^{161}Tb activity could be separated from Gd.
Target mass: 40.0 mg ^{160}Gd, c(α-HIBA): 0.13 M; after 30.0 ml: 0.5 M.
Resin bed length: 17.3 cm, inner diameter: 0.5 cm, resin: macroporous cation exchange resin.
Column efficiency: 204.0 mg/cm^2.

99.96% of the total measured ^{161}Tb activity without any measurable ^{159}Gd could be separated. After 15.5 ml ^{161}Tb starts to elute. The main activity is contained in the fractions at 17.5 – 22.0 ml (volume = 4.5 ml). ^{159}Gd is eluted after 33.0 ml and has its main peak at 35.0 – 38.0 ml (volume = 3.0 ml).

By using the macroporous exchange resin the elution proceeds faster than with the BioRad resin (Figure 4-2). The Tb peak is eluted at about 14.0 – 17.0 ml (Figure 4-6) with the macroporous exchange resin and at about 31.0 – 35.0 ml with the BioRad resin. The target mass in this experiments was not the same (3.0 mg for the BioRad resin and 5.0 mg for the macroporous exchange resin) but it is not expected that a difference of 2 mg would cause a huge discrepancy.

By increasing the target mass up to 40.0 mg the Tb peak broadens and the activity is eluted in a larger volume. Also the elution starts later (14.0 ml at 20.0 mg, 15.5 ml at 40.0 mg).

In addition, a difference in the elution profile can be seen by using different concentrations of α-HIBA compared to the separations with the BioRad resin. By using 0.14 M the Tb activity is eluted from about 12.0 – 14.0 ml (Figure 4-5), by using 0.13 M from 14.0 – 17.0 ml (Figure 4-6).

The following experiments have been performed with a resin bed length of 14.3 cm.

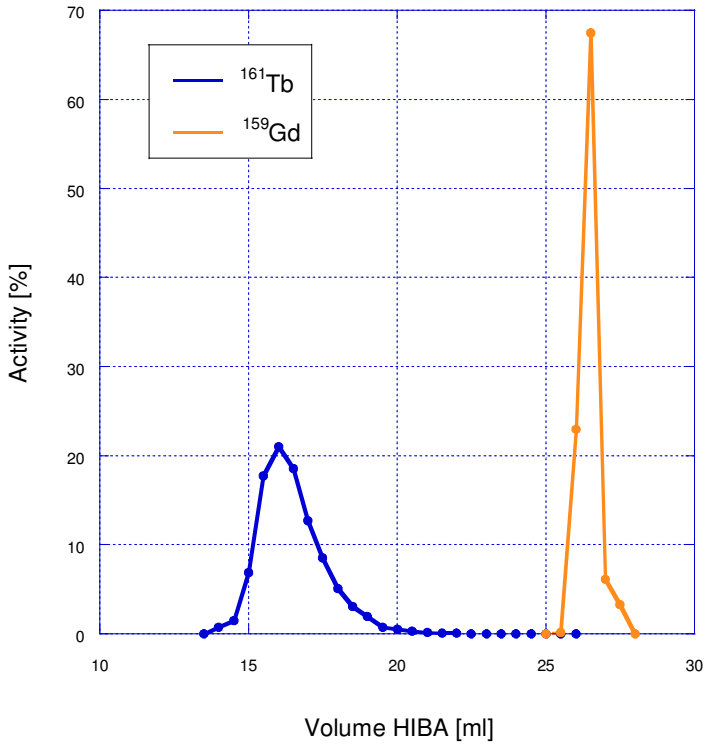

Figure 4-9: Elution profile of the Gd/Tb separation (macroporous resin, 10.0 mg, 0.13 M, 14.3 cm).
99.99% of the ^{161}Tb activity could be separated from Gd.
Target mass: 10.0 mg ^{160}Gd, c(α-HIBA): 0.13 M; after 23.0 ml: 0.5 M.
Resin bed length: 14.3 cm, inner diameter: 0.5 cm, resin: macroporous cation exchange resin.
Column efficiency: 51.0 mg/cm^2.

Within this separation it was possible to obtain 99.99% of the total measured ^{161}Tb activity without any measurable ^{159}Gd. ^{161}Tb starts to be eluted after 13.5 ml and has its main peak at 16.0 – 18.5 ml (volume = 2.5 ml). After 25.0 ml ^{159}Gd is eluted. Most of the ^{159}Gd activity is contained in the fraction at 26.5 and 27.0 ml (volume = 1.0 ml).

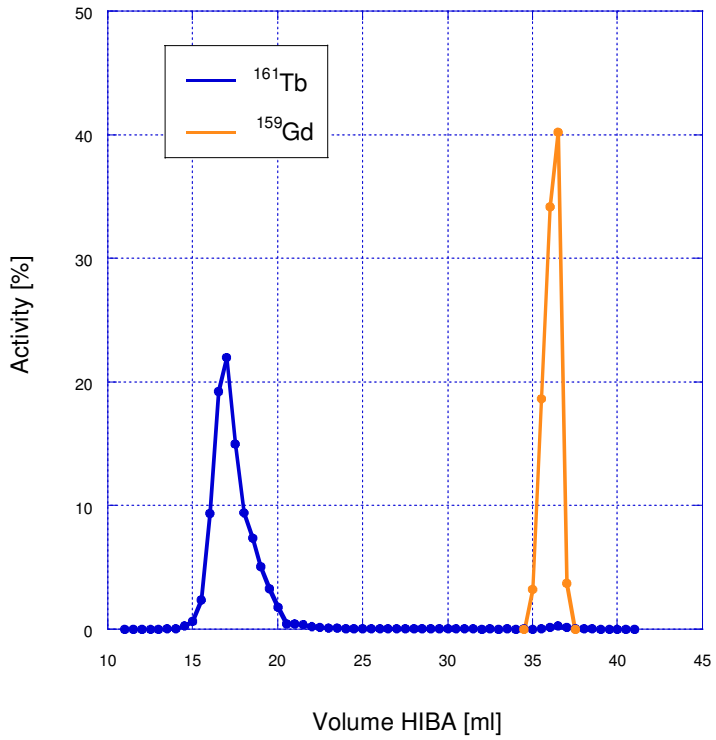

Figure 4-10: Elution profile of the Gd/Tb separation (macroporous resin, 20.0 mg, 0.13 M, 14.3 cm).
99.58% of the ^{161}Tb activity could be separated from Gd.
Target mass: 20.0 mg ^{160}Gd, c(α-HIBA): 0.13 M; after 35.5 ml: 0.5 M.
Resin bed length: 14.3 cm, inner diameter: 0.5 cm, resin: macroporous cation exchange resin.
Column efficiency: 102.0 mg/cm^2.

99.58% of the total measured ^{161}Tb activity without any measurable ^{159}Gd could be separated. After 10.0 ml ^{161}Tb starts to elute. The main activity is contained in the fractions at 16.0 – 19.0 ml (volume = 3.0 ml). ^{159}Gd is eluted after 34.0 ml and has its main peak at 36.5 and 37.0 ml (volume = 1.0 ml).

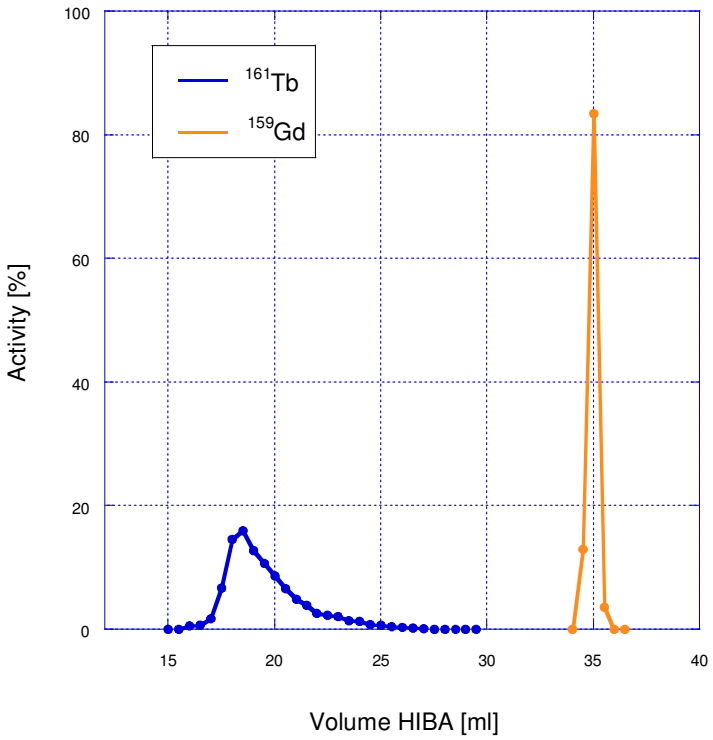

Figure 4-11: Elution profile of the Gd/Tb separation (macroporous resin, 40.0 mg, 0.13 M, 14.3 cm).
99.99% of the ^{161}Tb activity could be separated from Gd.
Target mass: 40.0 mg ^{160}Gd, c(α-HIBA): 0.13 M; after 26.0 ml: 0.5 M.
Resin bed length: 14.3 cm, inner diameter: 0.5 cm, resin: macroporous cation exchange resin.
Column efficiency: 204.0 mg/cm^2.

Within this separation it was possible to obtain 99.99% of the total measured ^{161}Tb activity without any measurable ^{159}Gd. ^{161}Tb starts to be eluted after 14.5 ml and has its main peak at 17.0 – 21.5 ml (volume = 4.5 ml). After 34.0 ml ^{159}Gd is eluted. Most of the ^{159}Gd activity is contained in the fraction at 34.5 and 35.0 ml (volume = 1.0 ml).

Using a shorter column (14.3 instead of 17.3 cm) of macroporous exchange resin also leads to good results in Tb/Gd separation. With a target mass of 20.0 mg there is a slight difference in the volume of α-HIBA that is required for the separation, 16.0 – 19.0 ml for 14.3 cm column length and 14.5 – 17.0 ml for 17.3 cm, respectively. At a target mass of 40.0 mg the used volume has almost the same amount of 17.0 – 21.5 ml for 14.3 cm column length and 17.5 – 22.0 ml for 17.3 cm. This small discrepancy cannot be sufficiently associated with the shortening of the used column.

A smaller resin bed leads to a decrease in interactions between the lanthanides and the ions of the resin. Nevertheless, the kinetics seem to be fast enough to provide an

efficient separation. Thus, a reduction of the column length from 17.3 to 14.3 cm does not interfere with the result of the separation.

4.2.3 Resin: AMINEX A6, resin bed length: 14.3 cm

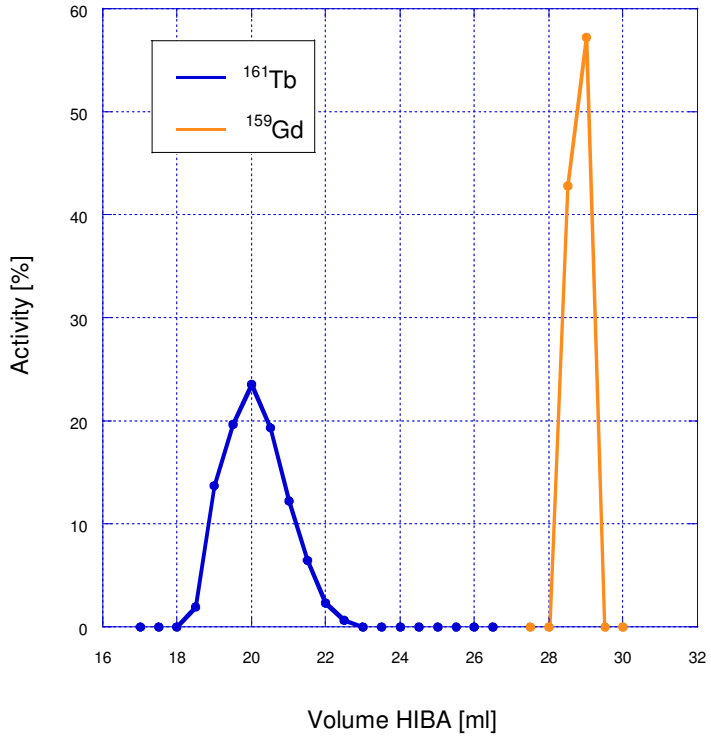

Figure 4-12: Elution profile of Gd/Tb separation (AMINEX, 5.0 mg, 0.13 M).
99.99% of the ^{161}Tb activity could be separated from Gd.
Target mass: 5.0 mg ^{160}Gd, c(α-HIBA): 0.13 M; after 25.0 ml: 0.5 M.
Resin bed length: 14.3 cm, inner diameter: 0.5 cm, resin: AMINEX A6.
Column efficiency: 25.5 mg/cm^2.

It was possible to obtain 99.99% of the total measured ^{161}Tb activity without any measurable ^{159}Gd. After 10.0 ml ^{161}Tb starts to elute. The main activity is contained in the fractions at 19.0 – 22.0 ml (volume = 3.0 ml). ^{159}Gd is eluted after 28.0 ml and has its main peak at 28.5 and 29.0 ml (volume = 1.0 ml).

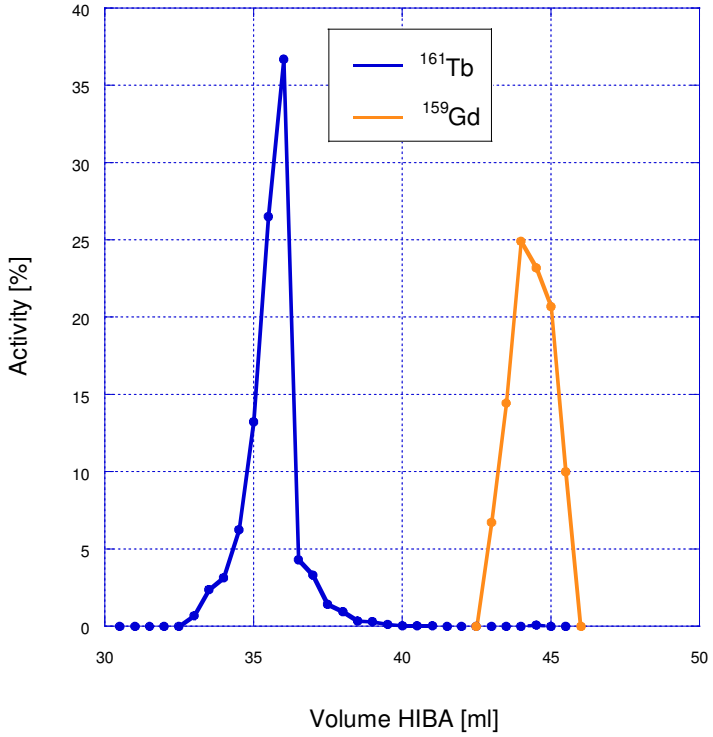

Figure 4-13: Elution profile of Gd/Tb separation (AMINEX, 20.0 mg, 0.13 M).
99.89% of the ^{161}Tb activity could be separated from Gd.
Target mass: 20.0 mg ^{160}Gd, c(α-HIBA): 0.13 M; after 40.5 ml: 0.5 M.
Resin bed length: 14.3 cm, inner diameter: 0.5 cm, resin: AMINEX A6 .
Column efficiency: 102.0 mg/cm^2.

After 30.0 ml the elution of ^{161}Tb begins. The range from 34.5 – 37.0 ml (volume = 2.5 ml) contains most of the activity. The ^{159}Gd-activity starts to elute after 43.0 ml. The main activity is contained in the fractions 44.0 – 45.5 ml (volume = 1.5 ml). 99.8% of the overall measured ^{161}Tb activity could be separated without any detectable content of ^{159}Gd.

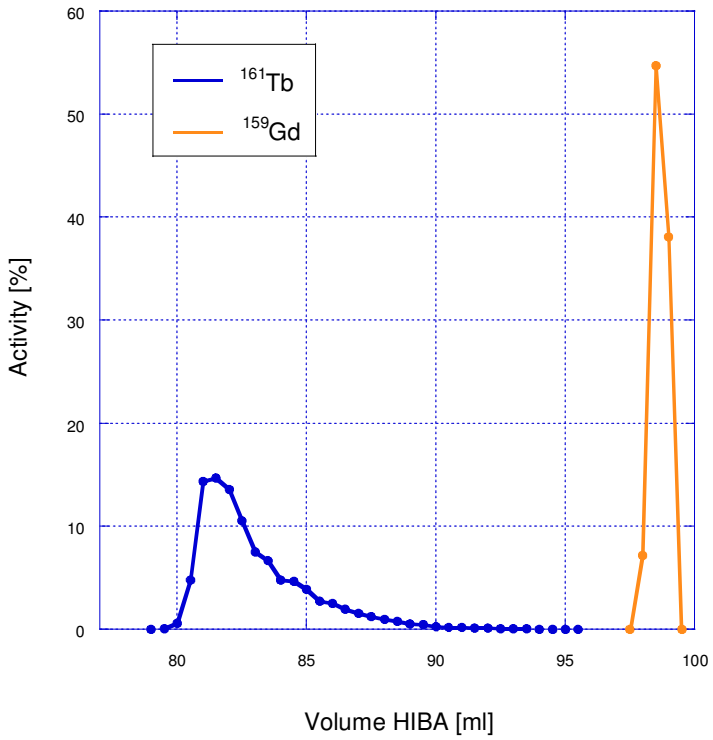

Figure 4-14: Elution profile of Gd/Tb separation (AMINEX, 40.0 mg, 0.13 M).
99.99% of the ^{161}Tb activity could be separated from Gd.
Target mass: 40.0 mg ^{160}Gd, c(α-HIBA): 0.13 M; after 90.0 ml: 0.5 M.
Resin bed length: 14.3 cm, inner diameter: 0.5 cm, resin: AMINEX A6.
Column efficiency: 204.0 mg/cm^2.

99.99% of the total measured ^{161}Tb activity without any measurable ^{159}Gd could be separated. After 78.0 ml ^{161}Tb starts to elute. The main activity is contained in the fractions at 80.5 – 85.0 ml (volume = 4.5 ml). ^{159}Gd is eluted after 96.5 ml and has its main peak at 99.0 and 99.5 ml (volume = 1.0 ml).

Using the AMINEX resin, the separations display the same characteristics as with the BioRad or the macroporous exchange resin. Also, with a higher target mass the lanthanides are eluted later and the Tb peak gets broader, which leads to a greater volume in which the activity is contained. A remarkable change can be observed in the volume of α-HIBA required to elute ^{161}Tb. The use of the macroporous exchange resin and a column of 14.3 cm length after 10.0 ml allows a detection of Tb (Figure 4-10). With the AMINEX resin 30.0 ml is needed (Figure 4-13). Likewise, with a target mass of 40.0 mg Tb is eluted after 15.0 ml using the macroporous resin (Figure 4-11) and after 78.0 ml with the AMINEX resin (Figure 4-14). However, with both resins

approximately the same volume of eluent containing the main activity of ^{161}Tb was needed (1.5 ml at 20 mg target mass, 4.5 ml at 40.0 mg target mass).

4.2.4 Elution of ^{161}Tb dependent on the resin

Figure 4-15 shows the elution profile of the Tb/Gd separation dependent on the used resin. The resin from macroporous cation exchange resin was compared with the BioRad and the AMINEX resin.

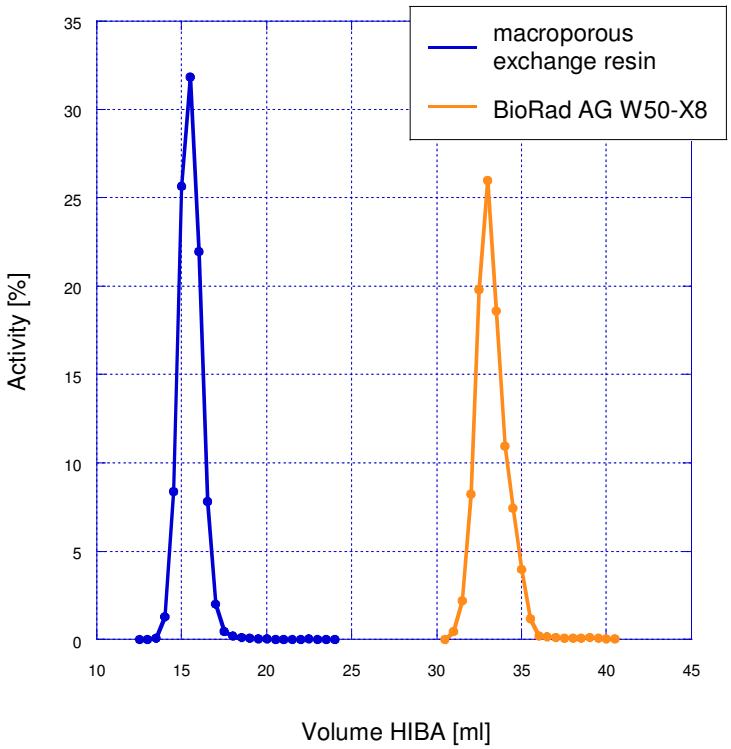

Figure 4-15: Comparison of the ^{161}Tb elution dependent to the resin.
Target mass: 5.0 mg ^{160}Gd, c(α-HIBA): 0.14 M.
Orange line: macroporous cation exchange resin, 17.3 cm resin bed.
Yellow line: BioRad AG 50W-X8, 17.3 cm resin bed.

Figure 4-15 shows the dependency of the ^{161}Tb elution profile on the used cation exchange resin. By using the macroporous cation exchange resin, the main ^{161}Tb activity is eluted from 13.0 – 14.0 ml (volume = 1.0 ml) and with the BioRad resin from 26.0 – 29.0 ml (volume = 3.0 ml). The highest value for the Tb peak is 54% with the macroporous cation exchange resin and 31% with the BioRad resin.

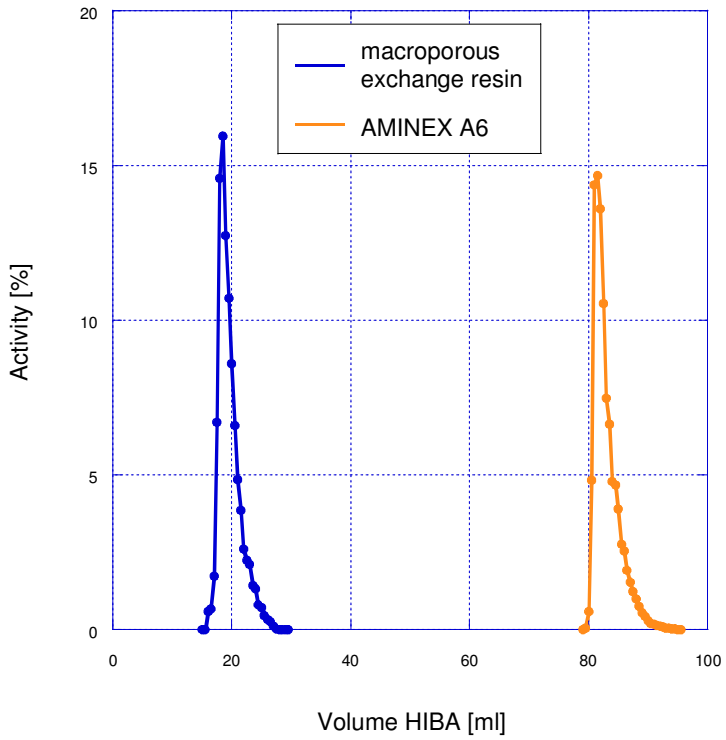

Figure 4-16: Comparison of the ^{161}Tb elution dependent to the resin.
Target mass: 5.0 mg ^{160}Gd, c(α-HIBA): 0.13 M.
Blue line: macroporous cation exchange resin, 16.3 cm resin bed.
Orange line: AMINEX resin, 16.3 cm resin bed.

The Tb-elution with the macroporous cation exchange resin compared to the AMINEX resin is shown in Figure 4-16. The main ^{161}Tb activity is eluted from 14.5 – 16.5 ml (volume = 2.0 ml) with the macroporous cation exchange resin and from 32.0 – 34.5 ml (volume = 2.5 ml) with the AMINEX resin. The highest peak value is 31.8% with the macroporous cation exchange resin and 28.1% with the AMINEX resin.

If the macroporous cation exchange resin is used the Tb-fraction is eluted earlier and the radiometal is solved in a smaller eluent volume than by using BioRad or AMINEX resin. Thus the macroporous cation exchange resin allows a faster separation of Gd and Tb and, due to the fact that less eluent is required, also the evaporation of the solvent is done in a shorter time. A reason for the faster elution of Tb with the macroporous cation exchange resin might be the cross linking of 16% compared to 8% for the BioRad and the AMINEX resin (Table 3-3). As a result, for production of ^{161}Tb for labeling experiments the macroporous cation exchange resin was used.

Shortening the macroporous exchange resin bed from 17.3 to 14.3 cm doesn't make any difference in the elution profile. So for further experiments a resin bed of 14.3 cm is used.

4.2.5 Elution of ^{161}Tb dependent on the concentration of the eluent

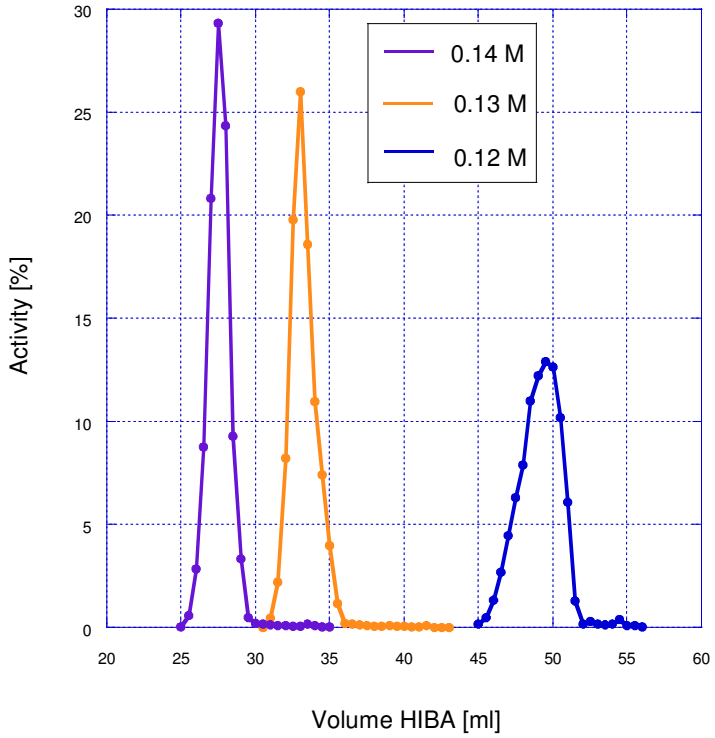

Figure 4-17: Comparison of the ^{161}Tb elution dependent to concentration of the eluent. Target mass: 3.0 mg ^{160}Gd, resin: BioRad AG W50-X8, resin bed length: 16.3 cm. Violet line: 0.14 M α-HIBA, orange line: 0.13 M α-HIBA, blue line: 0.12 M α-HIBA.

Figure 4-17 depicts that with 0.14 M α-HIBA the main ^{161}Tb activity is eluted from 5.0 – 11.0 ml (volume = 6 ml), with 0.13 M α-HIBA from 17.0 – 24.0 ml (volume = 7.0 ml) and with 0.12 M α-HIBA from 46.0 – 55.0 ml (volume = 9.0 ml). The highest peak value is 30% at 0.14 M, 26% at 0.13 M and 13% at 0.12 M.

Tb is eluted earlier when the concentration of α-HIBA increases. In addition, the peak is smaller and therefore the lanthanide is eluted in less volume. Even higher concentrations than 0.14 M might be appropriate but, if the concentration exceeds a certain value, Gd will be eluted earlier and the Tb-fraction overlaps with the Gd-

fraction. Accordingly, for the following ^{161}Tb productions a concentration of α-HIBA of 0.13 M was chosen.

4.2.6 Elution of ^{161}Tb dependent on the target mass

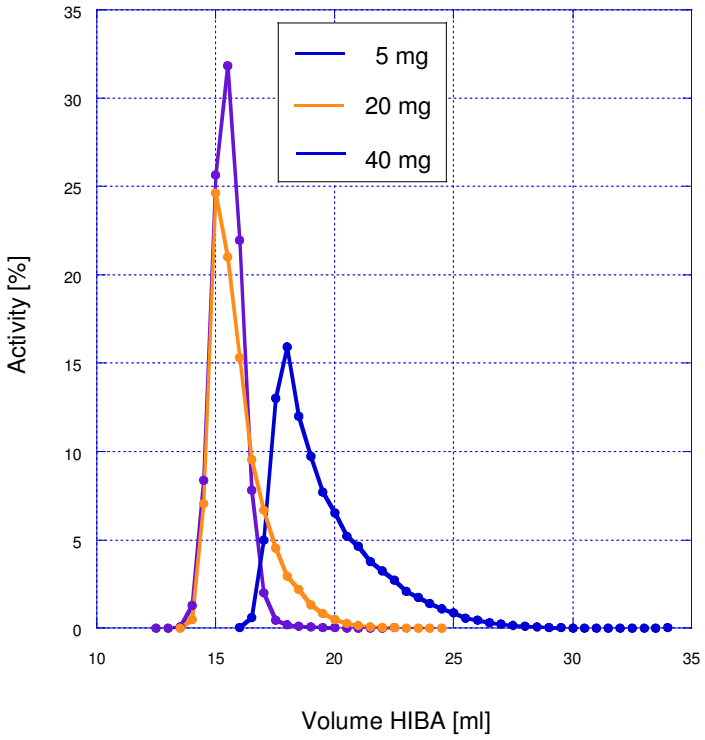

Figure 4-18: Comparison of the ^{161}Tb elution dependent to the target mass.
Resin: macroporous cation exchange resin, resin bed length: 17.3 cm, c(α-HIBA): 0.13 M.
Violet line: 5.0 mg ^{160}Gd, orange line: 20.0 mg ^{160}Gd,
blue line: 40.0 mg ^{160}Gd.

According to 4.2.2 at the lowest target mass, 5.0 mg, the main ^{161}Tb activity is eluted from 15.0 – 17.0 ml (volume = 2.0 ml), 20.0 mg target mass is eluted from 15.0 – 18.0 ml (volume = 3.0 ml) and the highest target mass, 40.0 mg, from 17.0 – 23.0 ml (volume = 6.0 ml). The highest peak value is 32% at 5.0 mg, 25% at 20.0 mg and 16% at 40.0 mg.

With increasing lanthanide mass, the elution of Tb sets in later. Furthermore, the peak gets higher and broader, consequently Tb is eluted in a larger volume. At a target mass of 40.0 mg, the elution profile shows a distinct peak tailing. With an even higher target mass an overlap of the Tb- and Gd-fraction might be observed. As a result, this column was used for separation of Tb and Gd with a target mass up to 40 mg.

4.3 Elution profile of the Dy/Gd separation

In addition, the behavior of Dy(III) in the system was studied by processing an irradiated sample containing a mixture of 10.0 mg ^{160}Gd and 0.2 mg ^{nat}Dy. The obtained elution profile is presented in Figure 4-19. The fraction of Dy is eluted first after about 10.0 ml (~ 7 FCV). Finally, a fraction of ^{161}Tb could be obtained with a Dy content reduced by a factor > 10^2.

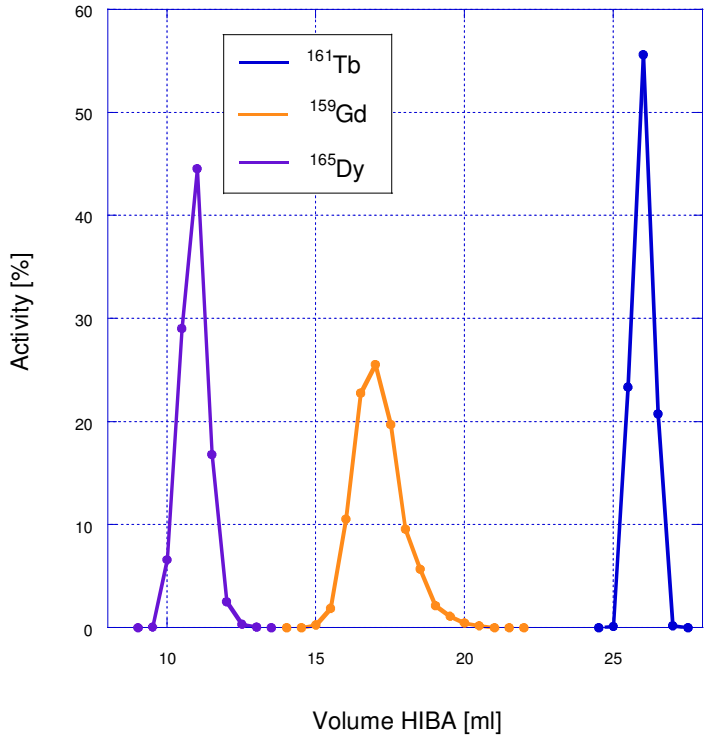

Figure 4-19: Elution profile of the Dy/Gd/Tb separation (macroporous resin, 3.0 mg, 0.13 M).
99.9% of the ^{161}Tb activity could be separated from Gd.
Target mass: 3.0 mg ^{160}Gd + 0.2 mg Dy, c(α-HIBA): 0.13 M; after 22.5 ml: 0.5 M.
Resin bed length: 17.3 cm, inner diameter: 0.5 cm, resin: macroporous cation exchange resin.
Column efficiency: 102.0 mg/cm^2.

^{165}Dy is eluted after 8.5 ml with its main activity at 10.5 – 11.5 ml (volume = 1.0 ml). Before the first ^{161}Tb activity was detectable, no ^{165}Dy could be measured in the fractions any more. ^{161}Tb is eluted after 13.5 ml with the main activity peaks at 16.5 – 18.0 ml (volume = 1.5 ml) and ^{159}Gd is eluted after 24.0 ml with the main activity at

26.0 ml (volume = 0.5 ml). 100.0% of the whole ^{161}Tb activity could be separated without any detectable ^{159}Gd.

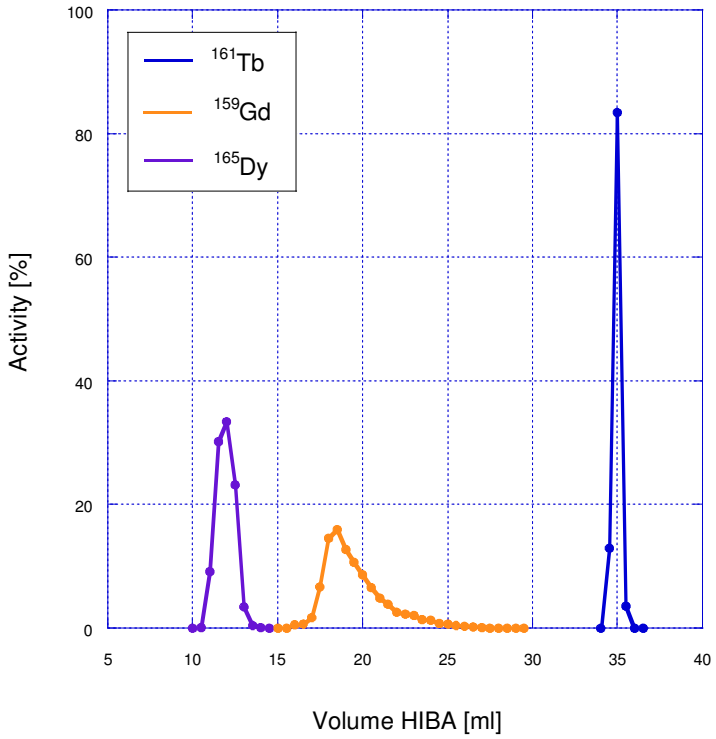

Figure 4-20: Elution profile of the Dy/Gd/Tb separation (macroporous resin, 40.0 mg, 0.13 M).
100.0% of the ^{161}Tb activity could be separated from Gd.
Target mass: 40.0 mg ^{160}Gd + 0.2 mg Dy, c(α-HIBA): 0.13 M; after 30.5 ml: 0.5 M.
Resin bed length: 16.3 cm, inner diameter: 0.5 cm, resin: macroporous cation exchange resin.
Column efficiency: 102.0 mg/cm^2.

With a target mass of 40.0 mg ^{165}Dy is eluted after 10.0 ml with its main activity at 10.5 – 13.0 ml (volume = 2.5 ml). In the first fraction of ^{161}Tb there was no ^{165}Dy measurable. ^{161}Tb is eluted after 15.0 ml with the main peaks at 17.5 – 21.0 ml (volume = 3.5 ml) and ^{159}Gd is eluted after 34.0 ml with the main activity at 35.0 ml (volume = 0.5 ml). 100.0% of the whole ^{161}Tb activity could be separated without any detectable ^{159}Gd.

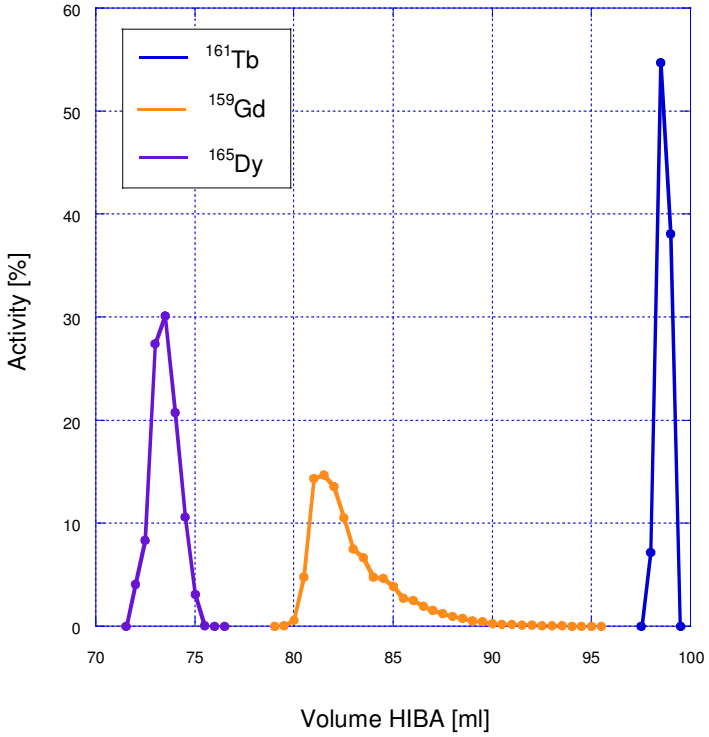

Figure 4-21: Elution profile of the Dy/Gd/Tb separation (AMINEX, 40.0 mg, 0.13 M).
100.0% of the ^{161}Tb activity could be separated from Gd.
Target mass: 400 mg ^{160}Gd + 0.2 mg Dy, c(α-HIBA): 0.13 M; after 96.5 ml: 0.5 M.
Resin bed length: 16.3 cm, inner diameter: 0.5 cm, resin: AMINEX.
Column efficiency: 102.0 mg/cm^2.

As with the other resins, by using the AMINEX resin, Dy can be separated completely from Tb. ^{165}Dy is eluted after 71.7 ml with its main activity at 72.0 – 73.0 ml (volume = 1.0 ml). No ^{165}Dy could be measured any more before the first fraction containing ^{161}Tb was eluted. ^{161}Tb is eluted after 78.5 ml with the main peaks at 80.5 – 85.0 ml (volume = 4.5 ml) and ^{159}Gd is eluted after 98.5 ml with the main activity at 99.5 ml (volume = 0.5 ml). 100.0% of the overall ^{161}Tb activity could be separated without any detectable ^{159}Gd.

Because of the further processing of the ^{161}Tb activity it is desirable to handle a volume as small as possible. Also, the separation has to be efficient and no Gd or Dy contamination should be detectable in the Tb fraction. In addition, for clinical routine, the separation is supposed to be performed in a short time period. Consequently, for all further productions of ^{161}Tb a column with 14.3 cm length, filled with the macroporous

exchange resin and an α-HIBA concentration of 0.13 M for a target mass up to 40 mg ^{160}Gd was used.

Table 4-2: Comparison of the ^{161}Tb and ^{160}Gd elution (c_{HIBA}: 0.13 M) from different resins.

resin	target mass [mg]	start elution ^{161}Tb [ml HIBA]	start elution ^{160}Gd [ml HIBA]	total volume main ^{161}Tb-fraction [ml HIBA]	figure
BIORAD AG 50W-X8	3.0	29.5	34.5	2.5	5-2
macroporous cation exchange resin	5.0	12.0	21.5	1.0	5-9
	20.0	10.0	34.0	3.0	5-10
	40.0	14.5	34.0	4.5	5-11
AMINEX A6	5.0	10.0	28.0	3.0	5-12
	20.0	30.0	43.0	2.5	5-13
	40.0	78.0	96.5	4.5	5-14

4.4 Labeling of DOTATATE (DOTA-Tyr^3-octreotate)

4.4.1 Labeling yield as a function of molar ratio and pH-value

Up to 23 GBq of ^{161}Tb could be produced by long-term irradiations of massive ^{160}Gd targets. The targets were processed in the manner described above with the established semi-automated system. The radionuclide was transferred into the chloride form. The complete procedure could be performed within 1.0 – 1.5 days. Finally, up to 16 GBq were obtained in 200 – 300 µl 0.05 M HCl. The activity was used for preparation of ^{161}Tb- DOTA-Tyr^3-octreotate. The yield of the radiolabeling reaction as a function of peptide mass is given in Figure 4-22. DOTA-peptide could be successfully radiolabeled with > 99% yield by incubation of 400 MBq ^{161}Tb and 10 µg of DOTATATE corresponding to a ^{161}Tb to DOTATATE mol ratio of 1:12.

At pH 4.5 the formation of ^{161}Tb-DOTATATE as a function of the molar ratio of ^{161}Tb:DOTATATE (1:6, 1:12 and 1:18) was determined (Figure 4-22).

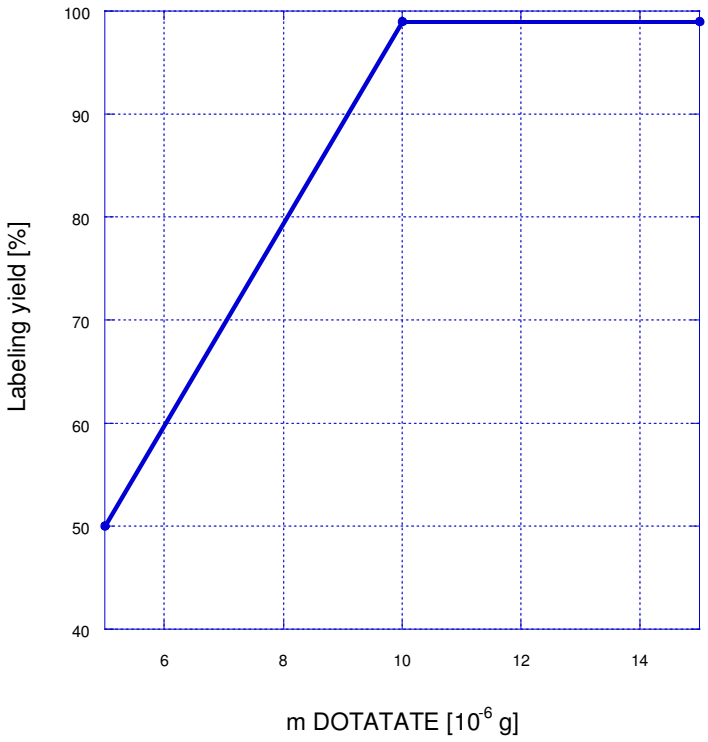

Figure 4-22: Formation of ^{161}Tb-DOTATATE as a function of $m_{(DOTATATE)}$.
Heating for 30 min at 100 °C, measured by TLC.
$A_{(Tb\text{-}161)}$ = 400 MBq per labeling, pH = 4.5, $n_{(Tb\text{-}161)}$:$n_{(DOTATATE)}$ = 1:6 (5 µg DOTATATE), 1:12 (10 µg DOTATATE), 1:18 (15 µg DOTATATE).

With increasing mass of DOTATATE the yield of the ^{161}Tb-DOTATATE formation increases. At about $n_{(Tb\text{-}161)}$: $n_{(DOTATATE)}$ = 1:12 the optimized concentration of DOTATATE is achieved with a yield of 98.9%. An increase of the amount of DOTATATE to $n_{(Tb\text{-}161)}$: $n_{(DOTATATE)}$ = 1:18 leads to an increased yield of 99.16%.

An increase of the peptide above the optimal dose increases the competition of unlabeled and labeled receptor ligand for the same receptor resulting in a lower uptake of the tracer (Breeman, et al., 2003). So a ratio of $n_{(Tb\text{-}161)}$: $n_{(DOTATATE)}$ = 1:12 seems to be ideal.

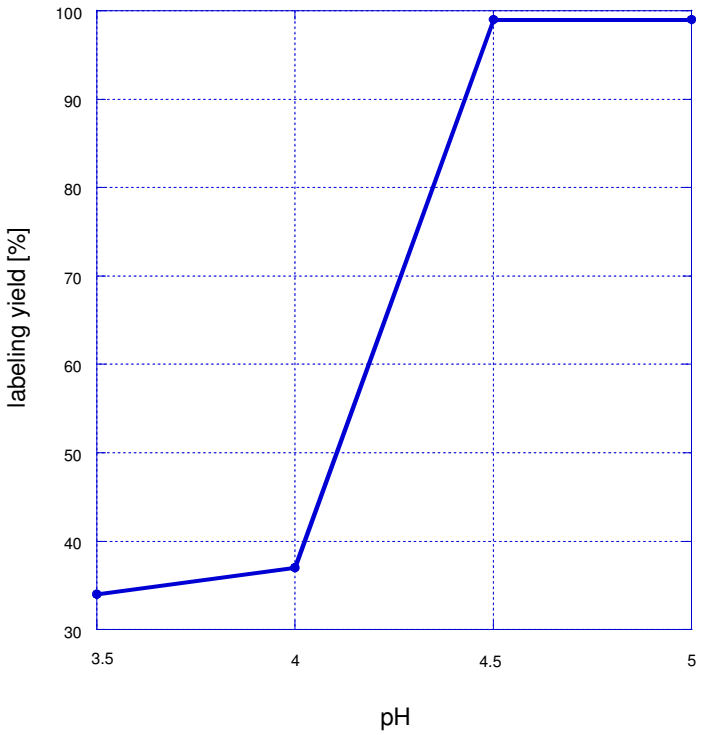

Figure 4-23: Formation of ^{161}Tb-DOTATATE as a function of the pH-value.
Heating for 30 min at 100 °C, measured by TLC.
$A_{(Tb\text{-}161)}$ = 400 MBq per labeling, $m_{(DOTATATE)}$ = 10 µg, $n_{(Tb\text{-}161)}$:$n_{(DOTATATE)}$ = 1:12.

Formation of ^{161}Tb-DOTATATE as a function of pH is presented in Figure 4-23. The highest radiolabeling yield could be achieved at pH 4.5 – 5. Only about 37% and 33% reaction yield was obtained at a pH of the mixture of 3.5 and 3, respectively. This was expected compared to the formation of ^{177}Lu-DOTATATE, with the highest labeling yield > 99% at about pH 4 (Breeman, et al., 2003).

The high specific activity of ^{161}Tb-DOTA-peptide confirms the high quality of the produced radionuclide. Reaction with the commercially available *n.c.a.* ^{177}Lu could be performed with even higher radiolabeling efficiency. Thus, > 99% yield could be achieved already at a 1:5 molar ratio. High radiochemical yields (98.9 ± 0.3%) were obtained for reaction mixtures containing 10 µg of DOTATATE and 7.4 MBq of $^{177}LuCl_3$ employing acetate buffer pH 4.5 as reaction medium as well (Araujo, et al., 2009).

We believe that higher quality and higher specific activity of ^{161}Tb-labeled compounds can be achieved as well by increasing the batch activity resulting in a suppression of general impurities in the system (e.g. Fe(III), Al(III), Pb(II), etc.).

4.4.2 Stability of labeled peptides in human serum

After labeling of DOTA-peptides, the stability of ^{161}Tb- and ^{177}Lu-labeled DOTA-compounds in human serum albumin (20%) at 37 °C was examined over 26 days. The counting rate of bound radiometal was controlled via γ-spectroscopy (Table 4-3).

Table 4-3: Stability of ^{161}Tb- and ^{177}Lu-labeled DOTA-compounds in human serum albumin (20%) at 37 °C.

time [d]	^{161}Tb free [cpm]	^{161}Tb bound [cpm]	^{161}Tb yield [%]	^{177}Lu free [cpm]	^{177}Lu bound [cpm]	^{177}Lu yield [%]
0	1.95	1073	**99.8**	2.65	1295	**99.8**
1	5.1	1269	**99.6**	3.6	1275	**99.7**
2	8.46	1490	**99.5**	5.4	889	**99.4**
3	3.32	584	**99.4**	7.54	1035	**99.3**
4	17.4	1370	**98.7**	8.34	2790	**99.7**
8	2.31	536	**99.5**	1.39	558	**99.7**
9	11.7	1040	**98.9**	3.24	749	**99.6**
10	7.59	728	**98.9**	16.04	420	**96.3**
11	10.9	610	**98.2**	13.8	1010	**98.6**
12	17.6	1216	**98.5**	8.9	983	**98.8**
26	5.2	90.5	**94.6**	5.9	85.1	**93.5**

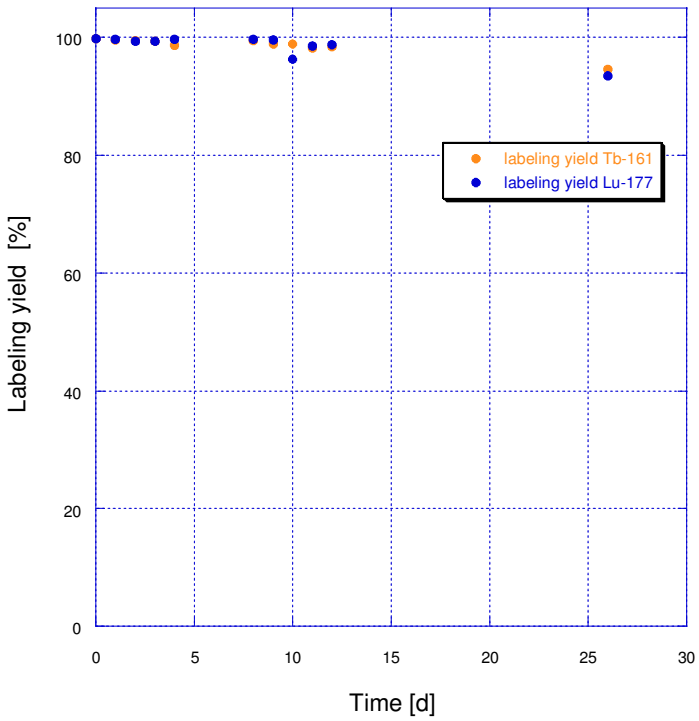

Figure 4-24: Stability of ^{161}Tb- and ^{177}Lu- DOTA-compounds in human serum. Radiolabeling yield was controlled by TLC on aluminum sheets, silica gel 60 and 0.1 M Na_3Citrate pH 4.5 as a mobile phase.

Labeling yield of ^{161}Tb- and ^{177}Lu-DOTA-compounds is quite constant for about two weeks (~ 98.5 – 99.5%). The conjugates were stable for at least 26 days (almost four half-lives). It must not be expected that the free radionuclide will occur *in vivo* because of the nearly complete decay of a radionuclide after ten half-lives. So ^{161}Tb- and ^{177}Lu-DOTA-compounds should be applicable for endoradiotherapy.

In addition, the stability of ^{161}Tb labeled peptides is comparable with ^{177}Lu labeled DOTA-compounds. So for use in nuclear medicine, free ^{161}Tb is not expected to occur *in vivo* (Jurkin, 2009).

4.5 Labeling of the monoclonal antibody chCE7

4.5.1 Ligand substitution of chCE7 with different molar excess of DOTA-NCS

Before labeling with ^{161}Tb, the monoclonal antibody chCE7 has to be substituted to the bifunctional chelator DOTA-NCS (p-isothiocyanatobenzyl-1,4,7,10-tetraazacyclo-dodecane-N-N'-N''-N'''-tetraacetic acid). Different numbers of ligands were coupled to the antibody, depending on the molar excess of DOTA-NCS. The number of linked chelators to the mAb was determined by mass spectroscopy. With a molar excess of 11 DOTA-NCS an average number of 2.5 (Figure 4-25), and with a molar excess of 22 DOTA-NCS an average number of 4.6 chelators have been coupled to the antibody (Figure 4-26).

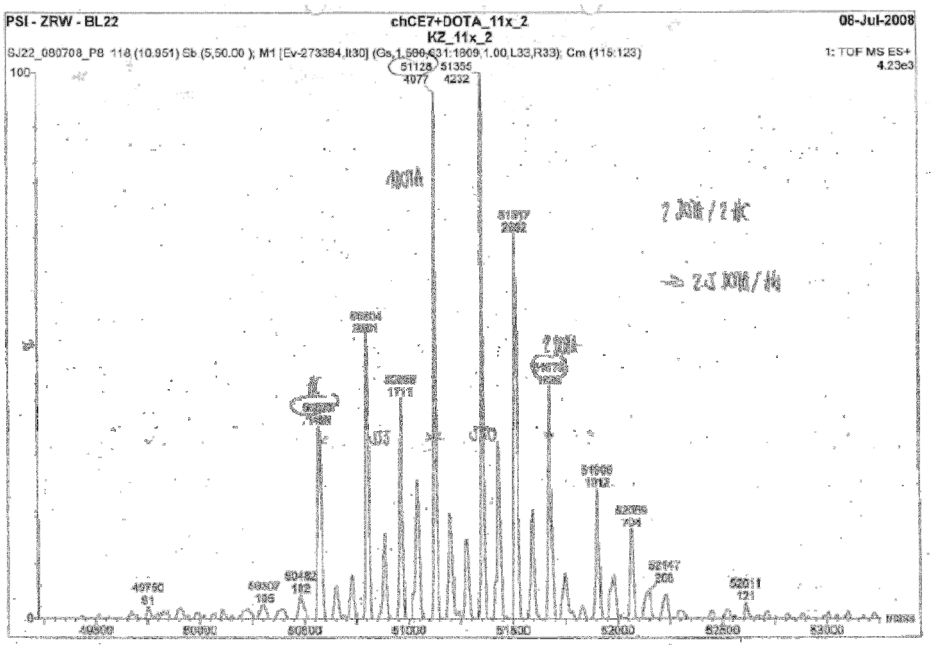

Figure 4-25: Mass spectra of the heavy chain of chCE7.
DOTA-NCS coupled to the mAb with a molar excess of 11 DOTA-NCS.
An average number of 2.5 DOTA-NCS is coupled to the mAb.

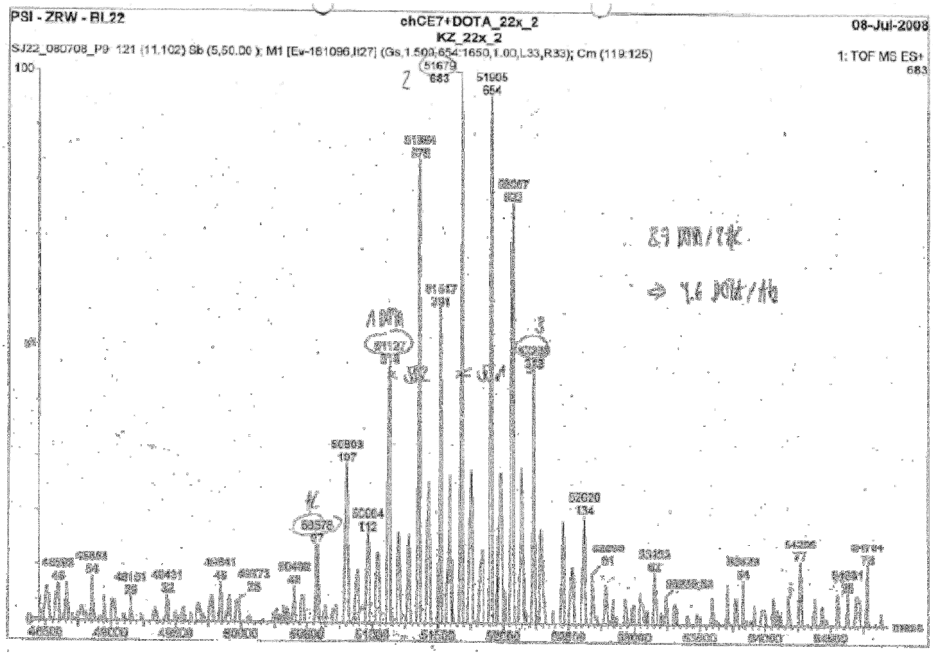

Figure 4-26: Mass spectra of the heavy chain of chCE7.
DOTA-NCS coupled to the mAb with a molar excess of 22 DOTA-NCS.
An average number of 4.6 DOTA-NCS is coupled to the mAb.

4.5.2 Labeling of DOTA-NCS-chCE7 with ^{161}Tb

After labeling of ^{161}Tb with DOTA-NCS-chCE7, the product was separated from unbound ^{161}Tb and different aggregates of the antibody by FPLC. The retention time of the eluted products is dependent on the size of the molecules. Lighter molecules are eluted earlier than heavy ones. The measurement was performed by γ-spectroscopy. After the labeling reaction EDTA was added to complex remaining ^{161}Tb to allow the calculation of the labeling yield.

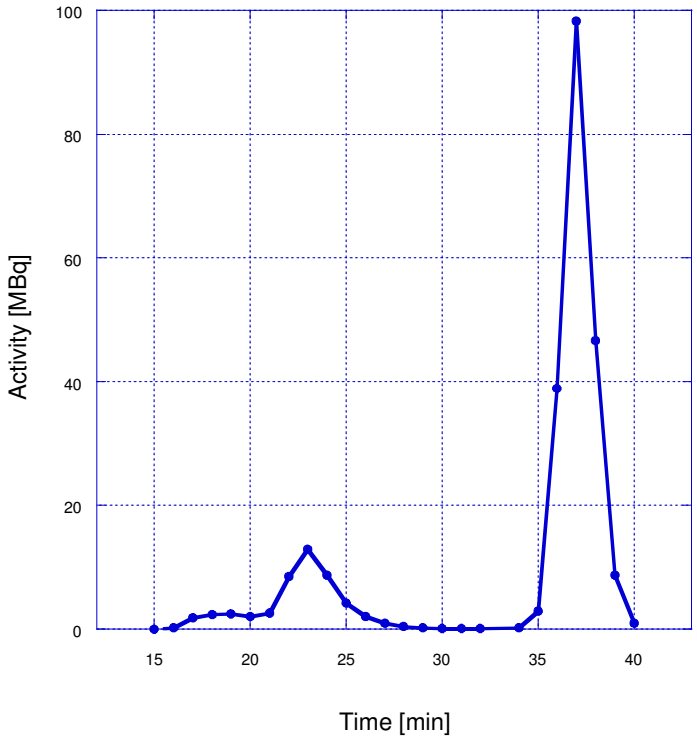

Figure 4-27: Elution profile of the labeling of DOTA-NCS-chCE7 (2.5 ligands) with ^{161}Tb (reaction time: 30 min). First different aggregates of the antibody are eluted (17-21 min), from 21-26 min ^{161}Tb labeled DOTA-NCS-chCE7 and the last peak represents ^{161}Tb bound to EDTA.

At about 16 to 20 min different aggregates of the antibody are eluted. From 21 to 26 ml ^{161}Tb labeled chCE7 can be obtained. The last peak from 35 to 40 min contains EDTA-bound ^{161}Tb that was not complexed by DOTA.

For the following experiments fraction number 23 (eluted after 23 min) was used. It contains 64.9 µg antibody in 0.5 ml with an ^{161}Tb activity of 12.9 MBq. The labeling yield for this reaction was 20.5% of the total measured activity.

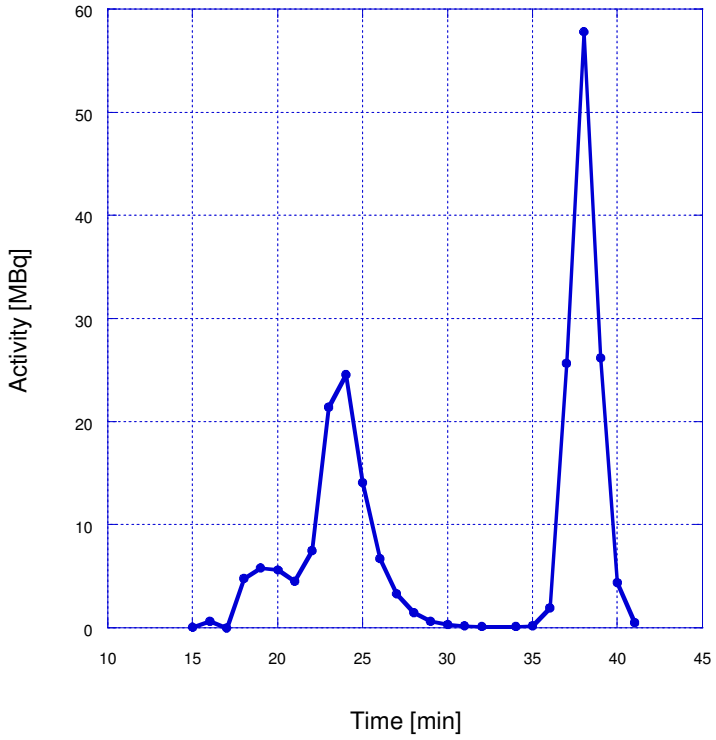

Figure 4-28: Elution profile of the labeling of DOTA-NCS-chCE7 (4.6 ligands) with ^{161}Tb (reaction time).
First different aggregates of the antibody are eluted (16-20 min), from 20-27 min ^{161}Tb labeled DOTA-NCS-chCE7 and the last peak represents ^{161}Tb bound to EDTA.

For the following experiments fraction number 23 was used. It contains 65.1 µg antibody in 0.5 ml with an ^{161}Tb activity of 24.6 MBq. The labeling yield for this reaction was 46.37% of the total measured activity.

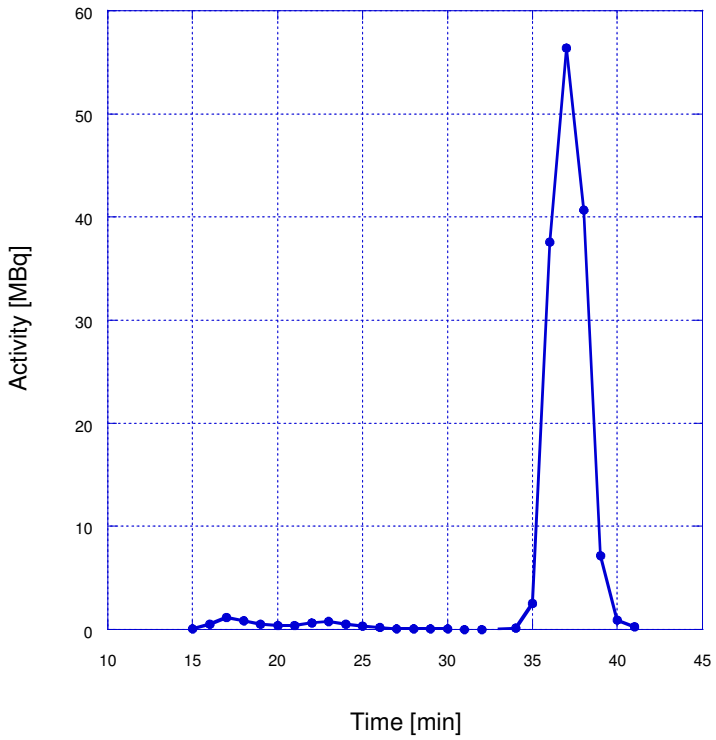

Figure 4-29: Elution profile of the labeling of DOTA-NCS-chCE7 (2.5 ligands) with ^{161}Tb (reaction time: 16 h).
First different aggregates of the antibody are eluted (17-20 min), at ~ 23 min ^{161}Tb labeled DOTA-NCS-chCE7 and the last peak represents ^{161}Tb bound to EDTA.

The labeling yield for this reaction was about 2% of the total measured activity. Because of this low value this labeling experiment was not used for any further trials.

Figure 4-27 and Figure 4-28 show that it was possible to label the mAb chCE7 with ^{161}Tb with a labeling yield of 20.5% (2.5 ligands) and 46.37% (4.6 ligands). The chosen fractions contained an activity to protein ratio suitable for further experiments (64.9 µg antibody:12.9 MBq ^{161}Tb at 2.5 ligands and 65.1 µg antibody : 24.6 MBq ^{161}Tb at 4.6 ligands). A reaction time of 30 min seems to be enough for adequate labeling results. If the reaction solution is incubated for several hours (over night) at 37 °C, the DOTA molecules presumably bind impurities in the solution, given that the antibody is not degraded and eluted at the same time as with the reaction mixtures incubated for 30 min.

These labeling experiments have to be performed with different numbers of ligands bound to the antibody to examine the influence of bound DOTA-ligands on the labeling yield.

4.6 Cell experiments with ^{161}Tb-chCE7 and ^{177}Lu-chCE7

The binding relations have been examined via two different binding assays. As cancer cells SKOV3ip human ovarian carcinoma cells have been used.

4.6.1 Scatchard analysis

Binding of ^{161}Tb-labeled antibodies to SKOV3ip cells was measured by incubating cells with Tb-labeled tracers in a concentration range between 800 and 1 ng. Nonspecific binding in the presence of 10 µg of unlabeled mAb chCE7 was subtracted and data was analyzed with the GraphPad prism program using the Scatchard method.

Table 4-4: Scatchard analysis of ^{161}Tb-DOTA-NCS-chCE7 (2.5 ligands).

ab cold [ng]	input [cpm]	bound [cpm]	bound [ng]	free [ng]	bound/free [ng]
800	38642	208	4.31	795.69	0.005
400	38642	540	5.59	394.41	0.014
200	38642	1194	6.18	193.82	0.032
100	38642	2528	6.54	93.46	0.070
50	38642	3558	4.60	45.40	0.101
1	38642	4738	0.12	0.88	0.140

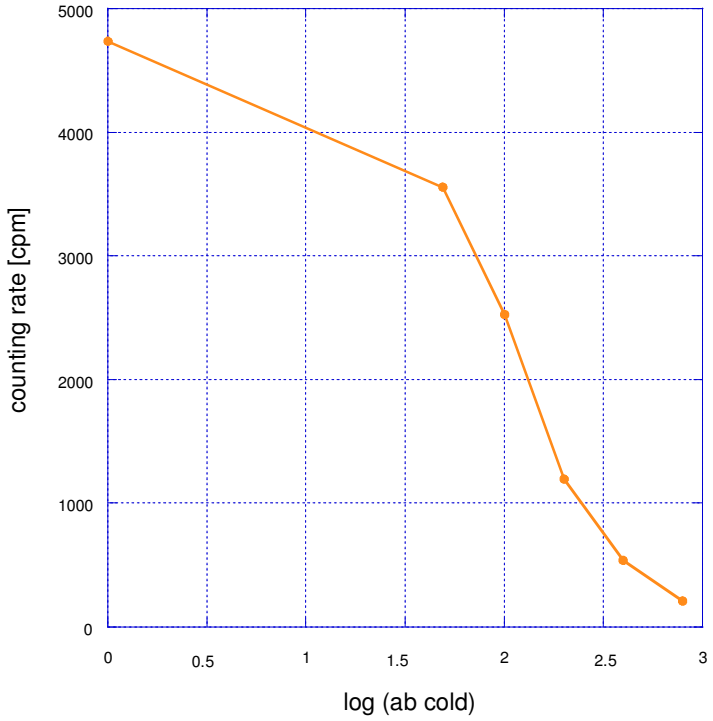

Figure 4-30: Scatchard analysis of ^{161}Tb-DOTA-NCS-chCE7 (2.5 ligands).

Complete displacements can be achieved with about 800 ng of competitors. Fifty percent displacement (IC_{50}) occurred at 90.67 ng. The equation for this calculation can be found in 3.2.6.2.

Table 4-5: Scatchard analysis of ^{161}Tb-DOTA-NCS-chCE7 (4.6 ligands).

ab cold [ng]	input [cpm]	bound [cpm]	bound [ng]	free [ng]	bound/free [ng]
800	234380	524.67	1.79	798.21	0.002
400	234380	1686.67	2.88	397.12	0.007
200	234380	3408.00	2.91	197.09	0.015
100	234380	8758.67	3.74	96.26	0.039
50	234380	10914.00	2.33	47.67	0.049
1	234380	15015.33	0.06	0.94	0.068

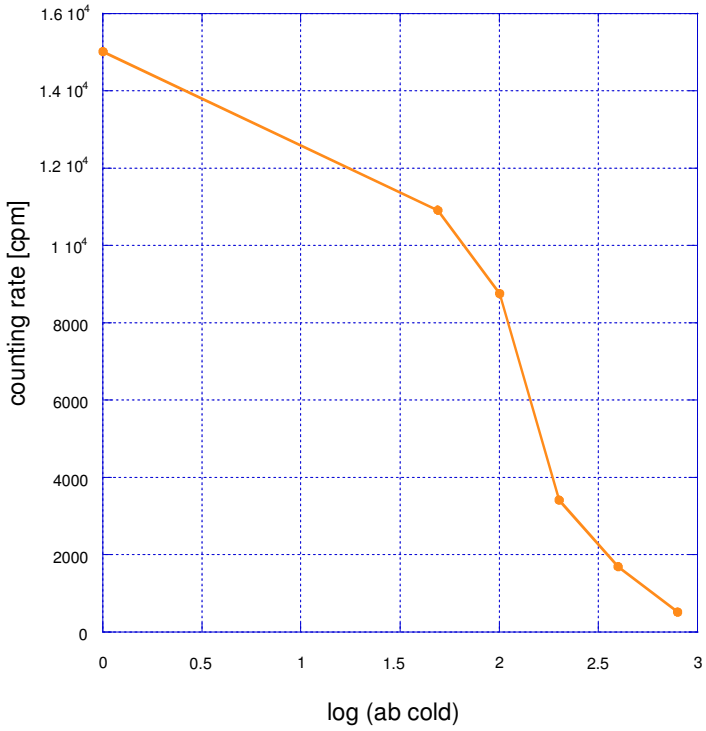

Figure 4-31: Scatchard analysis of ^{161}Tb-DOTA-NCS-chCE7 (4.6 ligands).

Complete displacements can be achieved with about 800 ng of competitors. Fifty percent displacement (IC_{50}) occurred at 85.79 ng.

These results are comparable with ^{177}Lu labeled chCE7. Scatchard analysis of chCE7 substituted with 7 DOTA groups showed an IC_{50} of 82 ng unmodified chCE7 and 119 ng at chCE7 substituted with 12 chelator groups (Knogler, et al., 2006).

With 2.5 ligands, a higher mass of competitors is required (90.67 ng) until IC_{50} is reached. Consequently, the binding can be considered more stable than with 4.6 ligands (85.79 ng of competitors).

4.6.2 Immunoreactivity assay

The immunoreactive fraction is an important parameter in evaluating the quality of radiolabeled antibody preparations and has a direct impact on the percentage uptake of the Ab in targeted tissues and the nonspecific toxicity of the Ab when used for cancer therapy (Konishi, et al., 2004).

Immunoreactive fractions of radiolabeled monoclonal antibodies can be examined easily by determination of the highest fraction of radiolabeled mAb that is able to bind in an assay which includes a series of increasing cell concentrations. The assay was set up using 6 concentrations of live SKOV 3IP cells in 1:2 dilutions from 6 to 0.18 million cells/ml and the final concentration of ^{161}Tb-labeled chCE7 was 6.5 ng/ml and 4.5 ng/ml respectively. Figure 4-32, Figure 4-34 and Figure 4-36 show the double inverse plot according to equation 3 of the total applied counting rate over specific binding as a function of the inverse cell concentration. The immunoreactive fraction for conditions representing infinite antigen excess can be determined by linear extrapolation to the ordinate.

Table 4-6: Counting rate of bound and non specific bound chCE7 antibody labeled with ^{161}Tb

(2.5 ligands, 6.5 ng protein).

cells (million cells)	measured [cpm]		T= input [cpm]
	bound	non specific	
6	4900	701	79479
	4838	701	
	4868	701	
3	6010	1650	
	5524	1650	
	6472	1650	
1.5	7656	2022	
	8686	2022	
	9416	2022	
0.75	6594	271	
	6360	271	
	6428	271	
0.375	4962	327	
	4910	327	
	4404	327	
0.1875	2882	273	
	3194	273	
	2648	273	

Table 4-7: Calculation of total applied radioactivity (T) over specific binding (S)

(2.5 ligands, 6.5 ng protein).

1/cells	average bound	average non specific	S = average specific	T/S
0.17	4869	701	4167.67	19.07
0.33	6002	1650	4352.00	18.26
0.167	8586	2022	6564.00	12.11
1.33	6461	271	6189.68	12.84
2.67	4759	327	4431.66	17.93
5.33	2908	273	2635.00	30.16

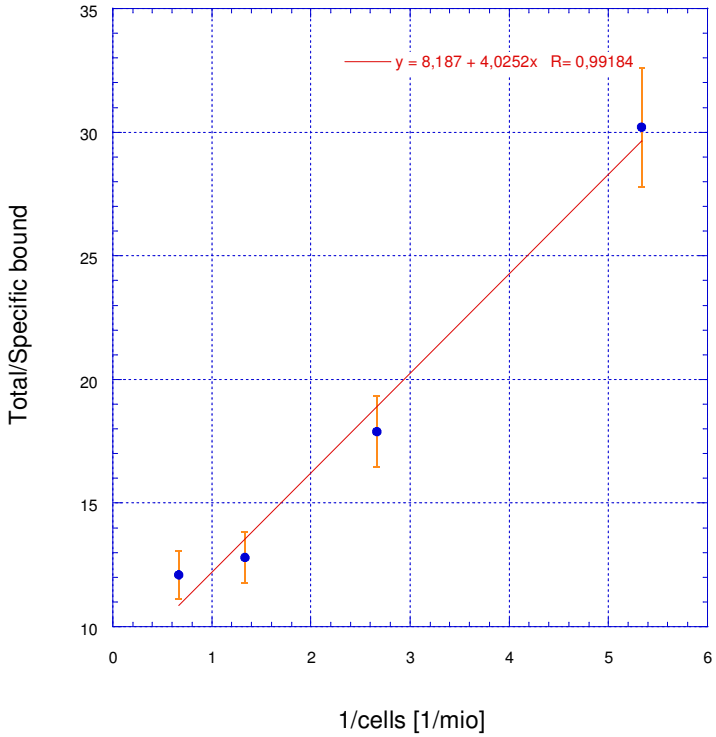

Figure 4-32: Lindmo-Plot ^{161}Tb-chCE7 (2.5 ligands), 6.5 ng protein.
The ratio total activity/specific bound activity is plotted against 1 over number of cells
Immunoreactive fraction: I = 12.2%.

The immunoreactive fraction of ^{161}Tb-chCE7 (2.5 ligands, 6.5 ng protein) in this first Lindmo-assay is 12.2%.

For calculation see 3.2.6.3.

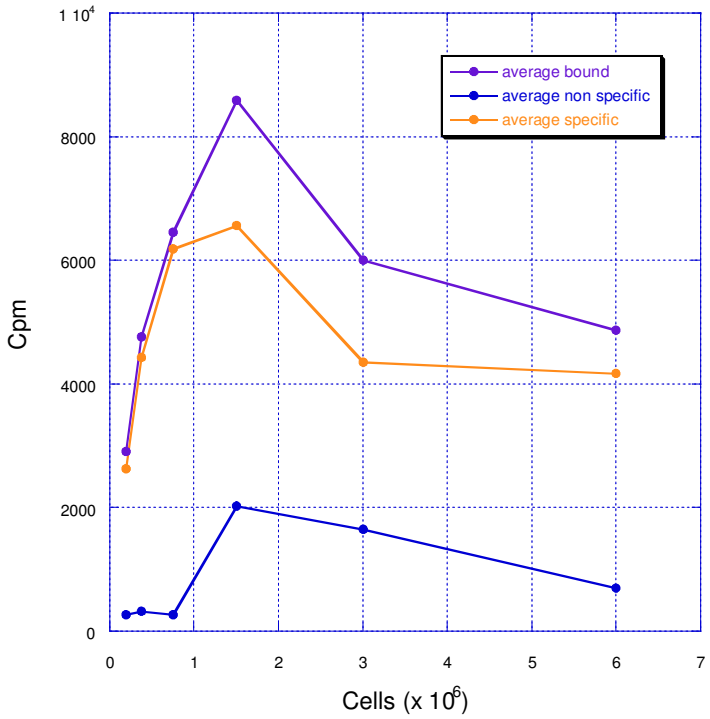

Figure 4-33: Saturation binding of ^{161}Tb-chCE7 (2.5 ligands, 6.5 ng proteine) to SKOV3ip cells. The value of specific binding approaches a limit of about 4500 cpm.

The value of the specific binding of the saturation binding curve (2.5 ligands, 6.5 ng proteine) approaches a limit of about 4500 cpm. The total applied counting rate is 79479 cpm, consequently about 57% of the antibodies are binding ones.

Table 4-8: Counting rate of bound and non specifically bound chCE7 antibody labeled with ^{161}Tb

(4.6 ligands, 6.5 ng protein).

cells (million cells)	measured [cpm]		T= input [cpm]
	bound	non specific	
6	32588	13704	234380
	36796	13704	
	31350	13704	
3	50534	12864	
	47480	12864	
	51252	12864	
1.5	23844	5090	
	35680	5090	
	24306	5090	
0.75	17808	2292	
	18606	2292	
	16942	2292	
0.375	19472	11088	
	20192	11088	
	11428	11088	
0.1875	7498	1184	
	6796	1184	
	6670	1184	

Table 4-9: Calculation of total applied radioactivity (T) over specific binding (S)

(4.6 ligands, 6.5 ng protein).

1/cells	AV bound	AV non spec.	S=AV spec.	T/S
0.17	33578	13704	19874.00	11.79
0.33	49755	12864	36891.33	6.35
0.67	27943	5090	22853.33	10.26
1.33	17785	2292	15493.33	15.13
2.67	17031	11088	5942.67	39.44
5.33	6988	1184	5804.00	40.38

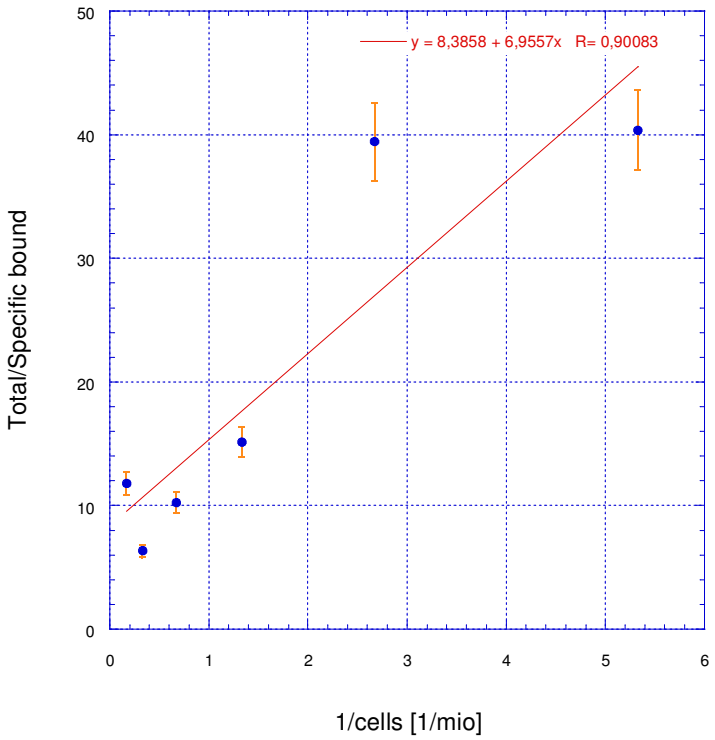

Figure 4-34: Lindmo-Plot ^{161}Tb-chCE7 (4.6 ligands), 6.5 ng protein.
Immunoreactive fraction: I = 9.1%.

If the Ab with 4.6 ligands is used (Figure 4-34), the immunoreactive fraction with 9.1% is slightly lower than with 2.5 ligands (immunoreactive fraction: 12.2%, Figure 4-32).

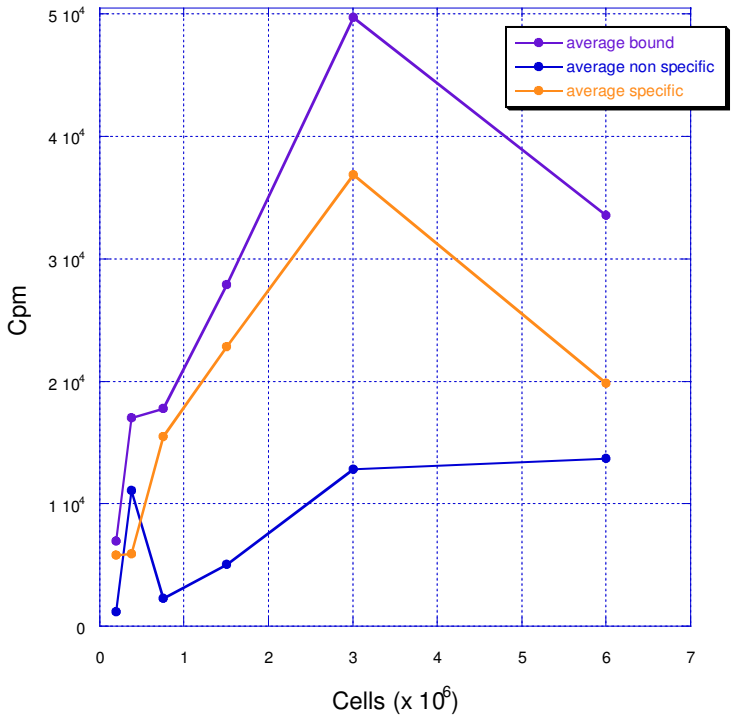

Figure 4-35: Saturation binding of ^{161}Tb-chCE7 (4.6 ligands, 6.5 ng proteine) to SKOV3ip cells.
The value of specific binding approaches a limit of about 35000 cpm.
Because of its deviation the last time point was not considered.

The value of the specific binding of the saturation binding curve (4.6 ligands, 6.5 ng proteine) approaches a limit of about 35000 cpm (because of its deviation the last point was not considered). With a total counting rate of 234380 cpm about 14.9% of the antibodies are binding ones.

Table 4-10: Counting rate of bound and non specifically bound chCE7 antibody labeled with ^{161}Tb

(2.5 ligands, 4.3 ng protein).

cells (million cells)	measured [cpm]		T= input [cpm]
	bound	non specific	
2	8002	3834	8066
	7708	3834	
	4536	3834	
1	4898	1968	
	7756	1968	
	4902	1968	
0.5	4333	532	
	4458	532	
	4402	532	
0.25	4076	448	
	4264	448	
	3988	448	
0.175	2694	646	
	3354	646	
	3322	646	
0.0875	2902	1082	
	3306	1082	
	3082	1082	

Table 4-11: Calculation of total applied radioactivity (T) over specific binding (S)

(2.5 ligands, 4.3 ng protein).

1/cells	AV bound	AV non spec.	S = AV spec.	T/S
0.5	6748	3834	2914.67	2.77
1	5852	1968	3884.00	2.08
2	4397	532	3865.67	2.09
4	4109	448	3661.33	2.20
5.71	3123	646	2477.33	3.26
11.43	3096	1080	2014.67	4.00

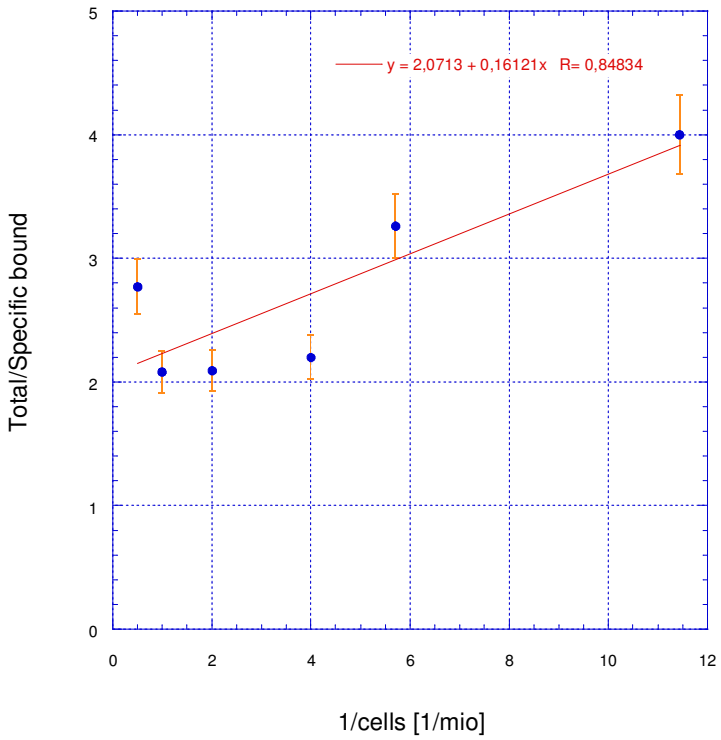

Figure 4-36: Lindmo-Plot ^{161}Tb-chCE7 (2.5 ligands), 4.3 ng protein.
Immunoreactive fraction: I = 48.6%.

By lowering the amount of proteine to 4.3 ng the immunoreactive fraction has the highest value of 48.6% (Figure 4-36) compared to 12.2% with 6.5 ng (Figure 4-32).

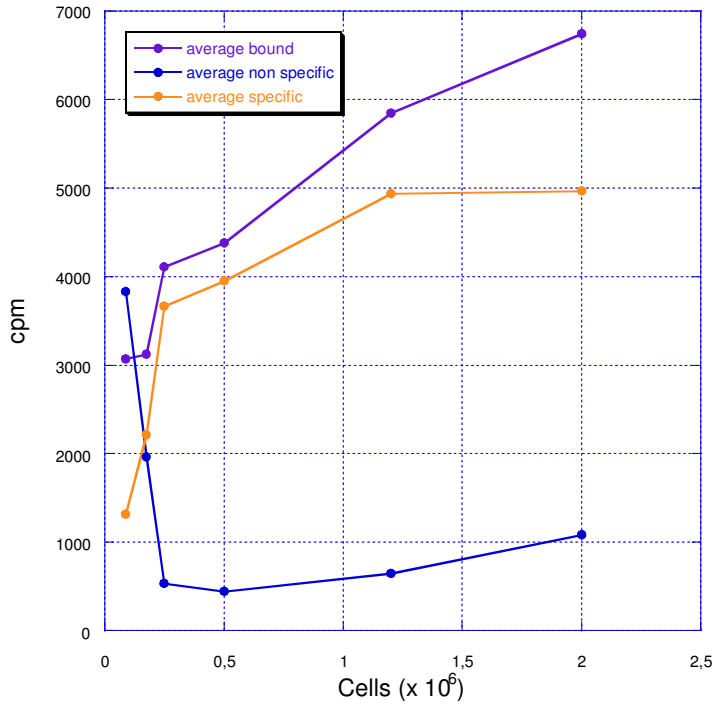

Figure 4-37: Saturation binding of ^{161}Tb-chCE7 (2.5 ligands, 4.3 ng proteine) to SKOV3ip cells. The value of specific binding approaches a limit of about 5000 cpm.

The value of specific binding of the saturation binding curve (2.5 ligands, 4.3 ng proteine) approaches a limit of about 5000. The total counting rate is 8066 cpm, therefore ~ 62% of the antibodies are binding mAb.

If the number of DOTA molecules is lower, the fraction of binding antibody increases (57% at 2.5 ligands, 15% at 4.6 ligands). The quantity of protein does not seem to have any influence in the number of binding mAb (57% at 6.5 ng, 62% at 4.3 ng).

Here, the value also depends on the number of linker attached to the protein. With 2.5 ligands per antibody the immunoreactive fraction is about 12%, with 4.6 ligands 9% if 6.5 ng proteine is used. Lowering the amount of protein to 4.3 ng (66% of protein mass) leads to an increase of immunoreactivity to 49%. The value of the specific binding differs from 15% (4.6 ligands, 6.5 ng protein), 57% (2.5 ligands, 6.5 ng protein) to 62% (2.5 ligands, 4.3 ng protein). Hence, the number of linker attached to the antibody indicates a great influence on the immunoreactive fraction. In contrast, influences from protein mass changes can be neglected.

In the literature, an immunoreactive fraction of 80 – 100% for ^{67}Cu labeled chCE7 can be found, determined by binding to SKOV3ip cells (Knogler, et al., 2007). Consequently, the experiments have to be repeated with different reaction conditions to be able to increase the value for immunoreactivity of ^{161}Tb labeled chCE7.

4.7 SDS-PAGE electrophoresis (western-blot)

The migration of protein particles in the electrophoresis gel depends on the length (molecular weight) of the polypeptide chains. Proteins get negatively charged in the acrylamide gel and migrate to the positively charged electrode. Smaller proteins are able to migrate faster through the gel than larger molecules.

By using reducing agents like Dithiothreitol (DTT), the antibody is denaturated. Thus, it is possible to separate the heavy- from the light-chain by their different molecular weight.

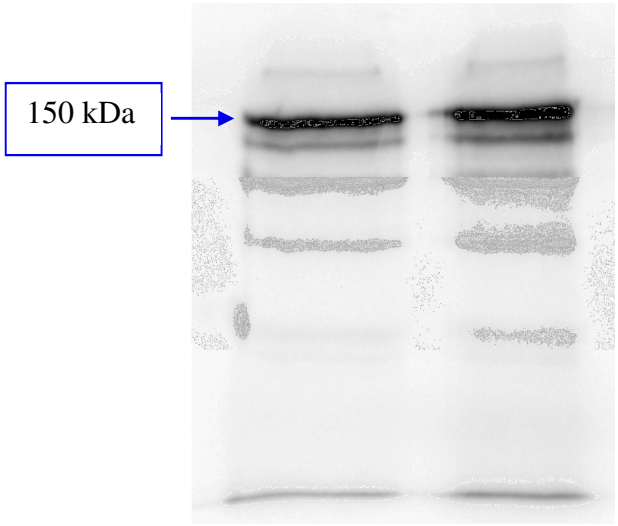

Figure 4-38: Gel electrophoresis without reducing agent.
Left side: 2.5 ligands; right side: 4.6 ligands.
At 150 kDa the activity bound to chCE7 can be seen.
The darker the band, the more activity is bound.

SDS-PAGE analysis of ^{161}Tb-chCE7 shows a dark labeled band at 150 kDa. The broader band for the antibody with 4.6 ligands in Figure 4-38 indicates that there is more activity bound to the antibody if there are more DOTA attached to the protein.

The lighter bands above 150 kDa are smaller labeled impurities or degradation products of the antibody.

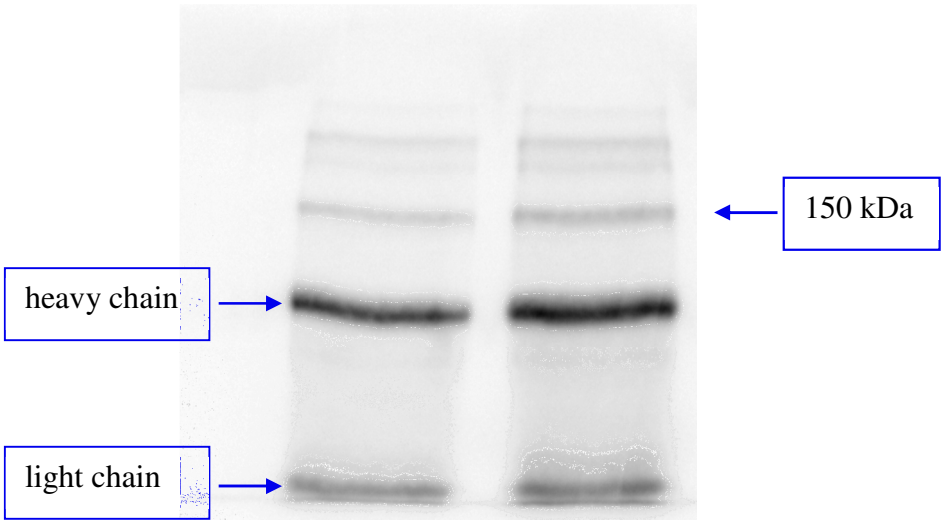

Figure 4-39: Gelelectrophoresis with DTT.
Left side: 2.5 ligands; right side: 4.6 ligands.

The chCE7 mAb is split in a heavy- and a light-chain by the reducing agent DTT. The light chain is placed at 25 kDa, the heavy chain at 50 kDa. The heavy chain is darker colored in the phosphorimage than the light chain. These results suggest that the radionuclide is mostly associated to the heavy chain.

The lighter bands above 50 kDa are labeled impurities or aggregation products of chCE7.

This SDS-PAGE analysis reveals that after labeling the antibody is still intact. So labeling with ^{161}Tb is not inducing any damage in the chCE7 structure. For further tests, this SDS-PAGE should be examined with ^{177}Lu labeled chCE7 mAb in order to allow a comparison.

4.8 Internalization of labeled chCE7

Uptake and subsequent cellular degradation have important consequences for the tumor targeting. Internalizing antibodies are required when radiation has to be delivered specifically to the nuclear DNA.

The grade of intracellular accumulation of ^{161}Tb-chCE7 was determined by measuring the internalized activity and the activity bound on the cell surface; the internalized activity of ^{161}Tb is then divided by the total applied one. For the activity profiles, the internalized activity [% of total activity] is plotted against the time of internalization.

Table 4-12: Calculation of the internalized ^{161}Tb counting rate referred to the total applied activity (2.5 ligands, 2.5 ng protein).

time elapsed	cell surface bound	internalized	total [cpm]	internalized [% of total]
0	101062	3400	317724	1.07
	103660	3640		
	102764	3198		
mean value	**102495**	**3413**		
1 h	71928	21396	297484	9.22
	73432	35306		
	69798	25624		
mean value	**71719**	**27442**		
3 h	43078	37274	235660	15.20
	42532	35198		
	42556	35022		
mean value	**42722**	**35831**		
4 h	40800	41610	246796	16.90
	41124	42076		
	39716	41470		
mean value	**40547**	**41719**		
24 h	15856	39132	174376	23.78
	16644	40072		
	17464	45208		
mean value	**16655**	**41471**		

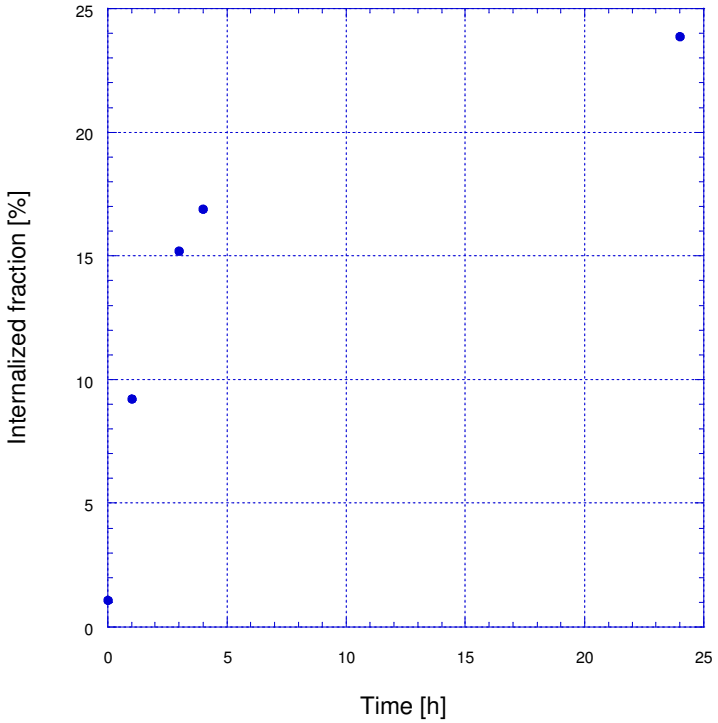

Figure 4-40: Profile of time dependent ^{161}Tb-chCE7 internalization (2.5 ligands, 6.5 ng protein)
After 23 h, 24.28% are internalized

Figure 4-40 presents the internalized ^{161}Tb bound to chCE7 (2.5 ligands, 6.5 ng proteine) into SKOV3ip cells. 23 h after starting the internalization, 24.28% of the ^{161}Tb activity is internalized.

The chCE7 molecule seems to be stable even if it is labeled with ^{161}Tb, where annihilation by radiolysis might occur. Because of the increasing degree of intracellular accumulation, the antibody is not degraded and remains in the tumor cell.

Table 4-13: Calculation of the internalized ^{161}Tb counting rate referred to the total applied activity (2.0 ligands, 2.9 ng protein).

time elapsed	cell surface	internalized	total [cpm]	internalized [% of total]
	2613	449		
0	2859	491	9092	4.84
	2299	381		
mean value	**2590**	**440**		
	1697	1147		
1	1707	1303	8552	14.23
	1497	1201		
mean value	**1634**	**1217**		
	1099	979		
3	1033	1015	6258	15.97
	1127	1005		
mean value	**1086**	**1000**		
	786	988		
4	902	1028	5288	18.18
	716	868		
mean value	**801**	**961**		
	237	1095		
24	217	775	3286	26.43
	227	735		
mean value	**227**	**868**		
	294	1146		
27	238	1308	4352	27.21
	268	1098		
mean value	**267**	**1184**		

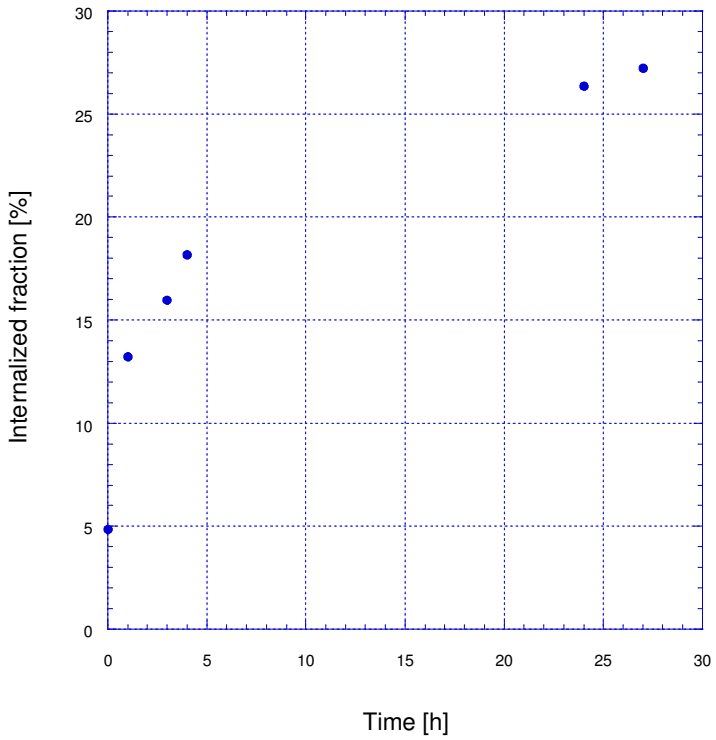

Figure 4-41: Profile of time dependent ^{161}Tb-chCE7 internalization (2.0 ligands, 2.9 ng protein). After 27 h, 27.2% are internalized.

In Figure 4-41 the internalization of ^{161}Tb-chCE7 (2.0 ligands), using 2.9 ng protein, is shown. After 27 h, 27.2% of the total activity is internalized into SKOV3ip cells.

Table 4-14: Calculation of the internalized ^{177}Lu counting rate referred to the total applied activity (2.0 ligands, 2.9 ng protein).

time elapsed	cell surface bound	internalized	total	internalized [% of total]
	5465	967		
0	6159	907	19910	4.59
	5543	869		
mean value	**5722**	**914**		
	4697	3503		
1	4753	3501	23932	14.30
	4215	3263		
mean value	**4555**	**3422**		
	5487	4747		
3	5343	4699	29902	15.44
	5225	4401		
mean value	**5351**	**4615**		
	3500	3190		
4	3794	3634	20990	16.22
	3480	3392		
mean value	**3591**	**3405**		
	1297	4377		
24	1291	4233	16402	25.74
	1147	4057		
mean value	**1245**	**4222**		
	1114	4306		
27	1040	4046	15338	26.52
	980	3852		
mean value	**1044**	**4068**		

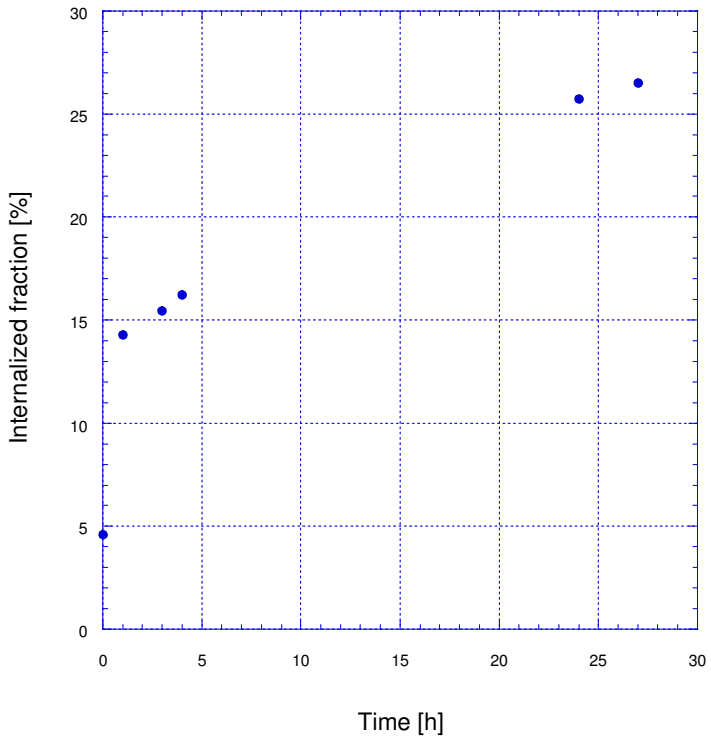

Figure 4-42: Profile of time dependent ^{177}Lu-chCE7 internalization (2.0 ligands, 2.9 ng protein). After 27 h, 26.5% are internalized.

The internalization of ^{177}Lu-chCE7 (2.0 ligands) is shown in Figure 4-42. After 27 h, 26.5% of the total ^{177}Lu activity is internalized into the tumor cells.

These results clearly indicate that there is no difference in degree of intracellular accumulation using ^{161}Tb- or ^{177}Lu-chCE7. If the mass of protein is compared, after 24 h with 2.5 ng protein 23.78% of the ^{161}Tb activity is internalized and with 2.0 ng protein 26.43%. Therefore, the grade of internalization is not dependent on the amount of protein. Because of the increasing degree of the internalization in the measured time period, the antibody is not degraded and remains in the tumor cell. These experiments should be repeated over an even longer time period in order to observe the clearance of the antibody from the cells.

These results are comparable with the grade of internalization of ^{125}I-chCE7. After 24 h, about 35% of the total activity is internalized into SKN-AS cells. The internalization of ^{67}Cu-chCE7 conjugates into tumor cells is even better, for example, 80% in SKOV3ip cells and 80% in SKN-AS cells (Knogler, et al., 2007; Novak-Hofer, et al., 1995)

4.9 Stability of labeled chCE7 in human serum

In order to examine if ^{161}Tb and ^{177}Lu DOTA-chCE7 (2 ligands) conjugates are stable *in vivo*, this complex has been incubated in human plasma at 37 °C. Samples were analyzed via fast protein liquid chromatography. The major peaks eluted at a retention time of about 23 min, are indicating the DOTA-chCE7 conjugates.

The labeling yield of DOTA-chCE7 was 45% for ^{161}Tb and 48% for ^{177}Lu.

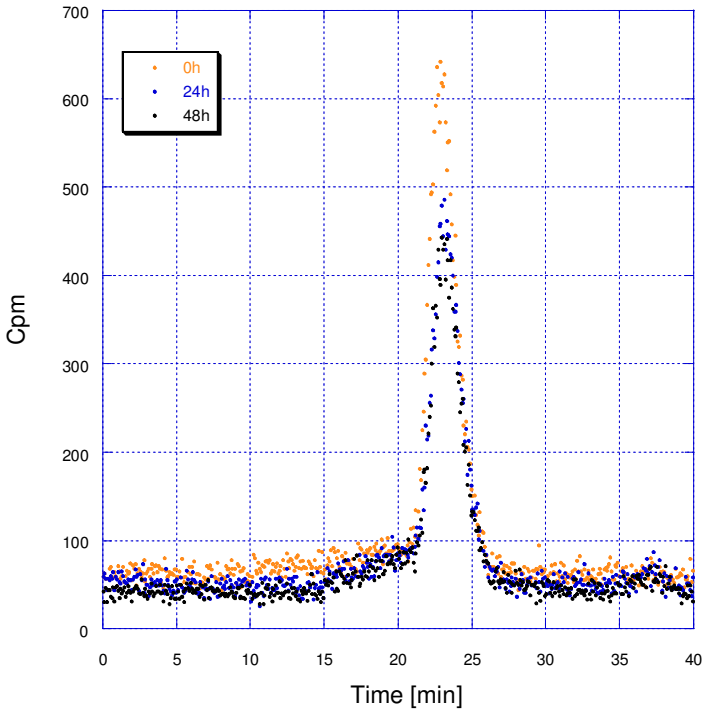

Figure 4-43: Stability of ^{161}Tb-DOTA-chCE7 (2 ligands) in human serum.
Samples were analyzed via fast protein liquid chromatography.
Orange line: 0 h, blue line: after 24 h incubation at 37 °C.

The peak eluted between 22 to 25 min contains stable labeled chCE7. The small peak at about 36 to 38 min is free chCE7 bound to EDTA. So it can be seen that most of the labeled antibody (~ 98%) is stable for at least 48 h in human plasma.

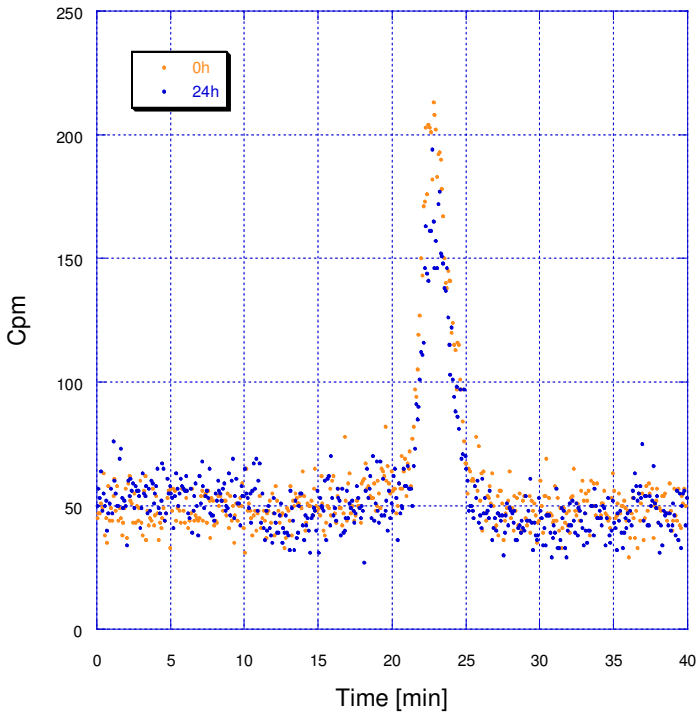

Figure 4-44: Stability of ^{177}Lu-DOTA-chCE7 (2 ligands) in human serum.
Samples were analyzed via fast protein liquid chromatography.
Orange line: 0 h, blue line: after 24 h incubation at 37 °C.

As can be seen in Figure 4-44, stable labeled chCE7 is eluted in the time between 22 to 25 min. There is no small peak at about 36 to 38 min originating from radiometal bound to EDTA identifiable. Thus, it can be seen that most of the labeled antibody (~ 96%) is stable for at least 24 h in human plasma.

In the direct comparative study, the stability of ^{161}Tb- and ^{177}Lu-DOTA-chCE7 was investigated by incubation in human plasma. No difference in the stability could be observed. More precisely, about 96 - 98% (~ 99% at the start) of the ^{161}Tb- and ^{177}Lu-DOTATATE were intact after incubation for 24 and 48 hours, respectively.

The measured activity decreases from day to day (~ 10%) due to the β^- decay of ^{161}Tb and ^{177}Lu.

4.10 Conclusion of experiments with ^{161}Tb labeled compounds

It was possible to obtain ^{161}Tb-DOTA-Tyr^3-octreotate with a labeling yield of > 99%. This result is similar to the labeling yield of ^{177}Lu DOTA-peptides with commercially available *n.c.a.* ^{177}Lu applicable for clinical cancer treatment. As a result, the quality of the produced ^{161}Tb seems to be comparable and this fraction might be suitable for appliance in nuclear medicine. Subsequent stability tests in human plasma for two weeks showed that ^{161}Tb labeled peptides are as stable as ^{177}Lu labeled peptides. Also, stability experiments in human plasma with labeled mAb chCE7 led to similar results for ^{161}Tb and ^{177}Lu. Due to the fact that the stability is an important criteria for use in clinical treatments this is an additional evidence that ^{161}Tb might be useful in nuclear oncology.

Comparative cell experiments with ^{161}Tb and ^{177}Lu labeled mAb chcE7 showed analog results. The Scatchard analysis proved that the stability of the binding of labeled chCE7 to SKOV3ip tumor cells is similar for ^{161}Tb and ^{177}Lu labeled compounds. In addition, internalization of ^{161}Tb- and ^{177}Lu-chCE7 led to equal results indicating that there is no difference in degree of intracellular accumulation and the antibody is not degraded and remains in the tumor cell.

With regard to these results, ^{161}Tb seems to be an adequate candidate for cancer treatment and it would be worthwhile to carry out further investigations and comparisons to ^{177}Lu-labeled compounds.

4.11 SPECT imaging performance of ^{161}Tb

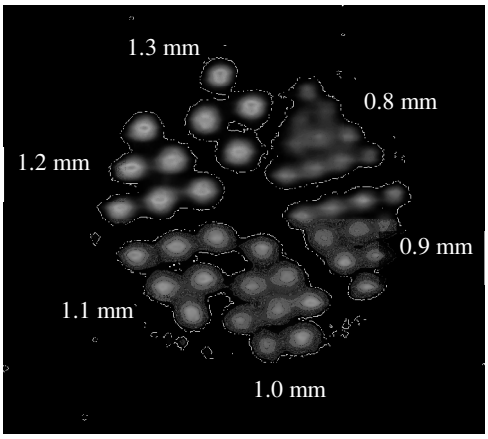

Figure 4-45: Dezentrino phantom small animal SPECT imaging with a Derenzo-phantom filled with $^{161}TbCl_3$ solution (hole diameter 0.8 to 1.3 mm). ^{161}Tb SPECT imaging is possible due to the 75 keV gamma-line of the nuclide. From bottom left (clockwise) 1.1, 1.2, 1.3, 0.8, 0.9 and 1.0 mm bars.

SPECT is an imaging technique for tomography in nuclear medicine using γ-rays. It provides a 3D presentation of tumours in human bodies. SPECT imaging with a Derenzo phantom shows if a radionuclide would be suitable for measurements in nuclear medicine.

Figure 4-45 shows the image of a Derenzo-phantom filled with $^{161}TbCl_3$ solution measured in a Dezentrino phantom small animal SPECT (hole diameter 0.8 to 1.3 mm). It is even possible to differentiate between individual bars at the smallest diameter of 0.8 mm. Hence, the few photons emitted per decay of ^{161}Tb are sufficient to be detected by γ-cameras used for SPECT. This shows the eligibility of ^{161}Tb for SPECT measurements in nuclear medicine diagnostics.

5 Conclusion and Outlook

Targeted radionuclide therapy involves the use of a radiolabeled molecule to deliver selectively radiation to tumor cells. The radiation dose received by the tumor has to be as high as possible while normal tissue may not be affected. There is already an increasing number of radioisotopes of heavy metals commercially used for therapy, but a further optimization that can intensify the therapeutic effect of the radiopharmaceuticals is still required.

Due to the relatively short range in the tissue and consequently high local damage, low energy electrons (e.g. Auger and conversion electrons) can provide a very high cytotoxicity and are therefore promising candidates for an improvement in endoradiotherapy. The low-energy electron emitter ^{161}Tb is a very attractive nuclide for therapeutic treatments in nuclear oncology. After β^- decay of ^{161}Tb a significant amount of conversion and Auger electrons is emitted. In addition to the energy provided by the β particle, about 27% of the mean β energy is released by secondary electrons emitted with energies between 3 and 50 keV. The physical and chemical characteristics of ^{161}Tb can be useful to improve therapeutic efficiency in applications with already established radiolabeling chemistry and targeting strategy or for the development of novel metalloradiopharmaceuticals.

^{161}Tb can be produced with adequate activities by neutron irradiation of highly enriched ^{160}Gd targets (98.2%). After radiochemical processing, the radionuclide can be obtained with highest specific activity, radionuclidic and chemical purity. The proposed strategy based on cation exchange chromatography allows effective isolation of 80 – 90% of ^{161}Tb from massive ^{160}Gd targets with gadolinium and ^{161}Dy content reduced by a factor $> 10^5$ and $> 10^2$, respectively. Three different resins have been used for separation of ^{161}Tb from ^{160}Gd-targets and ^{161}Dy produced by β^- decay of ^{161}Tb. Each resin was appropriate for production of *n.c.a.* ^{161}Tb, but the macroporous exchange resin turned out to be most suitable because of the fast procedure and the elution of the ^{161}Tb activity in a quite small volume. According to these results, the production of even higher ^{161}Tb activities for clinical use by increasing the mass of the target on a longer and broader column can be investigated. In addition, it would be desirable to obtain target material

with a higher grade of ^{160}Gd enrichment. The applied target material contained traces of stable terbium (46 ppm). Consequently, this reduces the specific activity from the maximum achievable one by about 35% and 7% for irradiations at FRM II, BER II, BR2 (SCK-CEN) and ILL, respectively, and decreases radionuclide purity by activation of ^{159}Tb to relatively long-lived ^{160}Tb.

^{161}Tb also was utilized for the preparation of ^{161}Tb-DOTA-peptides with adequate labeling yield. The stability of these compounds was compared with ^{177}Lu-DOTA-peptides in human serum albumin (20%) at 37 °C for 26 days. The labeling yield of both was comparable and stable over this time period. Therefore, it is not expected that free radionuclides will occur *in vivo*.

Further investigations were made with the monoclonal antibody chCE7. ^{161}Tb could be successfully used for preparation of ^{161}Tb-chCE7 with p-SCN-benzyl DOTA as linker. These compounds have been used for several cell experiments with SKOV3ip cells, like immunoreactivity and binding assay (Scatchard analysis), SDS-PAGE electrophoresis and internalization. In most of these, a dependence of the results on the number of linkers attached to the antibody could be observed. For example Scatchard analysis results indicate that the binding is more stable with 4.6 ligands than with 2.5. If 2.5 DOTA-molecules are attached to the mAb, a higher mass of competitors (90.7 ng compared to 85.8 ng for 4.6 DOTA-molecules) is required until IC_{50} is reached. Also the evaluation of the Lindmo-assay shows that the fraction of binding antibodies increases with lower number of DOTA-ligands (57% binding antibodies with 2.5 ligands in contrast to 15% with 4.6 ligands). Most likely, the reason is to be found in the steric configuration of the DOTA molecules which might have an effect on the stability of the antibody-linker binding.

Via Scatchard analysis, it was found that the stability of ^{161}Tb-chCE7 (IC_{50} = 82 ng with 7 DOTA molecules) is comparable to ^{177}Lu-chCE7 (IC_{50} = 91 ng with 2.5 DOTA molecules). The immunoreactivity of ^{161}Tb-chCE7 DOTA compounds was determined by Lindmo-assay. The highest obtained value in this study was ~ 49%. In literature, an immunoreactive fraction of 80 – 100% was found for ^{67}Cu labeled chCE7 determined by binding to SKOV3ip cells (Knogler, et al., 2007).

Reducing SDS-PAGE was utilized to examine the position of the activity in the antibody. Adjacent to a few labeled impurities and aggregation products ^{161}Tb is located on the heavy and the light chain. Hence, the radionuclide is still bound to the antibody even if the disulfide linkages are reduced and the quaternary protein structure is broken. In case of low energy electrons with a relatively short range it is essential that the radionuclide is internalized into the tumor cells. Since the mAb chCE7 is an internalizing antibody, the grade of internalization of ^{161}Tb-chCE7 was investigated. Over a few hours the internalized fraction increased continuously. After 27 hours about 27% of the total ^{161}Tb and ^{177}Lu activity was internalized into the SKOV3ip cells. These results clearly indicate that there is no difference in degree of internalization using ^{161}Tb or ^{177}Lu labeled compounds. With regard to the increasing internalization degrees over 24 h it can be concluded that the antibody is not degraded and remains in the tumor cells. These results are comparable to the internalization if ^{125}I and ^{67}Cu chCE7 conjugates, as well.

Similarly to DOTA-peptides, the labeling yield of ^{161}Tb- and ^{177}Lu-chCE7 was also investigated in human plasma. As linker molecule, p-SCN-benzyl-DOTA was used. The conjugates formed stable complexes with the lanthanides without release of radioactivity and without degradation or aggregation. ^{161}Tb is equally suitable for visualisation in SPECT-measurements.

According to these results, ^{161}Tb labeled mAb should be used for further experiments and investigations of their therapeutic efficiency compared to ^{177}Lu. First, the yield of the protein labeling has to be improved. Here, the labeling should be performed by increasing the batch activity resulting in a suppression of general impurities in the system (e.g. Fe(III), Al(III), Pb(II), etc.). In addition, different ratios of chCE7 to ^{161}Tb could be tested. It also would be interesting to perform the coordination of the BFC to the mAb with different excess of p-SCN-benzyl-DOTA and, additionally, the process for cleaning the chCE7-p-SCN-benzyl-DOTA compound from any impurities like uncoordinated educts could be made with different kinds of columns, eluents and concentrations of this eluents. Also chCE7 could be coordinated to different BFCs, for example p-SCN-benzyl-DTPA.

To exclude impurities from chemicals, for example buffer solutions, the use of GMP quality like compounds for the overall process could be considered.

The cell experiments performed in this work have to be repeated, for example by using the amount of ^{161}Tb activity which is required to reach a therapeutical cytotoxic effect. Also different protein concentrations should be tested and the results have to be compared directly to ^{177}Lu cell experiments. ^{161}Tb could be bound do different antibodies and, according to this, different kinds of cancer cells have to be used for this experiments.

If these cell experiments lead to successful results, further studies with mice have to be considered. This includes for example tumor uptake and biodistribution, a method for tracking in which organs the labeled compound is accumulated, e.g. blood, liver, kidney, lung and bone marrow. Also blood clearance studies should be performed and the maximum tolerated dose, the highest possible amount of activity that does not cause any unacceptable side effects, has to be found by using escalating doses. Finally, a survival curve of mice via radioimmunotherapy experiments has to be created, in order to get a concluding evidence for the therapeutic effect of ^{161}Tb labeled compounds for cancer treatment.

6 Appendix

6.1 References

International Atomic Energy Agency. 2003. Manual for reactor produced isotopes. *IAEA-TECDOC.* 2003.

Allen, B. J., et al. 2001. In vitro and preclinical targeted alpha therapy for melanoma, breast, prostate and colateral cancers. *Critical Reviews in Oncology/Hematology.* 2001, Vol. 39, pp. 139-146.

Amstutz, H., et al. 1993. Production and characterization of a mouse/human chimeric antibody directed against human neuroblastoma. *Int. J. Cancer.* 1993, Vol. 53, pp. 147-152.

Anthony, L. B., et al. 2002. Indium-111-Pentetreotide prolongs survival in gastroenteropancreatic malignancies. *Seminars in Nuclear Medicine.* 2002, Vol. 2, pp. 123 – 132.

Araujo, E. B., et al. 2009. A comparative study of ^{131}I and ^{177}Lu labeled somatostatin analogues for therapy of neuroendocrine tumours. *Applied Radiation and Isotopes.* 2009, Vol. 67, 2, pp. 227-233.

Bakker, W. H., et al. 1991. In vivo use of a radioiodinated somatostatin analogue: dynamics, metabolism, and binding to somatostatin receptor-positive tumors in man. *The Journal of Nuclear Medicine.* 1991, Vol. 32, 6, pp. 1184-1189.

Bakker, W. H., et al. 2006. Practical aspects of peptide receptor radionuclide therapy with ^{177}Lu DOTA-Tyr^3-octreotate. *The Quaterly Journal of Nuclear Medicine and Molecular Imaging.* 2006, Vol. 50, pp. 265-271.

Balasubramanian, P. S. 1994. Separation of carrier-free lutetium-177 from neutron irradiated natural ytterbium target. *Journal of Radioanalytical and Nuclear Chemistry.* 1994, Vol. 185, pp. 305-310.

Behr, T. M., et al. 2000. Therapeutic advantages of Auger electron over β^- emitting radiometals or radioiodine when conjugated to internalising antibodies. *European Journal of Nuclear Medicine.* 2000, Vol. 27, pp. 753 – 765.

Benali, N., et al. 2000. Somatostatin Receptors. *Digestion.* 2000, Vol. 62, 1, pp. 27-32.

Bernhardt, P., et al. 2001. Dosimetric comparison of radionuclides for therapy of somatostatin receptor-expressing tumors. *International Journal of Radiation Oncology, Biology, Physics.* 2001, Vol. 2, pp. 514 - 524.

Beyer, G. J., et al. 2004. Targeted alpha therapy in vivo: direct evidence for single cancer kill using ^{149}Tb-rituximab. *European Journal of Nuclear Medicine and Molecular Imaging.* 2004, Vol. 4, 31, pp. 547-554.

Breeman, W. A., et al. 2003. Optimising conditions for radiolabelling of DOTA-peptides with ^{90}Y, ^{111}In and ^{177}Lu at high specific activity. *European Journal of Nuclear Medicine.* 2003, Vol. 30, pp. 917-920.

Buchegger, F., et al. 2006. Auger radiation targeted into DNA: a therapy perspective. *European Journal of Molecular Imaging.* 2006, Vol. 33, pp. 1352-1363.

Buchmann, I., et al. 2005. Radioimmuntherapien zur Behandlung der akuten myeloischen Leukämie und des myelodysplastischen Syndrom: Konzeptionelle Chancen. *Nuklearmedizin.* 2005, Vol. 44, pp. 107-117.

Budinger, T. F., et al. 1977. Emission computer assisted tomography with single-photon and positron annihilation photon emitters. *Journal of Computer Assisted Tomography.* 1977, Vol. 1, 1, pp. 131-145.

Cooker, E. N. 2000. *Encyclopedia of Separation Science.* New York : Academic Press, 2000.

Cotton, S. 2006. *Lanthanide and Actinide Chemistry.* West Sussex : John Wiley and Sons, 2006.

Crabbe, J. 1990. Correct use of Scatchard plots. *Trends in Biochemical Science.* 1990, Vol. 15, pp. 12-13.

Daghighian, F., et al. 1996. Enhancement of radiation dose to the nucleus by vesicular internalization of iodine-125-labeled monoclonal antibody. *Journal of Nuclear Medicine.* 1996, Vol. 37, pp. 1052-1057.

de Goeij, J. J. and Bonardi, M. L. 2005. How do we define the concepts specific activity, radioactive concentration, carrier, carrier-free and no-carrier-added? *Journal of Radioanalytical and Nuclear Chemistry.* 2005, Vol. 263, 1, pp. 13-18.

de Jong, L. A., et al. 2005. Receptor–ligand binding assays: technologies and tpplications. *Journal of chromatography B.* 2005, Vol. 829, pp. 1-25.

de Jong, M., et al. 1995. Evaluation in vitro and in rats of ^{161}Tb-DTPA-octreotide, a somatostatin analogue with potential for intraoperative scanning and radiotherapy. *European Journal of Nuclear Medicine.* 1995, 22, pp. 608-616.

Denzler, F. O., et al. 1997. Production and radiochemical separation of ^{147}Gd. *Applied Radiation and Isotopes.* 1997, Vol. 48, pp. 319-326.

Dorfner, K. 1991. *Ion exchangers.* Berlin : Walter de Gryter, 1991.

Dörr, U., et al. 1993. First clinical results with the chimeric antibody chCE7 in neuroblastoma. *European Journal of Nuclear Medicine.* 1993, Vol. 20, p. 858.

Druce, M. R., Lewington, V. and Grossman, A. B. 2009. Targeted radionuclide therapy for neuroendocrine tumours: principles and application. *Neuroendocrinology.* 2009. published online.

Dunlavey, D. C. and Seaborg, G. T. 1953. Alpha activity of ^{146}Sm as detected with nuclear emulsions. 1953, Vol. 92, p. 206.

Dvorakova, S. 2007. *Dissertation: Production and chemical processing of ^{177}Lu for nuclear medicine at the Munich research reactor FRM II.* Lehrstuhl für Radiochemie Technische Universität München : s.n., 2007.

Dyer, A. 2000. *Encyclopedia of Separation Science, chapter Ion Exchange.* New York : Academic Press, 2000.

Essen, M., et al. 2007. Peptide receptor radionuclide therapy with ^{177}Lu-octreotate in patients with foregut carcinoid tumours of bronchial, gastric and thymic origin.

European Jorunal of Nuclear Medicine and Molecular Imaging. 2007, Vol. 34, pp. 1219-1227.

Firestone, B. R., et al. 1996. *Table of Isotopes.* 8. New York : John Wiley & Sons, Inc., 1996.

Fogel, M., et al. 2003. L1 adhesion molecule (CD 171) in development and progression of human malignant melanoma. *Cancer Letters.* 2003, Vol. 189, pp. 237-247.

Fogel, M., Huszar, M. and Ben-Arie, A. 2004. L1 (CD171) as a novel biomarker for ovarian and endometrial carcinomas. *Expert Review of Molecular Diagnostics.* 2004, Vol. 4, pp. 455-462.

Forsberg, J. H., Marcus, Y. and Moeller, T. 1983. *Gmelin handbook of Inorganic Chemistry: Sc, Y, La-Lu Rare Earth Elements.* Berlin : Springer-Verlag, 1983. Vols. 6, D6.

Forssell-Aronsson, F., et al. 1995. Indium-111 activity concentrations in tissue samples after intravenous injection of Indium-111-DTPA-D-Phe^{1}-octreotide. *Journal of Nuclear Medicine.* 1995, Vol. 36, pp. 7-12.

Friedli, A., et al. 2009. The soluble form of the cancer-associated L1 cell adhesion molecule is a pro-angiogenic factor. *The International Journal of Biochemistry Cell Biology.* 2009, 41, pp. 1572-1580.

FRM II. [Online] http://FRM2.tum.de.

Ghiorso, A., et al. 1955. New element mendelevium, atomic number 101. 1955, Vol. 98, pp. 1518-1519.

Glass, R. A. 1955. Chelating agents applied to ion-exchange separations of americium and curium. *Journal of American Chemical Society.* 1955, Vol. 77, pp. 807-809.

Grünberg, J., et al. 2003. High-yield production of recombinant antibody fragments in HEK-239 cells using sodium butyrate. *Biotechniques.* 2003, Vol. 34, pp. 968-972.

Gullick, W. J. 1991. Prevalence of aberrant expression of the epidermal growth factor receptor in human cancers. *British Medical Bulletin.* 1991, Vol. 1, pp. 87-98.

Harjula, R. and Lehto, J. 1995. The international workshop on uniform and reliable nomenclature, formulations and experimentation for ion exchange, Helsinki, Finland, May 30-June 1, 1994. *Reactive and Functional Polymers.* 1995, Vol. 27, pp. 127-135.

Hashimoto, K., Matsuoka, H. and Uchida, S. 2003. Production of no-carrier-added ^{177}Lu via the ^{176}Yb(n,γ)^{177}Yb $\xrightarrow{\beta^-}$ ^{177}Lu process. *Journal of Radioanalytical and Nuclear Chemistry.* 2003, Vol. 255, pp. 575–579.

Heeg, M. J. and Jurisson, S. 1999. The role of inorganic chemistry in the development of radiometal agents for cancer therapy. *Accounts of Chemical Research.* 1999, Vol. 32, pp. 1053-1060.

Heppeler, A., et al. 2000. Receptor targeting for tumor localisation and therapy with radiopeptides. *Current Medicinal Chemistry.* 2000, Vol. 7, 9, pp. 971-994.

Hoefnagel, C. A., et al. 2001. A comparison of targeting of neuroblastoma with mIBG and anti L1-CAM antibody mAb chCE7: therapeutic efficacy in a neuroblastoma xenograft model and imaging of neuroblastoma patients. *European Journal of Nuclear Medicine.* 2001, Vol. 28, pp. 359-367.

Horwitz, E. P and Bloomquist, C. A. 1975. Chemical separations for super-heavy element searches and irradiated uranium targets. *Journal of Inorganic and Nuclear Chemistry.* 1975, Vol. 37, pp. 425-434.

Horwitz, E. P, et al. 2005. A process for the separation of ^{177}Lu from neutron irradiated ^{176}Yb targets. *Appl. Radiation Isot.* 2005, Vol. 63, pp. 23 – 36.

Horwitz, E. P. and Bloomquist, C. A. 1972. The preparation, performance and factors affecting band spreading of high efficiency extraction chromatographic columns for actinide separations. *Journal of Inorganic and Nuclear Medicine.* 1972, Vol. 34, pp. 3851-3871.

Horwitz, E. P., et al. 1976. Radiochemical and isotope separations by high-efficiency liquid-liquid chromatography. *Journal of Chromatography.* 1976, Vol. 125, pp. 203-218.

International Atomic Energy Agency. 2003. *Manual for reactor produced radioisotopes.* Österreich : s.n., 2003.

Jurkin, D. 2009. *Dissertation: Etablierung der FISRE (Free-Ion Selective Radiotracer Extraction)-Technik zur Bestimmung der kinetischen Stabilitäten von Radionuklidkomplexen.* München : s.n., 2009.

Kassis, A. I., et al. 1987. Radiotoxicity of ^{125}I in mammalian cells. 1987, Vol. 111, pp. 305–318.

Knapp, F. F., et al. 2005. Production of therapeutic radiositotopes in the ORNL High Flux Isotope Reactor (HFIR) for applications in nuclear medicine, oncology and interventional cardiology. *Journal of Radioanalytical and Nuclear Chemistry.* 2005, Vol. 263, pp. 503-509.

Knogler, K. 2002. *Diplomarbeit: Expression, Reinigung und Charakterisierung rekombinanter anti-L1-CAM Antikörper chCE7.* Institut Pharmazeutische Wissenschaften Eidgenössische Technische Hochschule Zürich : s.n., 2002.

Knogler, K., et al. 2007. Copper-67 radioimmunotherapy and growth inhibition by anti-L1-cell adhesion molecule monoclonal antibodies in a therapy model of ovarian cancer metastasis. *Clinical Cancer Research.* 2007, Vol. 13, 2, pp. 603-611.

Knogler, K., et al. 2006. Evaluation of ^{177}Lu-DOTA-labeled aglycosylated monoclonal anti-L1-CAM antibody chCE7: influence of the number of chelators on the in vitro and in vivo properties. *Nuclear Medicine and Biology.* 2006, 33, pp. 883-889.

Knogler, K., Novak-Hofer, I. and Zimmermann, K. 2005. A comparison of biological properties of a chmieric ^{177}Lu labeled anti L1-CAM antibody chCE7 and different recombinant variants for targeting of L1-CAM positive tumors. *European Journal of Nuclear Medicine and Molecular Imaging.* 2005, Vol. 32, p. 239.

Konishi, S., et al. 2004. Determination of immunoreactive fraction of radiolabeled monoclonal antibodies: what is an appropriate method? *Cancer Biotherapy & Radiopharmaceuticals.* 2004, Vol. 19, 6, pp. 706-715.

Krenning, E. P., Kwekkeboom, D. J. and Bakker, W. H. 1993. Somatostatin receptor scintigraphy with [^{111}In-DTPA-Phe^{1}] and [^{123}In-Tyr^{3}]-octreotide: The rotterdam

experience with more than 1000 patients. *European Journal of Nuclear Medicine.* 1993, Vol. 20, pp. 716-731.

Kwekkeboom, D. J., et al. 2001. [^{177}Lu-DOTA^{0}, Tyr^{3}]octreotate: comparison with [^{111}In-DTPA^{0}]octreotide in patients. *European Journak of Nuclear Medicine.* 2001, Vol. 28, 9, pp. 1319-1325.

Kwekkeboom, D. J., et al. 2005. Overview of results of peptide receptor radionuclide therapy with 3 radiolabeled somatostatine analogs. *J. Nuc. Med.* 2005, Vol. 46, pp. 62S-66S.

Kwekkeboom, D., et al. 2003. Treatment of patients with gastro-entro-pancreatic (GEP) tumours with the novel radiolabelled somatostatin analogue [^{177}Lu-DOTA0,Tyr^{3}]octreatate. *European Journal of Nuclear Medicine.* 2003, Vol. 30, pp. 417-422.

Ladner, R. C. 1999. Polypeptides from phage display. A superior source of in vivo imaging agents. *The Quarterly Journal of Nuclear Medicine.* 1999, Vol. 43, 2, pp. 119-124.

Laemmli, U. K. 1970. Cleavage of structural proteins during the assembly of the head of bacteriophage T4. *Nature.* 1970, Vol. 227, pp. 680-685.

Lahiri, S., Volkers, K. J. and Wierczinski, B. 2004. Production of ^{166}Ho through ^{164}Dy(n,γ)^{165}Dy(n,γ)^{166}Dy$\xrightarrow{\beta^-}$^{166}Ho and separation of ^{166}Ho. *Applied Radiation and Isotopes.* 2004, Vol. 61, pp. 1157–1161.

Lamberts, S. W. J., Koper, J. W. and Reubi, J. C. 1987. Potenital role of somatostatin analogues in the treatment of cancer. *European Journal of Clinical Investigation.* 1987, Vol. 17, 4, pp. 281-287.

Laue-Langevin, Institut. Institut Laue-Langevin. [Online] http://www.ill.eu.

Lebedev, N. A., et al. 2000. Radiochemical separation of no-carrier-added ^{177}Lu produced via the ^{167}Yb(n,γ)^{177}Yb$\xrightarrow{\beta^-}$^{177}Lu process. *Applied Radiation and Isotopes.* 2000, Vol. 53, pp. 412 – 425.

Lefkowitz, R. J., Roth, J. and Pastan, I. 1970. Radioreceptor assay of adrenocorticotropic hormone: new approach to assay of polypeptide hormones in plasma. *Science.* 1970, Vol. 170, pp. 633-635.

Levene, A. P., Singh, G. and Palmieri, C. 2005. Therapeutic monoclonal antibodies in oncology. *Journal of the Royal Society of Medicine.* 2005, Vol. 98, 4, pp. 146-152.

Levi, H. 1976. George Hevesy and his concept of radioactive indicators - in retrospect. *European Journal of Nuclear Medicine.* 1976, Vol. 1, pp. 3-10.

Lieser, K. H. 1980. *Einführung in die Kernchemie.* Weinheim : Verlag Chemie, 1980.

Lin, X., Baumgärtner, F. and Li, X. 1997. The program "MULTINAA" for various standardization methods in neutron activation analysis. *Journal of Radioanalytical and Nuclear Chemistry.* 1997, Vol. 215, pp. 179-191.

Lin, X., et al. 2006. Neutron flux parameters at irradiation positions in the new research reactor FRM II. *Nuclear Instruments and Methods in Physics Research A.* 2006, Vol. 564, pp. 641-644.

Lindmo, T., et al. 1984. Determination of the immunoreactive fraction of radiolabeled monoclonal antibodies by linear extrapolation to binding at infinite antigen excess. *Journal of Immunological Methods.* 1984, pp. 77-89.

Liu, S. and Edwards, D. S. 2001. Bifunctional chelators for therapeutic lanthanide radiopharmaceuticals. *Bioconjugate chemistry.* 2001, Vol. 12, pp. 7-34.

Mäcke, H. R. and Good, S. 2003. Radiometals (non-Tc, non-Re) and bifunctional labeling chemistry. [book auth.] A. Vèrtes, S. Nagy and Z. Klencsàr. *Handbook of Nuclear Chemistry.* Amsterdam : s.n., 2003, pp. 279-314.

Mäcke, H. R. 2002. Recent advances in the use of radiometals for therapeutic applications. [book auth.] M. Nicolini and U. Mazzi. *Technetium, rhenium and other metals in chemistry and nuclear medicine.* Padua : SGE Editoriali, 2002, Vol. 6, pp. 35-41.

Magill, J., Galy, J. and Pfennig, G. 2006. *Karlsruher Nuklidkarte.* Karlsruhe : s.n., 2006.

Malja, S., Schomacker, K. and Malja, E. 2000. Preparation of ^{90}Y by the $^{90}Sr/^{90}Y$ generator for medical purpose . *Journal of Radioanalytical and Nuclear Chemistry.* 2000, Vol. 245, 2, pp. 403-406.

Marhol, M. 1982. *Ion exchanger in analytical chemistry: their properties and use in inorganic chemistry.* Prague : Academia, 1982.

Markl, P. 1972. Extraktion und Extraktions-Chromatographie in der Anorganischen Analytik. [book auth.] R. Kaiser, E. Pungor, W. Simon F. Hecht. *Methoden der Analyse in der Chemie.* Frankfurt/Main : Akadenische Verlagsgesellschaft, 1972, p. [13].

Martin, R. F. and Haseltine, W. A. 1981. Range of radiochemical damage to DNA with decay of iodine-125. *Science.* 1981, Vol. 213, pp. 896-898.

Mayer, S. W. and Freiling, E. C. 1953. Ion exchange as a separation method. VI. column studies of the relative efficiencies of various complexing agents for the separation of lighter rare earths. *Journal of American Chemical Society.* 1953, Vol. 75, pp. 5647-5649.

Meares, C. F., et al. 2003. Molecular tools for targeted imaging and therapy of cancer. *Journal of Molecular Recognition.* 2003, 16, pp. 255-259.

Meli, M., et al. 1999. Anti-neuroblastoma antibody chCE7 binds to an isoform of L1-CAM present in renal carcinoma cells. *International Journal of Cancer.* 1999, Vol. 83, pp. 401-408.

Meredith, R. F., et al. 1995. Initial clinical evaluation of iodine-125-labeled chimeric 17-1A for metastatic colon cancer. 1995, Vol. 36, pp. 2229–2233.

Michel, R. B., Brechbiel, M. W. and Mattes, M. J. 2003. A comparison of 4 radionuclides conjugated to antibodies for single-cell kill. *Journal of Nuclear Medicine.* 2003, Vol. 44, pp. 632 – 640.

Miederer, M. 2002. *Dissertation: In vitro Untersuchungen des zytotoxischen Effektes der alpha emittierenden Nuklide ^{213}Bi, ^{149}Tb und ^{225}Ac gekoppelt an monoklonale Antikörper und Bewertung der physikalischen und biologischen Eigenschaften der Nuklide und Antikörper.* Nuklearmedizinische Klinik und Poliklinik der Technischen Universität München : s.n., 2002.

Mikolajczak, R., Pawlak, D. and Parus, J. L. 2005. Separation of microgram quantities of ^{177}Lu from milligram amounts of Yb by the extraction chromatography. [book auth.] C. Chemaly, B. J. Allen and H. Bonet. *Proceedings of the 5th International Conference on Isotopes (5ICI).* Brussels, Belgium : s.n., 2005.

Miller, J.M. 1994. *Chromatographische Trennmethoden.* Stuttgart, New York : Georg Thieme Verlag, 1994.

National Nuclear Data Center. [Online] http://www.nndc.bnl.gov/.

Nijsen, J. F.W., Krijger, G. C. and van het Schip, A. D. 2007. The bright future of radionuclides for cancer therapy. *Anti-Cancer Agents in Medicinal Chemistry.* 2007, Vol. 7, pp. 271-290.

Novak-Hofer, I, et al. 1997. Tumor uptake and metabolism of copper-67-labeled monoclonal antibody chCE7 in nude mice bearing neuroblastoma xenografts. *Journal of Nuclear Medicine.* 1997, 38, pp. 536-544.

Novak-Hofer, I., et al. 2008. Antibodies directed against L1-CAM synergize with Genistein in inhibiting growth and survival pathways in SKOV3ip human ovarian cancer cells. *Cancer Letters.* 2008, 261, pp. 193-204.

Novak-Hofer, I., et al. 1995. Cellular processing of copper-67-labeled monoclonal antibody chCE7 by human neuroblastoma cells. *Cancer Research.* 1995, Vol. 55, pp. 46-50.

Novak-Hofer, I., et al. 1994. Internalization and degradation of monoclonal antibody chCE7 by human neuroblastoma cells. *International Journal of Cancer.* 1994, Vol. 57, pp. 427-432.

Novak-Hofer, I., et al. 1992. Radioimmunolocalization of neuroblastoma xenografts with chimeric antibody chCE7. *Journal of Nuclear Medicine.* 1992, 33, pp. 231-236.

Ong, G. L., et al. 2001. Single-cell cytotoxicity with radiolabeled antibodies. *Clinical Cancer Research.* 2001, Vol. 7, pp. 192-201.

Park, M., et al. 2008. Desing and fabrication of phantoms using stereolithography for small-animal imaging systems. *Molecular Imaging and Biology.* 2008, Vol. 10, 5, pp. 231-236.

Pauwels, E. K. and Erba, P. 2007. Radioimmunotherapy of non-Hodgkin's lymphoma: molecular targeting and novel agents. *Drug News & Perspectives.* 2007, Vol. 20, pp. 87-93.

Pillay, K. K. S. 1986. A review of the radiation stability of ion exchange materials. *Journal of Radioanalytical and Nuclear Chemistry.* 1986, Vol. 102, pp. 247-268.

—. 1986. The effects of ionizing radiations on synthetic organic ion exchangers. *Journal of Radioanalytical and Nuclear Chemistry.* 1986, Vol. 97, pp. 135-210.

Pomplun, E. and Sutman, G. 2004. Is Coulomb explosion a damaging mechanism for ^{125}IUdR. *International Journal of Radiation Biology.* 2004, Vol. 80, pp. 855 - 860.

Pomplun, E. 2000. Auger electron spectra. *Acta Oncologica.* [39] 2000, pp. 673 – 679.

Postema, E. J., Boerman, O. C. and Oyen, W. J. 2001. Radioimmunotherapy of b-cell non-hodgkins Lymphoma. *European Journal of Nuclear Medicine.* 2001, Vol. 28, pp. 1725-1735.

Primiano, T., et al. 2003. Identification of potential anticancer drug targets trough the selection of growth-inhibitory genetic suppressor elements. *Cancer Cell.* 2003, Vol. 4, pp. 41-53.

Prutton, M. and El Gomati, M. M. 2006. *Scanning Auger Electron Microscopy.* Weinheim : Wiley-VCH, 2006.

PSI. Einführung in die Pharmazie II. [Online] http://zrw.web.psi.ch/lectures/Einf_Pharma/EinfuehrungPharmazieII.pdf.

Ramos-Suzarte, M., et al. 1999. ^{99m}Tc-labeled antihuman epidermal growth factor receptor antibody in patients with tumors of epithelial origin: Part III. clinical trials safety and diagnostic efficiacy. *Journal of Nuclear Medicine.* 1999, Vol. 40, 5, pp. 768-775.

Raut, N. M., Jaison, P. G. and Aggarwal, S. K. 2002. Comparative evaluation of three alpha-hydroxycyrboxylic acids for the separation of lanthanides by dynamically modified reversed-phase high performance liquid chromatography. *Journal of Chromatography A.* 2002, Vol. 959, pp. 163-172.

Raymond, S. and Weintraub, L. 1959. Acrylamide gel as a supporting medium for zone electrophoresis. *Science.* 1959, Vol. 130, p. 711.

Reubi, J. C. 1997. Regulatory peptide receptors as molecular targets for cancer diagnosis and therapy. *The Quaterly Journal of Nuclear Medicine and Molecular Imaging.* 1997, Vol. 41, 2, pp. 63-70.

Robards, K. and Clarke, S. 1988. Advances in the analytical chromatography of the lanthanides. *Analyst.* 1988, Vol. 113, pp. 1757-1779.

Rösch, F. and Forssell-Aronsson, E. 2004. Radiolanthanides in nuclear medicine. [book auth.] A. Siegel and H. Siegel. *Metals Ions in Biological Systems.* New York-Basel : s.n., 2004, pp. 77 – 107.

Rösch, F. 2003. *Handbook of Nuclear Chemistry: Radiochemistry and radiopharmaceutical chemistry in life sciences, Volume 4.* Amsterdam : Kluwer Academic Publishers, 2003.

—. 2007. Radiolanthanides in endoradiotherapy: an overview. *Radiochimica Acta.* 95 2007, pp. 303-311.

Rosenthal, H. E. 1967. A graphiy method for the determination and presentation of binding parameters in a complex system. *Analytical Biochemistry.* 1967, Vol. 20, pp. 525-532.

Scatchard, G. 1949. The attraction of proteins for small molecules and ions. *Annals of the New York Academy of Science.* 1949, Vol. 51, pp. 660-672.

Schädel, M., Trautmann, T. and Hermann, G. 1977. Fast separation of lanthanides by high pressure liquid chromatography. *Radiochimica Acta.* 1977, Vol. 24, pp. 27–31.

Schmaljohann, J., Beirsack, H. J. and Guhlke, S. 2005. Radiotherapeutika: Herstellung und therapeutische Anwendung von Radiopharmaka. *Pharmazie in unserer Zeit.* 2005, Vol. 34, pp. 498-504.

Schwedt, G. 1994. *Chromatographische Trennmethoden.* Stuttgart, New York : Georg Thieme Verlag, 1994.

Shapiro, A. L., Vinuela, E. and Maizel, J. V. 1967. Molecular weight estimation of polypeptide chains by electrophoresis in SDS-polyacrylamide gels. *Biochemical and Biophysical Research Communications.* 1967, Vol. 28, pp. 815-820.

Shimizu, K., et al. 2004. Alkaline earth cation exchange with novel Na-3-mica: kinetics and thermodynamic selectivities. *Journal of material chemistry.* 2004, Vol. 14, pp. 1031-1035.

Sivaraman, N., et al. 2002. Separation of lanthanides using ion interaction chromatography with HDEHP coated columns. *Journal of Radioanalytical and Nuclear Chemistry.* 2002, Vol. 252, 3, pp. 491-495.

Smith-Jones, P. M., et al. 1998. Synthesis and characterisation of ^{90}Y-Bz-DTPA-oct: a ^{90}Y labeled octreotide analogue for radiotherapy of somatostatin receptor-positive tumours. *Nuclear Medicine & Biology.* 1998, Vol. 25, pp. 181-188.

Sochacka, R. J. and Siekierski, S. 1964. Reversed-phase partition chromatography with di-(2-ethylhexyl) orthophosphoric acid as the sttionary phase. Part I. separation of rare earths. *Journal of Chromatography.* 1964, Vol. 16, pp. 376-384.

Stahl, A., et al. 2006. [^{111}In]DOTATOC as a dosimetric substitute for kidney dosimetry during [^{90}Y]DOTATOC therapy: results and evaluation of a combined gamma camera/probe approach. *European Journal of Nuclear Medicine and Molecular Imaging.* 2006, Vol. 33, pp. 1328 - 1336.

Thompson, S. G., et al. 1954. Chemical Properties of Elements 99 and 100. *Journal of American Chemical Society.* 1954, Vol. 76, pp. 6229-6236.

Todd, M., et al. 2003. A rare earth-DOTA-binding antibody: probe properties and binding affinity across the lanthanide series. *Journal of the American Chemical Society.* 2003, Vol. 12, 125, pp. 3436-3437.

Tolmachev, V., et al. 2000. ^{114m}In, a candidate for radionuclide therapy: low-energy cyclotron production and labeling of DTPA-D-Phe-octreotide. *Nuclear Medicine and Biology.* 2000, Vol. 27, pp. 183-188.

Uusijärvi, H., et al. 2006. Electron- and positron-emitting radiolanthanides for therapy: aspects of dosimetry and production. *Journal of Nuclear Medicine.* 2006, Vol. 47, pp. 807 – 814.

Valkema, R., et al. 2002. Phase I study of peptide receptor radionuclide therapy with [^{111}In-DTPA^{0}]octreotide: the Rotterdam experience. *Seminars in Nuclear Medicine.* 2002, Vol. 2, pp. 110 – 122.

Volkert, W. A. and Hoffmann, T. J. 1999. Therapeutic Radiopharmaceuticals. *Chemical Reviews.* 1999, Vol. 99, pp. 2269-2292.

Waldherr, C., et al. 2002. Tumor response and clinical benefit in neuroendocrine tumors after 7.4 GBq ^{90}Y-DOTATOC. *Journal of Nuclear Medicine.* 2002, Vol. 43, pp. 610 – 616.

Warner, R. P. and O'Doriso, T. M. 2002. Radiolabeled peptides in diagnosis and tumor imaging: Clinical overview. *Seminars in Nuclear Medicine.* 2002, Vol. 32, pp. 79-83.

Weber, K. and Osborn, M. 1969. The reliability of molecular weight determinations by dodecyl sulfate polyacrylamide gel electrophoresis. *Journal of Biological Chemistry.* 1969, Vol. 244, pp. 4406-4412.

Welt, S., et al. 1996. Phase I/II study of iodine-125-labeled monoclonal antibody A33 in patients with advanced colon cancer. *Journal of Clinical Oncology.* 1996, Vol. 14, pp. 1787–1797.

Wilder, R. B., DeNardo, G. L. and DeNardo, S. J. 1996. Radioimmunotherapy: recent results and future directions. *Journal of Clinical Oncology.* 1996, Vol. 14, pp. 1383-1400.

Williams, C. D. 2000. *Encyclopedia of Separation Science, chapter Zeolites.* New York : Academic Press, 2000.

Wisemann, G. A., White, C. A. and Witzig, T. E. 1999. Radioimmunotherapy of relapsed non-Hodgkin's' lymphoma with zevalin, a ^{90}Y-Labeled anti CD20 monoclonal antibody,. *Clinical Cancer Research.* 1999, Vol. 5, pp. 3281-3286.

Wish, L., Freiling, E. C. and Bunney, L. R. 1954. Ion Exchange as a Separations Method. VIII. Relative Elution Positions of Lanthanide and Actinide Elements with Lactic Acid Eluant at 87°. 1954, Vol. 76, pp. 3444-3445.

Witzig, T. E., Cordon, L. I. and Cabanills, F. 2002. Randomized controlled trial of yttrium-90-labeled ibritumomab tiuxetan radioimmunotherapy versus rituximab immunotherapy for patients with relapsed or refractory low-grade, follicular, or transformed b-cell non-Hodgkin's' Lymphoma. *Journal of Clinical Oncology.* 2002, Vol. 20, pp. 2453-2463.

Xiao, M. and Selvin, P. R. 2001. Quantum yields of luminescent lanthanide chelates and far-red dyes measured by resonance energy transfer. *Journal of the American Chemical Society.* 2001, 123, pp. 7067-7073.

Yalow, R. S. and Berson, S. A. 1959. Assay of plasma insulin in human subjects by immunological methods. *Nature.* 1959, Vol. 184, pp. 1648-1649.

Zalutsky, M. R. 2003. Radionuclide Therapy. [book auth.] A., Nagy, S., Klencsár, Z Vértes. *Handbook of Nuclear Chemistry.* Amsterdam : s.n., 2003, pp. 315-350.

Zhernosekov, K. P., et al. 2007. A ^{140}Nd/^{140}Pr radionuclide generator based on physico-chemical transitions in ^{140}Pr complexes after electron capture decay of ^{140}Nd-DOTA. *Radiochimica Acta.* 2007, Vol. 95, pp. 319 – 327.

Zimmermann, K., et al. 1999. A triglycine linker improves tumor uptake and biodistributions of ^{67}Cu-labeled anti-neuroblastoma mAb chCE7 F(ab')2 fragments. *Nuclear Medicine and Bioloky.* 1999, Vol. 26, pp. 943-950.

6.2 List of Figures

6.3 List of Tables

6.4 Abbreviations

α-HIB	**α**-**h**ydroxy**i**sobutyrate
α-HIBA	**α**-**h**ydroxy**i**sobutyric **a**cid
BFC	**b**ifunctional **c**helator
Bn	**b**e**n**zyl
Bq	**b**ec**q**uerel
cps	**c**ounts **p**er **s**econd
cpm	**c**ounts **p**er **m**inute
CHX-A-DTPA	2-(p-isothiocyanatobenzyl)-**c**yclo**he**x**y**l-**d**iethylene**t**riamine**p**enta**a**cetic acid
BSA	**b**ovine **s**erum **a**lbumin
ddH_2O	**d**ouble-**d**istilled H_2O
DOTA	1,4,7,10-Tetraazacyclo**do**decane-1,4,7,10-**t**etraacetic**a**cid
DOTATATE	**DOTA**-(Tyr(3))octreo**tate**
DOTA-NCS	p-isothiocyanatobenzyl-1,4,7,10-tetraazacyclododecane-N-N'-N''-N'''-tetraacetic acid
DOTATOC	(**DOTA**-Phe(1)-Tyr(3))**oc**treotide
DTPA	**d**iethylene**t**riamine**p**entaacetic**a**cid
DTT	**d**i**t**hio**t**hreitol
EDTA	**e**thylene**d**iamine**t**etraacetic**a**cid
EGFR	**e**pidermal **g**rowth **f**actor **r**eceptor
FPLC	**f**ast **P**rotein **L**iquid **C**hromatography
FRM II	**F**orschungs**r**eaktor **M**ünchen II
HAS	**h**uman **s**erum **a**lbumin

HFR	**h**igh **f**lux **r**eactor
ILL	**I**nstitute **L**aue-**L**angevin
ITG	**I**sotope **T**echnologies **G**arching GmbH
ITM	**I**sotopen **T**echnologien **M**ünchen AG
LET	**l**inear **e**nergy **t**ransfer
mAb	**m**onoclonal **a**nti**b**ody
meq	**m**illi **eq**uivalent
n.c.a.	**n**o **c**arrier **a**dded
PBS	**p**hosphate **b**uffered **s**aline
PKM	**p**harmaco**k**inetic **m**odifier
RT	**r**oom **t**emperature
SCN	i**s**othio**c**ya**n**ato
SDS	**s**odium**d**odecyl**s**ulfate
SDS-PAGE	**s**odium**d**odecyl**s**ulfate **p**oly**a**crylamide **g**el **e**lectrophoresis
TEMED	N,N,N',N'-**te**tra**me**thylethylene**d**iamine
TND	**t**umor to **n**ormal **t**issue mean adsorbed dose ratio

Hiermit erkläre ich, dass ich diese Dissertation selbständig verfasst und nur mit den angegebenen Hilfsmittel gearbeitet habe.

_____

Silvia Lehenberger